# FLOW BIREFRINGENCE IN SOLUTIONS OF MACROMOLECULES

ROGER CERF[1] AND HAROLD A. SCHERAGA

*Department of Chemistry, Cornell University, Ithaca, New York*

*Received December 10, 1951*

CONTENTS



[1] Rockefeller Fellow, 1951, on leave from Centre d'Etudes de Physique Macromoléculaire, Strasbourg, France.

## I. Introduction

In the study of solutions of large molecules or colloidal particles the determination of size, shape, and flexibility of the solute particles is of major importance. Various physical-chemical methods have been developed for investigating this problem, a particularly fruitful approach being the study of the optical properties of solutions of macromolecules under the influence of an external field.

If an external field is applied to a normally isotropic pure liquid or solution, the system in most cases becomes birefringent. The production of double refraction in this manner is referred to as the Kerr effect, the Cotton–Mouton effect, or the Maxwell effect, depending upon whether the applied field is electric, magnetic, or hydrodynamic, respectively. In the particular case of interest here, i.e., that of a hydrodynamic field, flow birefringence is produced as a result of the shearing forces to which the system is subjected. Theoretical considerations indicate that if the solute molecules are rigid and geometrically asymmetric the double refraction of the system is due to an equilibrium between the orienting influence of the applied field and the disorienting effect of the Brownian motion. However, even though the particles may be spherical and optically isotropic in the absence of the field, this optical anisotropy can also appear in the system if the particles can be deformed by the shearing forces. The production of birefringence by a hydrodynamic field is a very useful method for the study of solutions of macromolecules, as it gives information about the geometrical, optical, and mechanical properties of the solute particles.

This subject has been reviewed by several investigators. Boehm's general article in 1939 contains many details about apparatus and experimental results (13). In 1942 a general review was presented by Edsall (38) and a discussion of the theory by Kanamaru and Tanaka (94). Peterlin and Stuart in 1943 considered the general problem of induced double refraction, including a discussion of flow birefringence (133). The purpose of this review is to present some of the important aspects of the method and also to point out some of the developments of the past decade. While some of the ideas established before 1942 will be referred

to here, the reader should consult Edsall's article for a discussion of these points in greater detail.

## II. Notation

The symbols employed in this review are defined below:

$a$ = radius of sphere,
$a$ = semi-major axis of ellipsoid,
$b$ = semi-minor axis of ellipsoid,
$b$ = hydrodynamic length of monomer,
$c$ = concentration in moles per liter,
$d$ = annular gap between cylinders; average thickness of statistical chain element,
$f$ = orientation factor,
$g_i$ = optical factor,
$\overline{h_0^2}$ = mean square end-to-end distance of a chain molecule,
$k$ = Boltzmann's constant,
$m, n$ = slope and intercept of $(\tan \alpha)_0$ *vs.* $\eta_0$ curve,
$n$ = average index of refraction of particle,
$n_0$ = index of refraction of solvent,
$n_1, n_2, n_3$ = principal indices of refraction of particle,
$n_x, n_y, n_z$ = principal indices of refraction of flowing solution,
$\partial n = n - n_0$,
$\delta n$ = refractive increment,
$\Delta n = n_z - n_x$ = magnitude of birefringence,
$p$ = axial ratio,
$r$ = cylinder radius,
$s$ = number of monomer units in a statistical chain element,
$t$ = time,
$v$ = volume of sphere,
$w$ = mechanical factor, and
$x, y, z$ = axes of index of refraction ellipsoid in flowing solution.

$A$ = average length of statistical chain element,
$F$ = distribution function for rigid particles,
$G$ = velocity gradient,
$L$ = hydrodynamic length of chain molecule,
$N$ = Avogadro's number,
$N$ = speed of rotor in R.P.M.,
$P, Q$ = designation of end-points of chain molecule,
$R = (p^2 - 1)/(p^2 + 1)$,
$T$ = absolute temperature,
$V$ = velocity of particle with respect to liquid; velocity of flowing liquid,
$X, Y, Z$ = fixed coördinate system in concentric cylinder apparatus, and
$Z$ = degree of polymerization.

$\alpha$ = ratio of velocity gradient to rotary diffusion constant,
$\alpha$ = inclination of initial slope of extinction angle curve,
$\alpha_1, \alpha_2, \alpha_3$ = principal polarizabilities of statistical chain element,
$\gamma$ = elastoöptical coefficient,
$\zeta$ = frictional coefficient,
$\eta_0$ = viscosity of solvent,
$\eta_i$ = internal viscosity,
$\eta_{sp}$ = specific viscosity,
$\vartheta, \varphi$ = orientation angles,
$\Theta$ = rotary diffusion constant,
$\lambda$ = wave length; also the Kuhn frictional factor,
$\mu$ = Lamé's shearing elasticity coefficient,
$\nu = \left(\frac{\Delta n}{G\eta_0 c}\right)_{c=0,\, G=0}$,
$\phi$ = volume fraction,
$\chi$ = extinction angle,
$\psi$ = position of axes of deformed particle, and
$\omega_\vartheta, \omega_\varphi$ = components of angular velocity.

## III. Method of Investigation

The application of shearing forces to a solution can be realized experimentally by forcing the solution through a capillary tube or by rotating one of two concentric cylinders of a Couette-type apparatus which contains the solution in the annular gap between the cylinders. For quantitative studies the arrangement of concentric cylinders is preferable, because in this type of apparatus one can best realize experimentally, by using a narrow annular gap, the ideal situation of two planes of infinite extent, one of which moves relative to the other. In the concentric cylinder apparatus the velocity, $V$, of the flowing liquid will vary across the annular gap, the velocity gradient, $G = \mathrm{d}V/\mathrm{d}r$, being in the direction of the cylinder radius. If the gap is small compared with the cylinder radius, the behavior of $G$ approaches that for the case of infinite planes, where it is constant.

The resultant birefringence is studied by the general methods used to examine optically anisotropic material, i.e., between crossed Nicol prisms with polarized light. These systems are studied with a linearly polarized light beam incident in such a direction that the ordinary and extraordinary beams are superimposed on each other. The resultant beam emerging from the medium is, in general, elliptically polarized.

If the annular gap is viewed between crossed Nicols, the field will appear dark when both cylinders are at rest. If one of the cylinders—for example, the outer one—is set in rotation, the field will then appear bright everywhere except in the region of a dark cross, the cross of isocline (125), as illustrated in figure 1.

In the birefringent system the index of refraction ellipsoid has three different principal axes $x$, $y$, $z$ with principal indices of refraction $n_x$, $n_y$, $n_z$ (defining the directions of the neutral lines) and therefore possesses the character of a biaxial crystal (133). However, since $x$ and $z$ lie in the streaming plane and $y$ is perpen-

dicular to it and coincident with the direction of the light beam, only $x$ and $z$ are observable. Thus, the system *appears* to have the character of a uniaxial crystal,[2] where the direction of the incident beam along $n_y$ does not permit the observation of this latter axis. Because the birefringent medium possesses the extinction character of a crystal, the smaller of the two angles between the cross

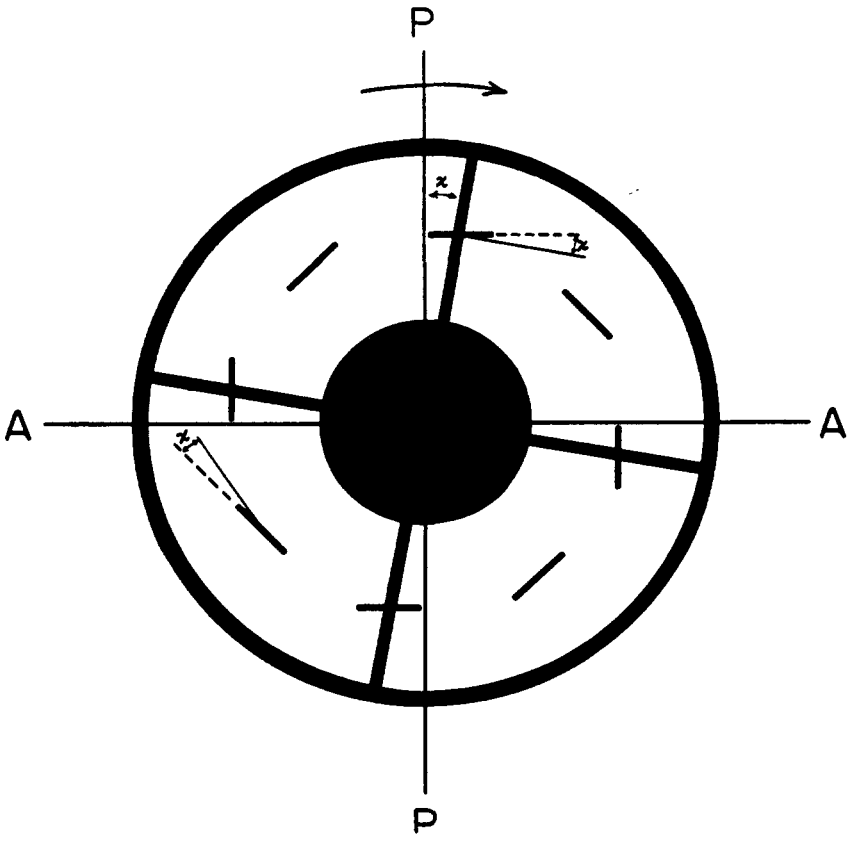


FIG. 1. View of the birefringent medium in the annular gap between the concentric cylinders. The cross of isocline is shown at an angle $\chi$ with respect to the plane of the polarizer for a rotating outer cylinder. The orientation of eight rod-like particles at an angle $\chi$ with respect to the stream lines at high velocity gradient is also indicated.

of isocline and the planes of transmission of the Nicol prisms is referred to as the extinction angle, $\chi$.

The double refraction may be characterized by $\Delta n = n_z - n_x$, the difference in the indices of refraction of light with electric vectors parallel to each of the neutral lines of the flowing solution. Depending on the relative magnitude of $n_x$ and $n_z$, the birefringence can be positive or negative. $\chi$ is the angle between the neutral line $z$ (index of refraction $n_z$) and the stream lines. This angle is also equal to the angle between the cross of isocline and the Nicol planes as previously defined (figure 1).

[2] For a uniaxial crystal $n_x = n_y$.

### A. EXPERIMENTAL BEHAVIOR

For those pure liquids which exhibit flow birefringence the extinction angle has been found to be 45° at all velocity gradients, while the birefringence is a linear function of velocity gradient in the region of laminar flow (18, 142, 143, 174).

In general, for solutions of macromolecules, the extinction angle approaches 45° as the gradient approaches zero and approaches 0° as the gradient attains high values. At sufficiently low concentration, where the solute–solute interaction is negligible, the $\chi$ *vs.* $G$ curve is independent of concentration. $n_z - n_x$ is zero at zero gradient, increases linearly at low gradients, and departs from linearity at higher gradients, the nature of the departure depending on the type of

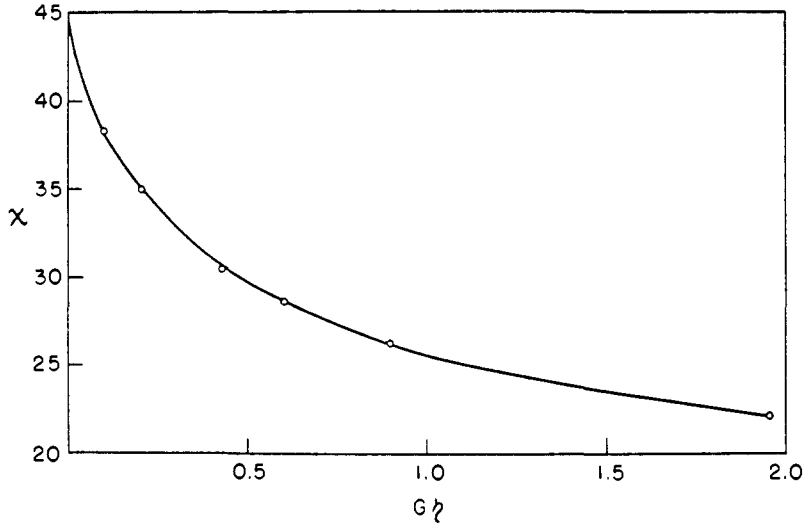


FIG. 2. Experimental data for the behavior of the extinction angle at low gradients in solutions of tobacco mosaic virus (Wissler (196)). $\eta$ is the solvent viscosity.

solute particle; for rigid particles $n_z - n_x$ approaches a limiting or saturation value (negative departure from linearity), while for non-rigid particles it may depart from linearity in a positive sense. At sufficiently low concentration $n_z - n_x$ is proportional to the volume fraction of the solute particles.

Some experimental results may be seen in figures 2 and 3, which represent Wissler's data (196) for tobacco mosaic virus, a macromolecule exhibiting the behavior of a rigid particle. Figure 2 shows the initial behavior of the extinction angle at low gradients, while figure 3 illustrates how the extinction angle and magnitude of the birefringence approach their limiting values at high gradients. Data of Tsvetkov and Frisman (186) for oppanol and vystanex (unfractionated polyisobutylenes) in figures 4 and 5 illustrate, respectively, the different character of the birefringence curves but the similar nature of the extinction angle curves for deformable particles. It may be noted that for tobacco mosaic virus

accurate measurements are possible for low gradients, as the effect is very large. Usually, for chain molecules the effect is very small and high velocity gradients

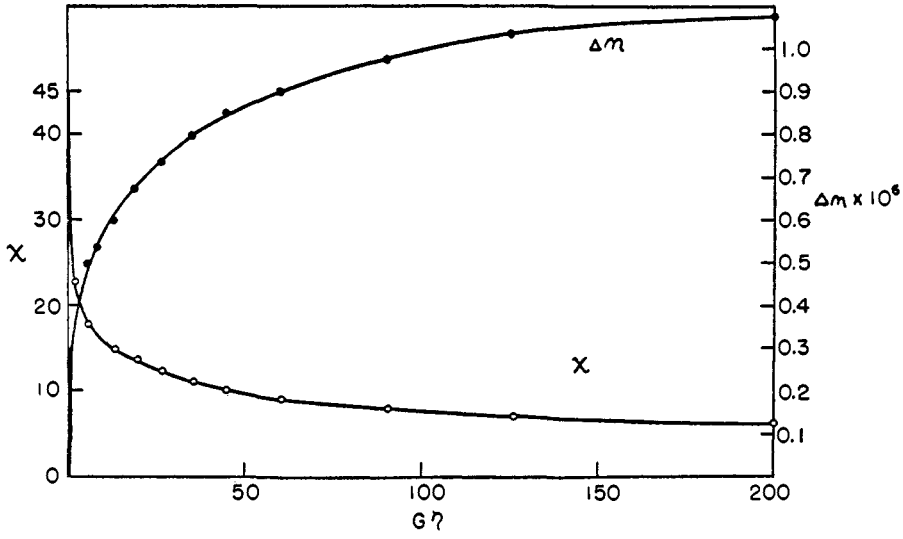


FIG. 3. Behavior of the extinction angle and the magnitude of the birefringence at high values of $G\eta$ in solutions of tobacco mosaic virus (Wissler (196)).

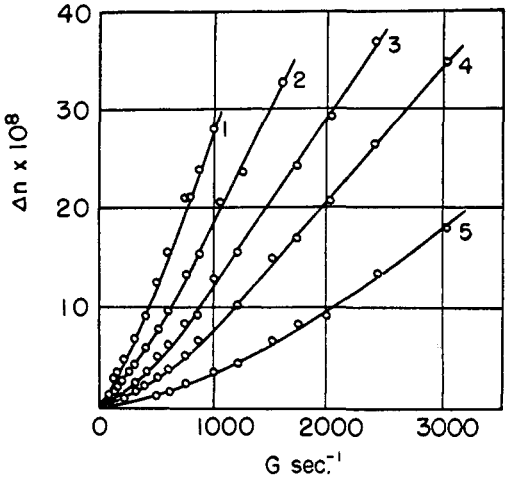


FIG. 4. Double refraction of oppanol solutions *vs.* velocity gradient for several concentrations, decreasing from 1 to 5 (Tsvetkov and Frisman (186)). The positive deviation from linearity should be noted.

are required. These are typical results for rigid and deformable particles, respectively, and must be explained by a suitable theory. It might be pointed out that many proteins, viruses, and other biological materials exhibit an effect suggestive of that of rigid particles, whereas chain molecules, such as many synthetic polymers, appear to be deformable.

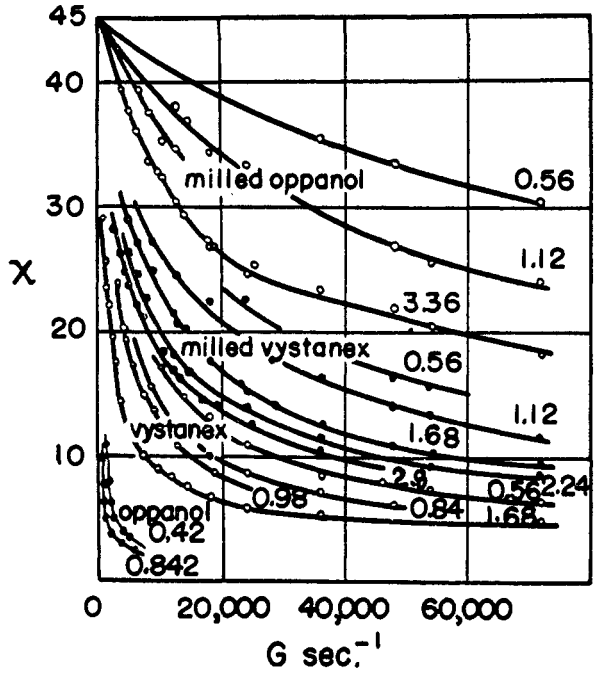


FIG. 5. Extinction angle at various velocity gradients for solutions of oppanol and vystanex (Tsvetkov and Frisman (186)). The numbers close to the curves indicate the volume concentration × 100. The two lowest curves for oppanol correspond to curves 1 and 4 of figure 4.

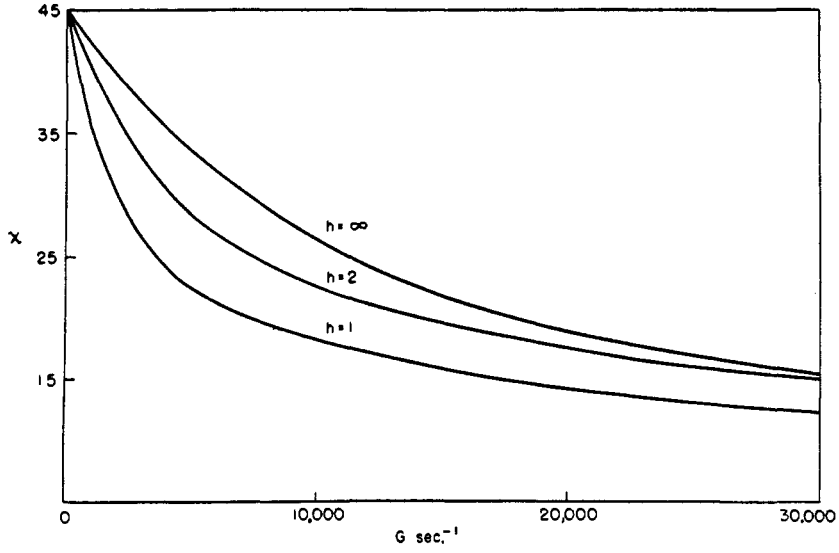


FIG. 6. Dependence of extinction angle on velocity gradient for a monodisperse system ($h = \infty$) of rigid ellipsoids and for polydisperse systems having a Gaussian distribution of particle lengths ($h = 1$ and 2) (152).

If the system is polydisperse, then the behavior of the extinction angle and birefringence curves is quite different from that indicated in figure 3, for example. If the various components of a polydisperse system have birefringence values of different sign, then the curves become more or less complicated (145, 147, 148). If the components have birefringence values of the same sign, the resultant curves may be qualitatively similar to those for monodisperse systems. Figure 6 represents a particular example of the theoretical curves for a Gaussian distribution of lengths in a system of rod-like particles having birefringence of the same sign (152). The curve for $h = \infty$ represents a monodisperse system, whereas the curves for lower values of $h$ indicate the effect of higher degrees of polydispersity.

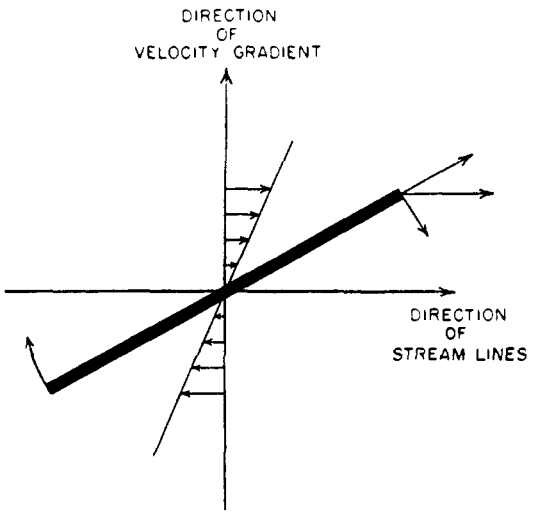


FIG. 7

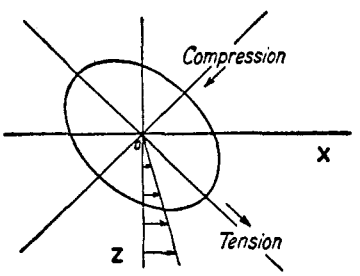


FIG. 8

FIG. 7. Effect of a velocity gradient on a rigid rod-like solute particle, showing the rotation caused by the hydrodynamic forces.

FIG. 8. Effect of velocity gradient on a deformable particle. The tensions and compressions are at 45° with respect to the stream lines in the $X$ direction. The orientation of the particle axes depends on the velocity gradient.

### B. RIGID PARTICLES

The origin of the phenomenon may be understood from the following outline of the method which employs the concentric cylinder apparatus with the liquid contained between the cylinders. We shall first discuss the case which has been known for some time (12, 60), where the effect is greatest and easiest to observe, that is, the orientation effect in a solution of rigid rod-like particles. This will be followed by a description of the effect for deformable particles.

In the absence of any shearing forces, rod-like particles are maintained in a state of random orientation due to the rotary Brownian motion. With the outer cylinder rotating, a velocity gradient is set up along a radius vector across the gap, with the stream lines normal to the radius vector. As a result the rods will rotate in the direction indicated in figure 7, with a tendency to be oriented

in the direction of the stream lines. This orientation will be opposed by the Brownian motion. In an equilibrium steady state the rotating rods will spend the greater portion of their time at a preferred orientation with respect to the stream lines. This degree of orientation may be characterized by the parameter $\alpha$. $\alpha = G/\Theta$, where $G = dV/dr$ is the velocity gradient in sec.$^{-1}$ and $\Theta$ is the rotary diffusion constant of the rod in sec.$^{-1}$ and will be defined later. $\Theta$ is a measure of the intensity of the Brownian motion (29, 129) and is a function of the size and shape of the solute particles.

There exists a cross of isocline for every velocity gradient. At any gradient there is a *distribution* of orientations of rod axes at any point in the liquid. The picture is particularly simple at high values of $\alpha$, where all the particles tend to become parallel to each other, i.e., there is then a very narrow distribution of particle orientations. We can thus assume that at high values of $G$ or $\alpha$ all the rods are oriented at an angle $\chi$ (small because $G$ is large) with respect to the stream lines, as illustrated for eight rods in figure 1. The origin of the cross of isocline then becomes apparent. If $PP$ and $AA$ represent the planes of transmission of the crossed polarizing and analyzing Nicols, respectively, then it can be seen that those rods lying on the cross of isocline are parallel to the planes of the Nicol prisms. If we assume that the axis of largest polarizability of the rod lies in the direction of its long axis, then for those rods on the cross, the linearly polarized light beam passes through the solution unaffected and is extinguished by the analyzer. For rods not lying on the cross, the electric vector of the incident beam will make some angle with the rod axis, giving rise to components parallel and perpendicular to this axis. The resultant elliptically polarized light cannot be completely extinguished by the analyzer. The appearance of the arms of the cross of isocline will depend on the velocity gradient, i.e., the arms will be rather diffuse at low $\alpha$ but will appear sharper as $\alpha$ increases.

### C. DEFORMABLE PARTICLES

In the flowing liquid there are tensions and compressions at right angles to each other and at 45° with respect to the direction of the stream lines in the range of velocity gradients under consideration here (77). As a result of these forces there will be a deformation effect superimposed on the orientation effect if the particles are deformable (the case of an elastic dumbbell (79, 110)), and the phenomena will differ from those already described for rigid particles, especially at high gradients.

Non-rigid spherical particles can also be deformed, giving double refraction of a different nature from that observed in solutions of rigid particles (the case of an elastic sphere (25, 77)). The behavior of such solutions has been compared to that of a suspension of liquid drops in another immiscible liquid (27). Figure 8 shows how the tensions and compressions deform the liquid drop. The section of the drop in the plane of flow has the form of an ellipse, the direction of whose axes will depend on the value of the gradient (182): for low velocity gradients the angle between the major axis and the stream lines approaches 45°; for higher gradients one axis becomes more and more parallel and the other more and more

perpendicular to the direction of the stream lines. A solution of such drops should show flow birefringence, the neutral lines of the solution coinciding with the axis of each ellipse, provided the drops are small enough so that the light can pass through the solution. The behavior of a macroscopic liquid drop is similar to that of an elastic sphere (25), for which the distribution of the orientations of the axes of the ellipses is very narrow even at low $G$ values, in contradistinction to the case of rigid particles which become parallel to each other only at high $G$ values.

The neutral lines of a solution of deformable particles show, qualitatively, the same behavior with varying $G$ as do those for a solution of rigid rods. The theory for deformable particles will be discussed, together with the experimental results, in Section VI.

### D. EXPERIMENTAL QUANTITIES

The experimentally determined quantities of the method of flow birefringence are the extinction angle, $\chi$, and the birefringence, $n_z - n_x$, at various velocity gradients $G$. The birefringence is related to the size, shape, and optical properties of the solute and solvent molecules, while the extinction angle depends only on the size and shape of the particles (132, 144).

It might be pointed out that in the method of flow birefringence the position of the neutral lines varies with the gradient, whereas in electric or magnetic birefringence, one of the neutral lines is in the direction of the applied field for all values of the field strength.

## IV. Apparatus

The range of velocity gradients required for satisfactory measurements depends very much on the material under investigation. Very long, rigid, asymmetrical molecules, like those of tobacco mosaic virus (120) or myosin (125), require extremely low gradients (of the order of 100 $sec.^{-1}$) to produce a large amount of birefringence. Smaller, less asymmetrical molecules like serum albumin (53) and most chain molecules like polystyrene (165) require very high velocity gradients (several thousand $sec.^{-1}$) to produce measurable effects. Thus, in a rough way, one may divide the systems to be studied into two categories, one involving low gradients and the other involving moderate or high gradients.

In a given solution larger effects which are more easily measured are observed at the higher gradients, whereas the smaller effects present at low gradients require more refined apparatus for precise measurement. Snellman (169, 171) has discussed some of the sources of error in streaming birefringence measurements. At high gradients one has to avoid the possibility of turbulence (142, 165) if the viscosity is low and of heating effects (10) if the viscosity is high. For deformable particles, the interpretation of the initial behavior of the birefringence and extinction angle is simpler, whereas for rigid particles the interpretation is possible over a wide range of gradients. In addition, if the system is polydisperse, it is desirable to make measurements at both low and high gradients (155).

Several different modifications of the concentric cylinder apparatus are in use by various investigators; details of many of these have been summarized by Boehm (13). In selecting the design of apparatus, one of the main considerations is the type of material for which the apparatus is to be used. In general, for molecules like myosin a large intercylinder gap (approximately 1 cm.) and slow speeds of rotation suffice for achieving high enough gradients. In such cases the optical alignment is a relatively simple problem. Where higher velocity gradients are required, it is necessary to have an apparatus capable of attaining high rotational speeds. Since the flow must remain laminar, the annular gap must be made small and the solution viscosity increased. This narrower gap introduces more stringent requirements as to the accuracy of the alignment of the optical system in order to avoid reflections from the cylinder walls. Frey-Wyssling and Weber (63) have suggested procedures to correct for these disturbances; Björnstahl (8) has discussed several methods for the accurate alignment of optical systems for studies of induced double refraction. In practice it is very difficult to apply Björnstahl's recommendations. In both slow-speed and high-speed systems flexibility can be achieved by using several interchangeable rotors to give various gap widths.

### A. INNER CYLINDER ROTATING

A typical apparatus, described by Edsall and coworkers (44), makes use of a high-speed, rotating inner cylinder. The cylinders which come in contact with the solution are made of Carpenter No. 4-Mo, type 316 stainless steel, which is satisfactory for use with protein solutions. The cylinder system is shown in figure 9. The shaft to which the rotor is attached is mounted on a set of preloaded precision ball bearings to enable maintenance of a uniform gap width during rotation. Various gap widths can be obtained by the use of several interchangeable rotors, the gap widths for the apparatus shown (153) being 0.12 mm., 0.26 mm., and 0.72 mm. Water is circulated through the outer jacket of the stator for the maintenance of constant temperature. The linearly polarized light beam passes down successively through a slot in the ball bearing housing, the upper glass window, and the solution in the annular gap, and emerges through the lower glass window. Further details of this cylinder system and the associated optical arrangement may be found in Edsall's original paper (44).

Figure 10 is a photograph of a complete assembly (153), showing the vertical optical bench on which is mounted a J-25 Western Union concentrated arc lamp at the focus of a suitable lens, a Farrand interference filter for obtaining light of wave length 544 m$\mu$, an iris diaphragm, the polarizing Nicol, the cylinder system, a mount for a quarter-wave plate serving as a Senarmont compensator to measure the birefringence ($n_z - n_x$), the analyzing Nicol, and a mirror which reflects the light into a telescope mounted on the adjoining table. The inner cylinder is driven by the drive shaft mounted on a side shelf. It can be operated in both senses of rotation in a speed range of 100–3000 R.P.M. with adequate power in solutions of viscosity as high as 1 poise. Speed is maintained constant to within 0.1 per cent by suitable controls and is measured stroboscopically.

Fredericq and Desreux (58) have also recently described an apparatus with rotating inner cylinder for use at high gradients. Like that of Snellman and Björnstahl (174), it makes use of a horizontal instead of a vertical optical system.

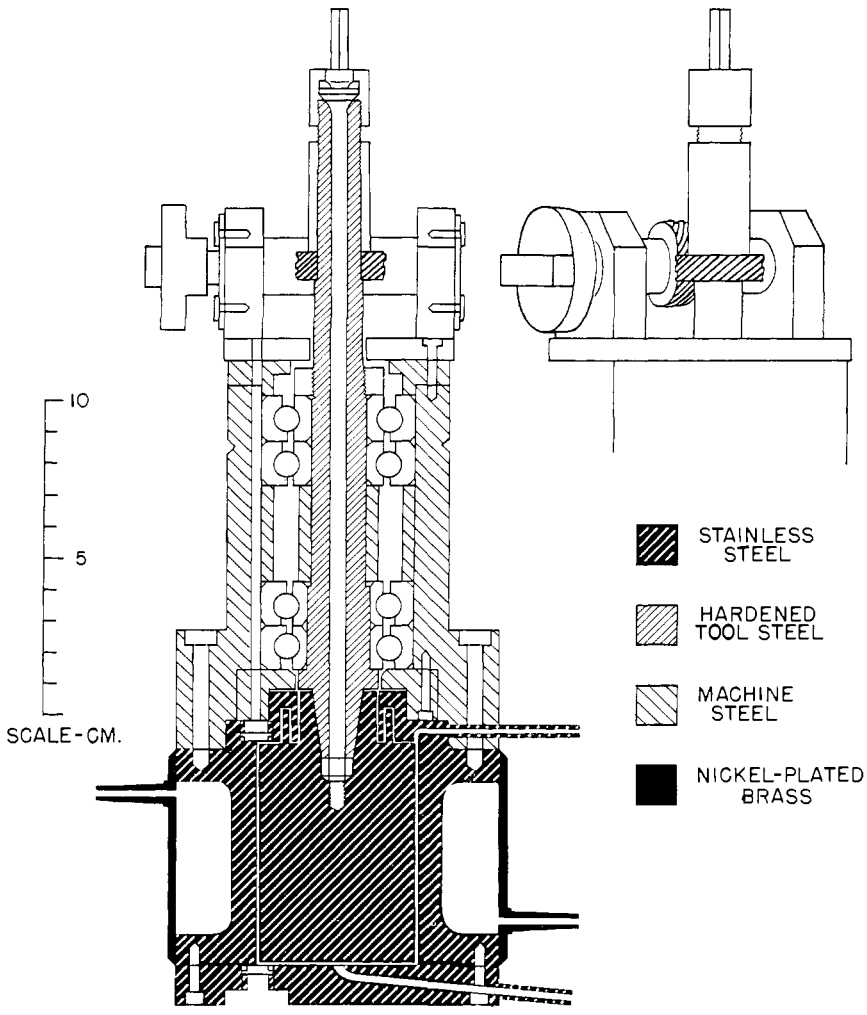


FIG. 9. Edsall high-velocity concentric cylinder apparatus (44)

Other high-speed apparatuses with rotating inner cylinders have been described by Kanamaru and Tanioku (100) and Tsvetkov and Petrova (189).

### B. OUTER CYLINDER ROTATING

According to the theoretical studies of Taylor (181, 183) it should be preferable to keep the inner cylinder fixed and the outer one rotating, since in this situation higher velocity gradients can be attained with relatively large annular

gaps and with the flow remaining laminar. The use of wider gaps makes the optical alignment easier. Also, if the outer cylinder rotates, the apparatus is easily

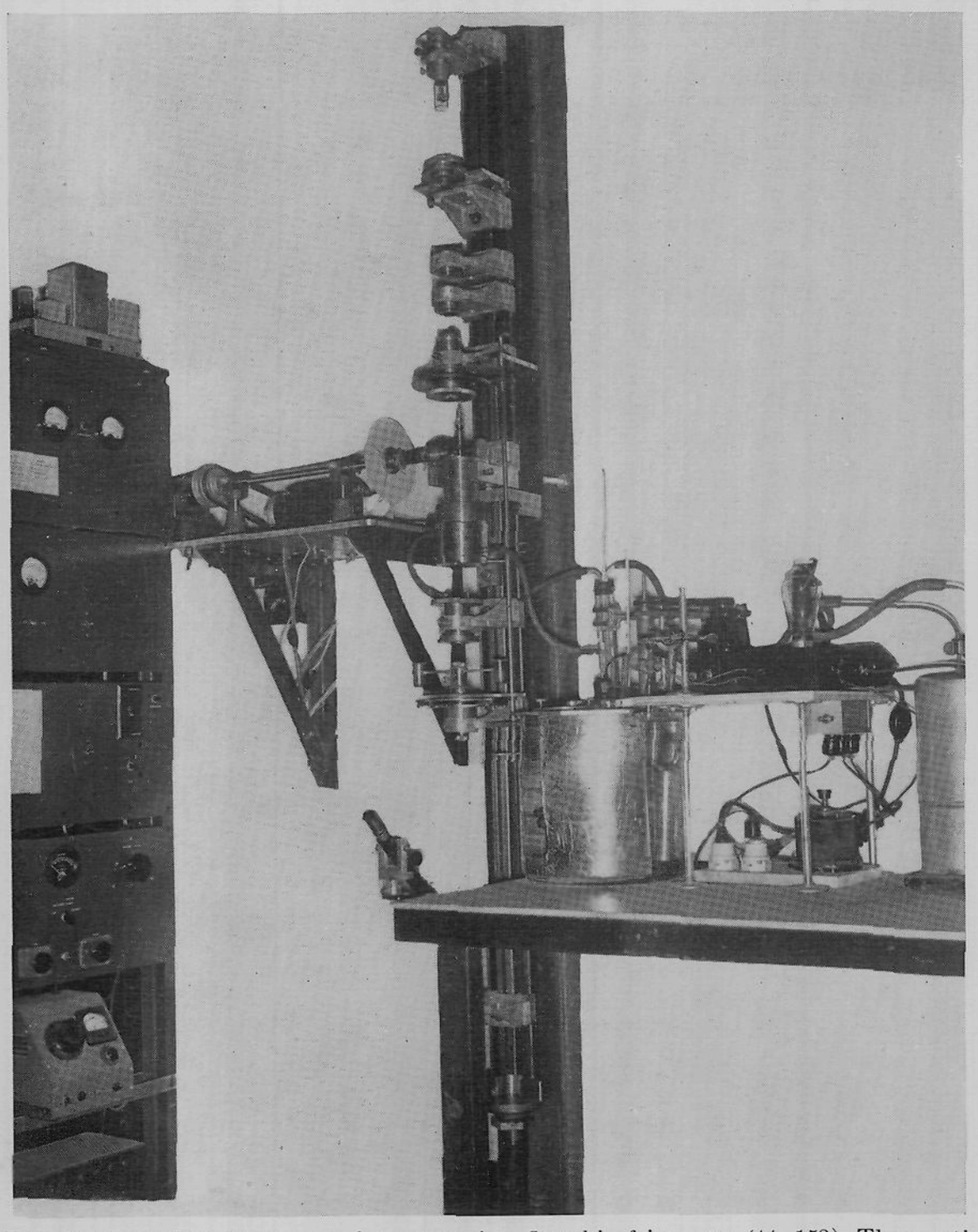

FIG. 10.—Complete apparatus for measuring flow birefringence (44, 153). The vertical optical bench contains the lamp, lens, monochromatic filter, diaphragm, polarizing Nicol, cylinder system, mount for quarter-wave plate, analyzing Nicol, and mirror which reflects light into the telescope on the adjoining table. The motor drive system and thermostat are also shown.

adaptable to viscosity measurements on the same solutions on which the flow birefringence measurements have been made. An apparatus of this design has been described by Gray and Alexander (74) and also by Lawrence, Needham,

and Shen (117). Figure 11 shows the apparatus with rotating outer cylinder used by Edsall, Rich, and Goldstein (46).

### C. OTHER DESIGNS OF APPARATUS

Several investigations of flow birefringence have been carried out with apparatus so designed that the fluid streams through a capillary tube instead of residing in a Couette cylinder apparatus (68, 115).

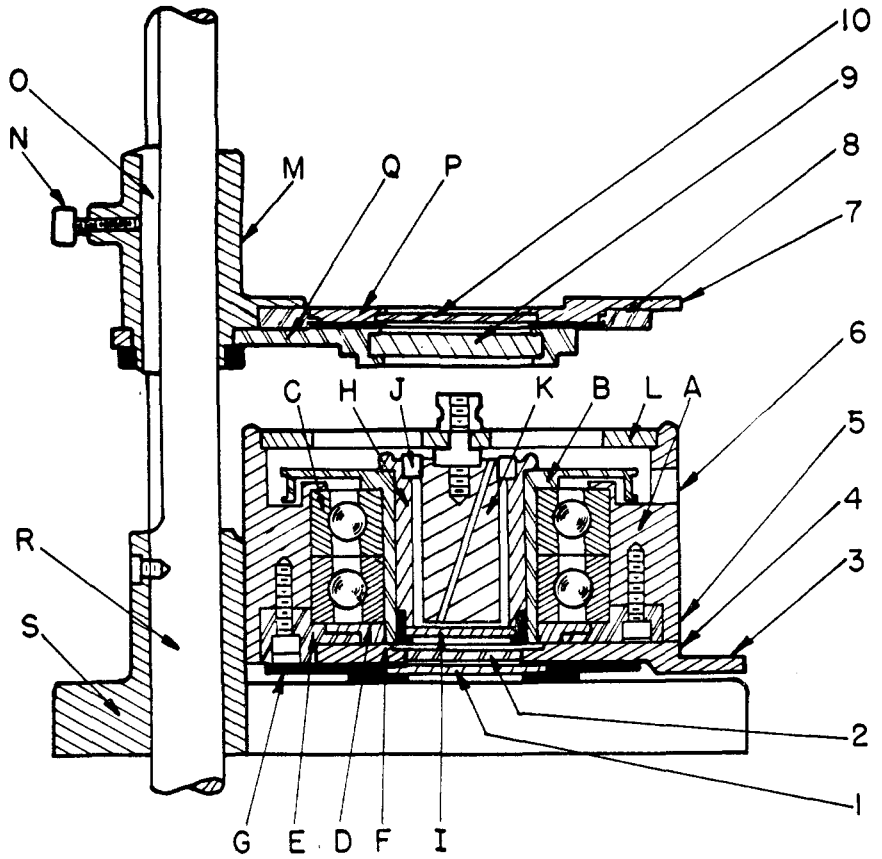


FIG. 11. Apparatus of Edsall, Rich, and Goldstein (46). K is the stationary inner cylinder; the rotating outer cylinder B holds a removable cup H in which the liquid is placed.

Conner and Donnelly (30) have recently constructed an apparatus to measure the relaxation time of flow birefringence in concentrated viscose solutions. This apparatus is similar to that reported earlier by Gonsalves (72). The rate of disappearance of the birefringence was followed photoelectrically after the flow through a cylindrical glass tube was suddenly stopped. The rate of decay of birefringence was compared on an oscilloscope screen with the rate of charging a condenser of known capacity, $C$, through a known resistance, $R$. For the solutions studied the decay with time was found to be essentially exponential, the

expected behavior for a single relaxation process. The charging of the condenser is exponential, with a time constant equal to the product of the capacity times the resistance. The voltage outputs from the photocell and condenser portions of the circuit were properly fed across the vertical and horizontal deflection plates, respectively, of the cathode-ray tube so that an oblique straight line appeared on the screen when the relaxation time was equal to the time constant of $C$ and $R$. The value of $C$ was thus varied until a straight-line trace appeared on the screen. The relaxation time, under these conditions, was equal to $CR$. Time constants from 0.001 to 2 sec. could be determined with a precision of about $\pm 5$ per cent.

### D. PROCEDURE

It can be seen in figure 1 that $\chi$, the angle between the neutral lines of the flowing solution and the stream lines, is also equal to the smaller of the two angles

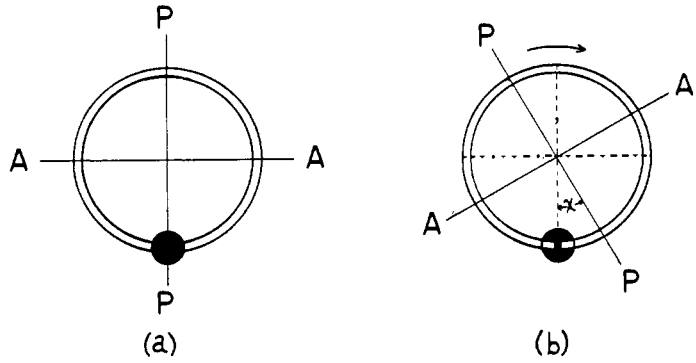


FIG. 12. Appearance of visible portion of annular gap between crossed Nicols for (a) cylinder at rest and (b) outer cylinder rotating. The coupled crossed Nicols are rotated to bring one of the arms of the cross of isocline into the center of the observable field.

between the cross of isocline and $PP$, and is thus experimentally determinable. In the type of cylinder system where a very narrow gap is used one observes only a small portion of it, as shown in figure 12. In such a case one rotates the coupled crossed Nicol prisms until the small visible portion of the cross of isocline is brought to the center of the field. The direction of rotation of the moving cylinder is reversed and the procedure repeated. The difference in the analyzer positions for both senses of rotation is then equal to $2\chi$.

$n_z - n_x$ determines the phase difference of the elliptically polarized light emerging from the cylinder system. This phase difference is usually rather small and may be satisfactorily measured by means of a quarter-wave plate which functions as a Senarmont compensator. If $\Delta$ is the angle of rotation of the analyzer, in degrees, when using the compensator, the birefringence is given by the relation

$$n_z - n_x = \frac{\lambda\Delta}{180S} \tag{1}$$

where $\lambda$ is the wave length of the incident light, *in vacuo*, and $S$ is the path length through the solution. For the apparatus shown in figure 9, this relation becomes (153), for light of wave length 544 m$\mu$:

$$n_z - n_x = 4.31 \times 10^{-8}\Delta \tag{2}$$

*Maintenance of laminar flow*

The apparatus must be used at speeds such that the flow is laminar if the results are to be interpreted quantitatively. The velocity gradient will be practically linear if the flow is laminar but will be more complicated if the flow is turbulent, as shown in figure 13a for the inner cylinder rotating and figure 13b for the outer cylinder rotating (86). Signer and Gross (165) first observed the effects of turbulence, while Sadron (142) studied these effects in detail in pure liquids as an experimental verification of the mathematical treatment of Taylor (181, 183).

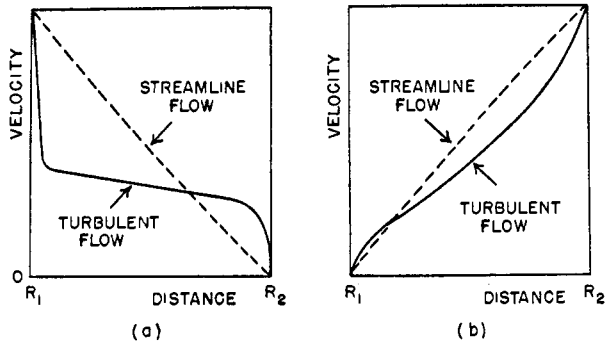


FIG. 13. Velocity distribution across the annular gap for (a) inner cylinder rotating and (b) outer cylinder rotating (after Wattendorf and Taylor, quoted by Jerrard (86)).

These results and their implications for studies of flow birefringence have been adequately discussed by Edsall (38). For the inner cylinder rotating, the maximum speed for which the flow will remain laminar can be increased by making the gap as small as possible. It can also be increased by increasing the solvent viscosity. This is usually accomplished by adding glycerol. This additive also serves the purpose of lowering the intensity of the Brownian motion, thus favoring molecular orientation. The problem of laminar flow in the various types of apparatus in use today has been reviewed by Jerrard (86). For a narrow gap the velocity gradient may be approximated by the expression

$$G = \frac{2\pi N}{60} \cdot \frac{r}{d} \tag{3}$$

where $N$ is the speed of the rotor in R.P.M., $r$ is the mean cylinder radius in centimeters, and $d$ is the gap width in centimeters. From figure 13 it can be seen that in such laminar flow all concentric layers of solution traversed by the beam of light are subject to the same velocity gradient if $d$ is much smaller than $r$. This is not the case in turbulent flow, and therefore the amount of birefringence ob-

served in turbulence will vary across the gap. As a result, one can find either a sharp break in the curve of birefringence against velocity gradient in the transition region between laminar and turbulent flow, or else no break at all in this region, depending on the portion of the gap traversed by the beam of light (143).

The effect of turbulence on the double refraction may be seen in figure 14 for the case where the inner cylinder is rotating (86). This behavior is a consequence of the character of the velocity gradient, as illustrated in figure 13a.

### E. ATTAINMENT OF PRECISION IN MEASUREMENTS OF THE EXTINCTION ANGLE

For studies of polystyrene and other such synthetic polymers, where the effect is much smaller than for many proteins, as already indicated, provision must be made for a more precise measurement of the extinction angle, especially at low velocity gradients. Such investigations have recently been carried out with Sadron's apparatus by Cerf (26), who improved the precision in the measurement of the extinction angle by using a Bravais double plate (23).

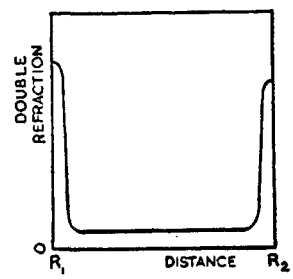


FIG. 14. Distribution of double refraction across annular gap in turbulent flow for the case of rotating inner cylinder (Jerrard (86)).

The Bravais double plate consists of two plates of quartz whose thickness is chosen in such a way that the plate introduces a phase difference of one wave length of yellow light. The neutral lines in both halves of the plate are mutually perpendicular and are parallel to the surface upon which the light is incident. Such a plate, when placed between crossed Nicols, exhibits a rose color if white light is used.

If a birefringent medium is placed between the polarizer and the Bravais double plate one half becomes red, the other blue; the two halves will have the same color only if the plane of the polarizing Nicol coincides with one of the neutral lines of the medium under investigation.

The most favorable condition for using the Bravais double plate in measurements of streaming double refraction is when it is coupled to the crossed Nicols so that the angle between the plane of the polarizer and the neutral lines of the double plate is very small (about 1°) (23). The use of the Bravais double plate to determine the extinction angle is therefore analogous to the use of the half-shadow plate in determining a plane of polarization. Both require high light intensity and are based upon a matching procedure which is independent of the memory of the eye.

When using a Bravais double plate for measurements of flow birefringence white light must be employed; to determine the magnitude of the birefringence, monochromatic light must be used.

In measuring small effects, i.e., for small birefringence, sources of error such as strain birefringence in the windows, reflections of light from the cylinder walls, etc., become very serious. These problems, together with details for mounting the Bravais double plate and the half-shadow plate, and some details of Sadron's apparatus have been discussed elsewhere (23, 26).

The precision obtained with the Bravais double plate may be seen in figure 15, showing the extinction angle curve and corresponding birefringence curve for a sample of polystyrene in cyclohexanone (26). One can see that the extinction angle can be determined with a precision of 1 or 2 degrees even when $\Delta n$ is as small as $10^{-8}$.

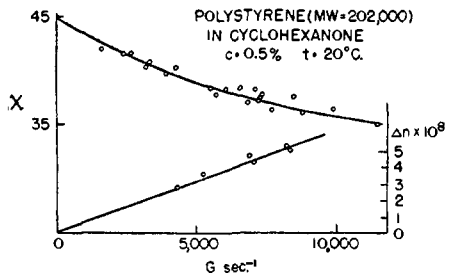


FIG. 15. Extinction angle and birefringence curves for a sample of polystyrene in cyclohexanone (Cerf (26)). It should be noted that $\Delta n$ is extremely small.

## V. Recent Developments for Solutions of Rigid Molecules

### A. THEORY FOR RIGID PARTICLES

#### *1. Introduction*

A suitable theory to account for the experimental observations depends ultimately on the model proposed for the solute particles. The theory for flow birefringence in solutions of macromolecules is intimately associated with that for the viscosity behavior of these same systems. The data for many proteins appear to be compatible with a rigid model (40), which, for purposes of calculation, has been assumed to be an ellipsoid of revolution. The treatment of infinitesimally thin rods by Boeder (12) in 1932 represented a major step in the ultimate solution of the problem. This, together with the work of Sadron (144) in 1937, provided a basis for the development by Peterlin and Stuart (130, 132) of the theory of rigid ellipsoids of revolution. The results of Peterlin and Stuart have been extended by Scheraga, Edsall, and Gadd (155) to the region of high velocity gradient by means of a mechanical computor. Snellman and Björnstahl (174) have considered the effect of absorption on the observed phenomenon. Stuart and Peterlin have also made an attempt to treat chain molecules by an orientation theory (179). However, for many of the synthetic polymers the rigid model

appears to be untenable, and various hydrodynamic and statistical treatments for chain molecules have been carried out by several investigators and will be discussed later. In cases where the particle is rigid, flow birefringence gives information about its size and shape; in cases where it is not rigid, this technique can furnish information about the internal motion of the molecule.

The following discussion of the theory for rigid particles will consider first the case of monodisperse systems and then the effects of polydispersity.

### *2. Orientation theory*

#### (a) Theory for rigid ellipsoids

In the theory of rigid ellipsoids of revolution of Peterlin and Stuart (130, 132) the particle is assumed to be homogeneous and dissolved in a continuous

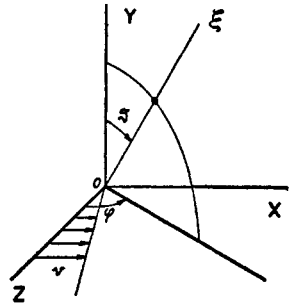


FIG. 16

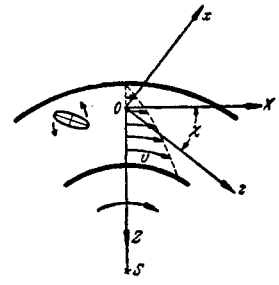


FIG. 17

FIG. 16. Position of the major axis of an ellipsoidal particle in the flowing solution as given by $\vartheta$ and $\varphi$. $\xi$ is the direction of the particle axis, $X$ is the direction of the stream lines, and $Z$ is the direction of the velocity gradient.

FIG. 17. Relative positions of the principal axes of the index of refraction ellipsoid $x, y, z$ and the fixed coördinate system $X, Y, Z$ in the concentric cylinder apparatus (Peterlin and Stuart (133)).

fluid medium which adheres to the particle surface. It is further assumed that the principal axes of the index of refraction ellipsoid of the *particle* are coincident with its geometrical axes and that the solution is dilute enough so that there are no interactions between the solute particles.

(*1*) *Distribution function:* As in the case of rod-like particles (see Section III,B), there exists at any gradient a distribution of orientations of the particle axes due to the combined effects of the hydrodynamic field and the Brownian motion. The state of the system may be characterized by the distribution function $F(\vartheta, \varphi, t)$ for the orientation of the major axes of the particles at any time, $\vartheta$ and $\varphi$ being the usual angles of spherical coördinates, as shown in figure 16. $X$ is the direction of the stream lines at 0; $Z$ is the direction of the velocity gradient between the concentric cylinders; $Y$ is parallel to the cylinder axis and is normal to the streaming plane. An *individual* particle has its major axis in the $\xi$ direction, where $\xi, \eta, \zeta$ is a set of axes fixed in the particle. $\vartheta$ is the angle between $Y$ and $\xi$, while $\varphi$ is the angle between the $YZ$ and $Y\xi$ planes. Figure 17 illustrates the relative position of the $X$, $Y$, $Z$ axes and $x$, $y$, $z$, the principal

axes of the resulting index of refraction ellipsoid of the biaxial birefringent system; the extinction angle, $\chi$, is the angle between the $z$ and $X$ axes, $x$ and $z$ being coplanar with $X$ and $Z$.

The distribution function, $F$, will depend on the relative magnitudes of the velocity gradient, $G$, and the rotary diffusion constant, $\Theta$; the ratio of these quantities, $G/\Theta$, is indicated by the parameter $\alpha$. The distribution function obeys the general diffusion equation

$$\frac{\partial F}{\partial t} = \Theta \Delta F - \text{div}\,(F\omega) \tag{4}$$

analogous to Fick's equation for translational diffusion. $\Delta$ is the Laplacian operator and $\omega$ is the angular velocity of the rotating ellipsoid due to the hydrodynamic forces and, according to Jeffery (85), has the components

$$\omega_\vartheta = \tfrac{1}{2} RG \sin\vartheta \cos\vartheta \sin 2\varphi \tag{5}$$

$$\omega_\varphi = \tfrac{1}{2} G(1 + R \cos 2\varphi) \tag{6}$$

where $R$ depends on the axial ratio, $p = a/b$, of the ellipsoid.

$$R = \frac{p^2 - 1}{p^2 + 1} \tag{7}$$

$R = 1$ for an infinitesimally thin rod, 0 for a sphere, and $-1$ for an infinitesimally flat disc.

If the particles are relatively small (no dimension greater than 10,000 Å.), then within a very short time after initiation of the rotation of the cylinder a steady state is reached in which $\partial F/\partial t = 0$. For the steady state Peterlin (130) integrated the diffusion equation for small $\alpha$, making use of equations 5 and 6, and thus characterized the distribution function $F$ in terms of $\alpha$ by means of slowly converging series of spherical harmonics

$$F = \sum_{j=0}^{\infty} R^j \left[ \frac{1}{2} \sum_{n=0}^{\infty} a_{n0,j} P_{2n} + \sum_{n=1}^{\infty} \sum_{m=1}^{n} (a_{nm,j} \cos 2m\varphi + b_{nm,j} \sin 2m\varphi) P_{2n}^{2m} \right] \tag{8}$$

The $a_{nm,j}$ and $b_{nm,j}$ coefficients are functions of $\alpha$. $P_{2n}$ are spherical functions of $\cos\vartheta$ and $P_{2n}^{2m}$ are their derivatives of order $2m$.

The minimum and maximum values of $F$ occur in the streaming plane ($\vartheta = 90°$). An intermediate value of $F$ is in the direction perpendicular to the streaming plane. The orientation of the directions of minimum and maximum $F$ depends on $\alpha$, being $+45°$ and $-45°$, respectively, with respect to the direction of the stream lines as $\alpha$ approaches zero but shifting to 90° and 0°, respectively, as $\alpha$ increases.

For very large $\alpha$ the particles are essentially subjected only to the hydrodynamic forces, the effect of the Brownian motion being negligible. As a result, one should anticipate the tendency for a rod-like particle to rotate into the plane of flow and also into the direction of the stream lines. If we can for the moment assume that the flow would remain laminar as $\alpha$ approaches infinity, then a solution of infinitesimally thin ellipsoids (i.e., rods) should have all particles

oriented parallel to the stream lines at $\alpha = \infty$. For solutions of ellipsoids of *finite* axial ratio all particles cannot achieve complete orientation in the direction of the stream lines, even at infinite $\alpha$, because of the forces acting on the surface of ellipsoids of finite thickness. The degree of orientation at infinite $\alpha$ would increase with increasing axial ratio. This is illustrated in figure 18, which shows the degree of orientation (in terms of the orientation factor defined in equation 12) as a function of axial ratio at infinite $\alpha$. Of course, in practice, the maximum value of $\alpha$ is limited by the conditions for the maintenance of laminar flow.

(*2*) *Dynamoöptical behavior:* When the partially oriented system interacts with the electric field of the incident linearly polarized light, the resultant index of refraction ellipsoid has two of its principal axes lying in the plane of flow (neutral lines) and the third perpendicular to the plane, as indicated in figure 17. The

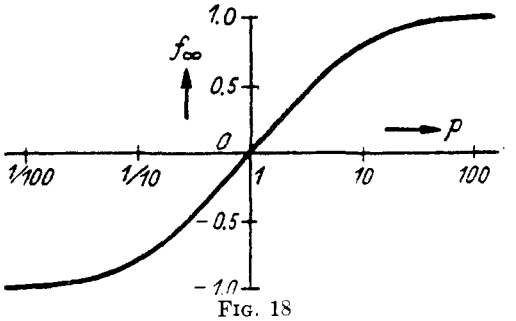


FIG. 18

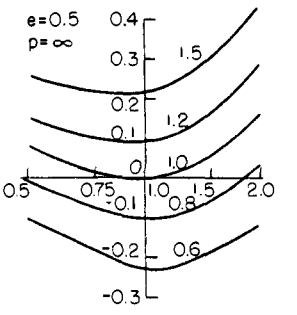


FIG. 19

FIG. 18. Effect of axial ratio $p$ on the orientation factor, $f_\infty$, at infinite velocity gradient (Peterlin and Stuart (132)).

FIG. 19. Behavior of the optical factor for an ellipsoidal particle of infinite axial ratio (Peterlin and Stuart (132)). See text for definition of coördinates.

extinction angle, $\chi$, is the smaller of the two angles between the stream lines and the two principal axes in the streaming plane. It is given by

$$-\tan 2\chi = \frac{\sum_{j=1}^{\infty} R^{j-1} b_{11,j}}{\sum_{j=1}^{\infty} R^{j-1} a_{11,j}} \tag{9}$$

It is seen that $\chi$ is determined by the coefficients $a_{11,j}$ and $b_{11,j}$, that is to say, by the orientation function $F$. It depends only on the size and shape of the solute particles and not on their optical properties. $\chi$ approaches 45° as $\alpha$ approaches zero and tends toward 0° as $\alpha$ increases.

The resultant birefringence, $n_z - n_x$, on the other hand, is given by the formula

$$n_z - n_x = \frac{2\pi\phi}{n_0} (g_1 - g_2) \cdot f \tag{10}$$

where $\phi$ is the volume fraction of the solute particles and $n_0$ is the refractive index of the solvent at rest. It is a product of an orientation factor, $f$, and an optical factor, $g_1 - g_2$, defined in equations 12 and 14, respectively. The magnitude of the birefringence is sometimes expressed in terms of a Maxwell constant defined as

$$M = \frac{1}{n_0 \eta_0} \left( \frac{\Delta n}{G\phi} \right)_{G=0, \phi=0} \tag{11}$$

where $\eta_0$ is the viscosity of the solvent. This is analogous to the definition, for example, of a Kerr constant for electrical birefringence (178).

The orientation factor, $f$, is

$$f = \frac{16\pi R}{5} \left[ \left( \sum_{j=1}^{\infty} R^{j-1} a_{11,j} \right)^2 + \left( \sum_{j=1}^{\infty} R^{j-1} b_{11,j} \right)^2 \right]^{1/2} \tag{12}$$

For $\alpha = 0, f = 0$. As $\alpha$ increases, the orientation factor, $f$, increases, because of the greater degree of orientation of the particles. The increase, which is linear for small values of $\alpha$, becomes less for higher values of $\alpha$. For very high values of $\alpha$, $f$ tends toward a saturation value $f_\infty$, shown in figure 18 as a function of axial ratio. The birefringence, $n_z - n_x$, which is proportional to $f$, according to equation 10, follows the same dependence on $\alpha$, i.e., the same velocity gradient dependence, as $f$.

Thus it is seen that the velocity gradient dependence of both $\chi$ and $n_z - n_x$ is in agreement with the experimental behavior for rigid particles (figures 2 and 3).

$g_1$ and $g_2$ are calculated on the basis of the quasi-static theory for the propagation of light in dispersed media and are functions of $n_1$ and $n_2$, the principal indices of refraction of the particle, $n_0$, the refractive index of the solvent, and $L_1$ and $L_2$, functions expressing the anisotropy of the inner field (132). $L_1$ and $L_2$ are functions of a form factor, $e$, which depends only on the axial ratio of the ellipsoid (132).

$$g_i = \frac{n_i^2 - n_0^2}{4\pi + \frac{n_i^2 - n_0^2}{n_0^2} L_i} \tag{13}$$

where $i = 1$ or 2. This expression for $g_i$ is valid when the quasi-static treatment can be applied, i.e., if the solvent medium can be regarded as a continuum with respect to the solute particles and if the following condition holds:

$$\frac{2\pi a n_0}{\lambda} < 1$$

where $a$ is the radius of a spherical particle. In practice the continuum theory is applicable if the smallest dimension of the particle is greater than 10 Å., and the above condition is satisfied for $a < 500$ Å. In other words, for a non-spherical particle no dimension should be greater than 1000 Å. for visible light.

From equation 13, the expression for the optical factor is

$$g_1 - g_2 = \frac{1}{4\pi} \frac{(n_1^2 - n_2^2) + e\dfrac{(n_1^2 - n_0^2)(n_2^2 - n_0^2)}{n_0^2}}{\left[\dfrac{n_1^2 + 2n_0^2}{3n_0^2} - \dfrac{2e}{3}\dfrac{n_1^2 - n_0^2}{n_0^2}\right]\left[\dfrac{n_2^2 + 2n_0^2}{3n_0^2} + \dfrac{e}{3}\dfrac{n_2^2 - n_0^2}{n_0^2}\right]} \tag{14}$$

The numerator of equation 14 consists of two terms, the first one arising from the intrinsic anisotropy and the second one from the form anisotropy, which depends on the relative indices of refraction of the particle and the solvent, and also on the particle shape. Equation 14 indicates that it is possible to cause a change of sign in $g_1 - g_2$, and thus in $n_z - n_x$, by suitable variation of the index of refraction of the solvent, if $n_1 < n_2$. If $n_1 > n_2$, $n_z - n_x$ is positive for all values of the index of refraction of the solvent. The optical behavior is illustrated in figure 19 for a prolate ellipsoid of infinite axial ratio where the ordinate

$$\frac{2\pi(g_1 - g_2)}{\frac{1}{3}(n_1^2 + 2n_2^2)}$$

is plotted against the abscissa

$$\frac{n_0^2}{\frac{1}{3}(n_1^2 + 2n_2^2)}$$

the various curves corresponding to different values of $n_1^2/n_2^2$. The possibility of an inversion of the sign of $n_z - n_x$ had already appeared in the theoretical work of Sadron (144). The method of determining $n_1$ and $n_2$ will be described later.

It may be mentioned at this point that the optical behavior of the Maxwell effect indicated in equation 14 is similar to that discussed much earlier by Wiener (195) and Weber (194) in terms of the form and intrinsic birefringence in fibers, where the fundamental structures in these biological materials have the possibility of orientation in their natural state. The question of form and intrinsic double refraction has also been considered more recently by Frey-Wyssling (61, 62), Hegetschweiler (78), Snellman (171), Gerendas and Matoltsy (69), and Backus and Scheraga (2).

(*3*) *Absorption:* Snellman and Björnstahl (174) have extended the theory by taking into account the absorption of the particles. They assumed that the principal axes of absorption coincide with the principal indices of refraction. In such a case the directions of the principal indices of refraction of the streaming solution, and therefore the extinction angle and orientation factor, are unaffected by the absorption. There will result, however, a change in the optical factor, $g_1 - g_2$, with possible effects on the magnitude and sign of the birefringence, $n_z - n_x$.

Björnstahl (9) also treated the case where the suspended particles are optically active, but his results are not easily interpretable in terms of the parameters of the streaming solution. It is suggested that an optically active solvent be

used to compensate the optical activity of the suspended particles so that the solution would be optically inactive.

(4) *Experimental determination of rotary diffusion constant:* For small $\alpha$ ($\alpha < 1.5$), the first terms of the solutions of equations 9 and 12 are, according to Peterlin and Stuart (132),

$$\chi = \frac{\pi}{4} - \frac{\alpha}{12} = \frac{\pi}{4} - \frac{G}{12\Theta} \tag{15}$$

and

$$f = \frac{\alpha R}{15} = \frac{GR}{15\Theta} \tag{16}$$

Thus, the initial slope of the extinction angle curve, $d\chi/dG$, is $-1/12\Theta$.

From an experimental curve for the extinction angle it is thus possible to evaluate the rotary diffusion constant $\Theta$, using either equation 15 or the more complete solutions (155) discussed below, depending on the range of available precise experimental data. $\Theta$, in turn, depends on the dimensions of the particle. Gans (66) and Perrin (129) have treated this dependence of $\Theta$ on particle dimensions, the equations of Perrin for the case of a high degree of asymmetry ($p > 5$) being

$$\Theta = \frac{3kT}{32\eta_0 b^3} \quad \text{for oblate ellipsoids} \tag{17}$$

$$\Theta = \frac{3kT}{16\pi\eta_0 a^3}\left(-1 + 2\ln\frac{2a}{b}\right) \quad \text{for prolate ellipsoids} \tag{18}$$

In these equations $a$ and $b$ are the semi-axes of the ellipsoids. $a > b$ for prolate ellipsoids; $b > a$ for oblate ellipsoids. $\eta_0$ is the solvent viscosity, $T$ is the absolute temperature, and $k$ is the Boltzmann constant. The reader is referred to Edsall's review (38) for a more complete discussion of the relationship between rotary diffusion constant and molecular size and shape.

Using equation 17 or 18, the dimensions of the solute particles may be determined from a knowledge of $\Theta$. In order to use equation 18 the axial ratio, $a/b$, must be determined from another type of measurement, usually intrinsic viscosity. The relation between particle dimensions and extinction angle has also been represented graphically (151) and is illustrated in figure 20.

It might be mentioned that small particles having very large rotary diffusion constants ($\Theta_{20,w} \sim 10^5$–$10^6$ sec.$^{-1}$) cannot be easily oriented in a flow birefringence experiment. In such cases the relaxation time, which is related to the rotary diffusion constant, can be determined by the method of dielectric dispersion (128), using electric fields in a wide range of frequencies.

From Perrin's equations and equation 15 it can be seen that the initial slope, $(\tan\alpha)_0$, of the extinction angle curve is

$$-\left(\frac{d\chi}{dG}\right)_{G=0,\phi=0} \equiv (\tan\alpha)_0 = \frac{1}{12\Theta} = \text{constant} \cdot \frac{\eta_0}{T} \tag{19}$$

where the constant depends on the size and shape of the solute particle. Equation 19 has been used for ascertaining whether a particle is rigid or deformable (26), as will be discussed in more detail in Section VI.

(*5*) *Concentration dependence:* The foregoing theory applies only to an infinitely dilute solution of uncharged particles. Experimentally one finds a concentration dependence of the extinction angle and birefringence curves. In order to interpret measurements at finite concentrations, the practice seems to have

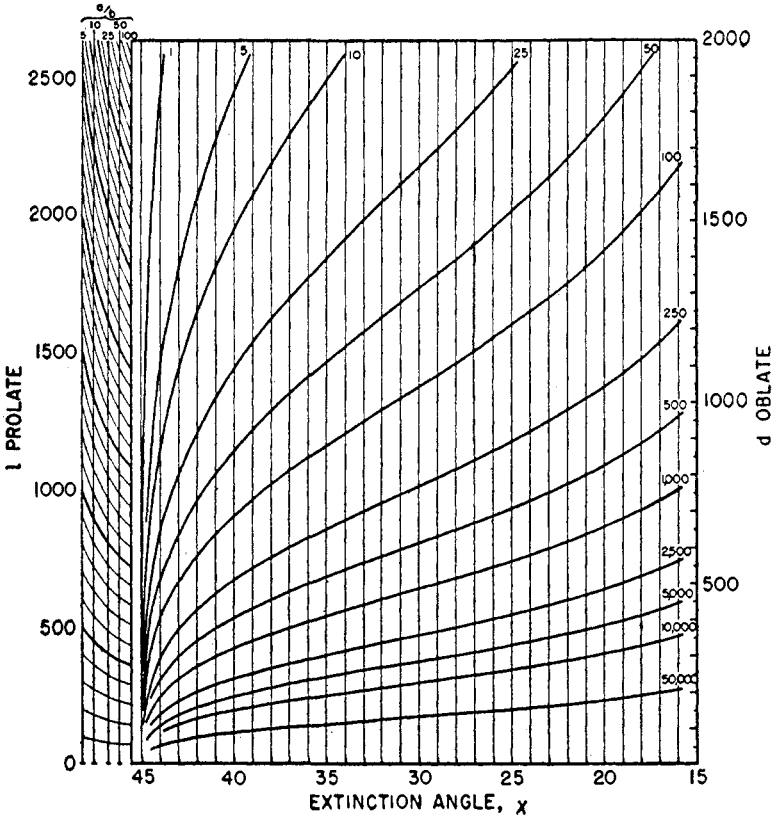


FIG. 20. Relation between extinction angle and molecular dimensions for oblate and prolate ellipsoidal models at various values of $G\eta$ (151).

been to perform the experiment at sufficiently low concentration, where the concentration dependence is negligible. However, in the cases where one cannot reach the concentration-independent range, it is still a question of theoretical and also practical significance of how to perform properly the extrapolations to zero concentration. For example, it has been found empirically for desoxypentosenucleic acid of squid testis that $1/\Theta$ is a linear function of concentration (47, 139). In other cases, such as detergent micelles and bovine fibrinogen, the apparent length has been found to vary linearly with concentration (2, 154). To date, no satisfactory treatment of the concentration dependence of the apparent

rotary diffusion constant has been given. Kanamaru, Tanaka, and Yamamoto have proposed empirical relations for the concentration dependence of the extinction angle and birefringence to account for their experimental data on nitrocellulose solutions. These samples showed a behavior somewhat similar to that of rigid particles (99).

(6) *Experimental determination of the index of refraction of the particles:* If the orientation behavior of the rigid particles has been determined from measurements of the extinction angle at various velocity gradients, the orientation factor, $f$, is then characterized. A simultaneous determination of $n_z - n_x$ then provides enough data to calculate the optical factor, $g_1 - g_2$, from equation 10. To evaluate $g_1$ and $g_2$ separately one must have another relation between $g_1$ and $g_2$, which can be obtained from the refractive increment, $\delta n$, of the solution over that of the solvent. According to Peterlin and Stuart (133),

$$\delta n = \frac{2\pi\phi}{n_0} \frac{g_1 + 2g_2}{3} \tag{20}$$

Thus, measurements of refractive increment in conjunction with flow birefringence data are sufficient for the calculation of $g_1$ and $g_2$ (20). From $g_1$ and $g_2$, $n_1$ and $n_2$ can be calculated from equation 13.

The intrinsic anisotropy of the solute particle is thus determinable. A knowledge of this anisotropy enables one, in principle, to draw conclusions about the polarizability of the molecule in various directions and thus to learn something of the arrangement of the bonds in the molecule. A knowledge of the principal indices of refraction is also useful for the calculation of depolarization factors (83).

Edsall and Foster (41) have used equation 14 for proteins, obtaining the index of refraction of the protein from the Lorentz–Lorenz relation. The Lorentz–Lorenz equation gives the same result as equation 20 if the index of refraction of the particle is near that of the solvent. If the difference in the index of refraction is very high, the use of equation 20 is preferable.

(7) *Simultaneous application of electric and hydrodynamic fields:* Tolstoi (185) has taken into account the effect of a simultaneous application of electric and hydrodynamic fields for a particle having an anisotropic polarizability but no permanent dipole moment wherein the electric field, $E$, is applied in the direction of the velocity gradient. Generalizing the results of Peterlin and Stuart for small $\alpha$, he has found that the extinction angle is not 45° as $\alpha$ approaches zero but deviates from 45° by an amount $\varphi'$, where

$$\tan 2\varphi' = \frac{2 \tan \varphi'}{1 - \tan^2 \varphi'} \sim \frac{E^2}{G} \tag{21}$$

In addition, an expression has been given for the dependence of the birefringence on $E$ and $G$, which may be written in the form:

$$\left.\frac{\partial(\Delta n)}{\partial(E^2)}\right|_{\substack{E=0 \\ G=\text{constant}}} = 0 \tag{22}$$

Tolstoi has applied these results for colloidal solutions to the limiting case of pure liquids wherein equations 21 and 22 were found to hold for a sample of purified transformer oil. By introducing the effect of the electric field into the Raman and Krishnan (137) theory for pure liquids, the following equations have been obtained

$$\frac{2 \tan \varphi'}{1 - \tan \varphi'} \sim \frac{E^2}{G} \tag{23}$$

and

$$\frac{\partial(\Delta n)}{\partial(E^2)}\bigg|_{\substack{E=0 \\ G=\text{constant}}} \neq 0 \tag{24}$$

which are in disagreement with the experiments just mentioned. Tolstoi, therefore, concluded that the experiments were in agreement with an orientation-type theory (Peterlin and Stuart) and in disagreement with the Raman and Krishnan theory. The disagreement of the latter theory with experiments on pure liquids had also been indicated earlier by Sadron (142).

### (*b*) *Solution for high velocity gradients*

It has been pointed out (155) that the approximate equations 15 and 16 often are not sufficient to characterize the solute particles, since the precision of the data is often quite poor at low $\alpha$, being much better at high $\alpha$ values where the approximate equations do not hold. Also, as will be seen later, it is necessary to make measurements over a large range of $\alpha$ values in order to obtain information about polydisperse systems (152, 155). The evaluation of the complete series in equations 9 and 12 is, therefore, required to increase the usefulness and applicability of the theory for rigid particles.

Values for $\chi$ and $f$ given by equations 9 and 12 have been obtained for a wide range of values of the parameter $\alpha$ with the help of a mechanical computor and are available in tabular form (155, 156). The resulting dependence of the extinction angle and orientation factor on $\alpha$, together with the dependence on axial ratio, $p$, is illustrated in figures 21 and 22. These curves are of the same type as those obtained experimentally in monodisperse protein systems which behave like solutions of rigid particles. The effect of polydispersity will be discussed below.

## *3. Polydispersity*

The foregoing discussion applies to a monodisperse solution of particles. If the system is polydisperse, then the observed behavior, as pointed out by Sadron (145, 148), can be quite different from that presented here. From both theoretical and experimental considerations it has been shown that the apparently anomalous experimental observations of extinction angle and birefringence in polydisperse systems can be accounted for by the fact that the longer particles will be oriented more readily at the lower gradients and, as the gradient increases, the shorter particles become oriented. Sadron's results for polydisperse systems have also been reviewed by Edsall (38). Quantitatively, the extinction angle and

birefringence, for a polydisperse system, can be obtained from the following expressions:

$$\tan 2\chi = \frac{\sum_i \delta_i \sin 2\psi_i}{\sum_i \delta_i \cos 2\psi_i} \tag{25}$$

$$(\Delta n)^2 = (\sum_i \delta_i \sin 2\psi_i)^2 + (\sum_i \delta_i \cos 2\psi_i)^2 \tag{26}$$

where the summations are carried out over the $i$ species of particles which, if present alone in the flowing solution, would give the observed values $\psi_i$ and $\delta_i$, of the extinction angle and birefringence, respectively, at the same velocity gradient. Equations 25 and 26 have the same restriction with respect to the absence of particle interactions as the theory for monodisperse systems. Sadron and Mosimann have applied these formulas to experimental studies of binary systems of chain molecules (148), although they are, of course, quite general and

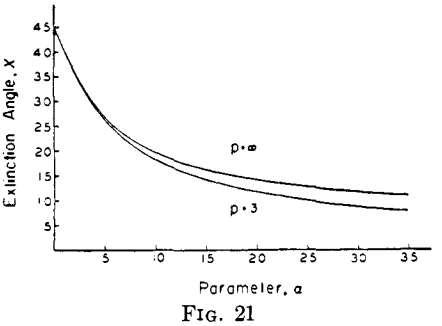


FIG. 21

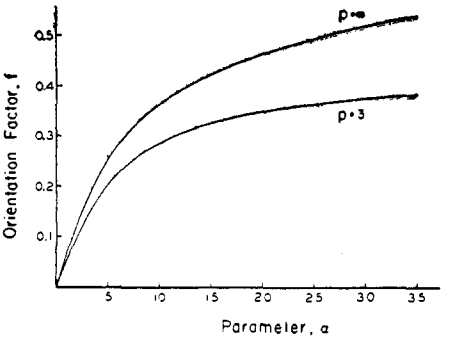


FIG. 22

FIG. 21. Extinction angle as a function of the parameter $\alpha$ together with its dependence on axial ratio (Scheraga, Edsall, and Gadd (155)).

FIG. 22. Orientation factor as a function of the parameter $\alpha$ together with its dependence on axial ratio (Scheraga, Edsall, and Gadd (155)).

hold for any number of components in a system exhibiting induced double refraction, *independent of the nature of the particle or of the origin of the effect.* It should be possible, using these equations, to characterize the distribution of particle sizes from studies of the flow birefringence of polydisperse systems. Figure 6 shows the behavior for a Gaussian distribution of particles all having the same optical factor (152). Calculations have also been carried out for polydisperse systems of rigid rod-like molecules, where the polydispersity was assumed to arise from random degradation of a system of molecules all having the same length initially. For such systems, Goldstein (71) used the distribution function of Montroll and Simha.

Equation 25 has been reported in another useful form by Donnet (35):

$$\frac{1}{\theta} = \frac{\sum \frac{\phi_i}{\theta_i^2}}{\sum \frac{\phi_i}{\theta_i}} \tag{27}$$

where $\Theta$ is the apparent rotary diffusion constant of the polydisperse system at *zero* gradient and $\Theta_i$ is the rotary diffusion constant of the $i^{th}$ species of volume fraction $\phi_i$. In deriving equation 27 from equation 25, it is assumed that $g_1 - g_2$ is the same for all components of the polydisperse system.

### B. EXPERIMENTAL RESULTS FOR RIGID PARTICLES

The use of the flow birefringence technique has become quite widespread in the past decade. Some of the results of these recent investigations for rigid particles are reported herein.

From the foregoing discussion of the theory for rigid particles it is clear that flow birefringence studies of these systems can give a value for the rotary diffusion constant and, thereby, the particle length from equations 17 or 18, and also, in conjunction with measurements of refractive increment, the principal indices of refraction of the particle from equations 10, 13, 15, 16, and 20. Such determinations of size are necessary not only to characterize the individual particles but also to study interaction and aggregation phenomena such as polymerization and micelle formation. In discussing the results of flow birefringence studies of solutions of rigid particles it should be kept in mind that it is not necessary for the particle to be extremely rigid in order to be oriented, i.e., even a somewhat deformable particle will exhibit a phenomenon which is predominantly one of orientation.

Spherical particles can give flow birefringence only if deformable. Rigid spherical particles like southern bean mosaic virus (136), on the other hand, do not exhibit flow birefringence (135).

Many systems have been investigated for which the evidence is either nonexistent or inconclusive for establishing the degree of rigidity of the particles. Nevertheless, the tendency seems to have been to apply the theory for rigid particles to obtain some idea of the linear dimensions and, thereby, an indication of the particle weight. Thus, in the following presentation, the quotation of a particle length from flow birefringence data does not carry the implication that the particle is unequivocally rigid. Also, it should be kept in mind that many applications have been made to molecules which are larger than the required limit for validity of the quasi-static theory of propagation of light in disperse media. In order to facilitate the discussion, the results are divided into two groups: (*A*) studies on those particles which not only appear to be rigid but also have been studied by other methods which give data which may be compared to the flow birefringence results, and (*B*) studies on those particles which have been investigated using the method of flow birefringence as a tool for the determination of molecular parameters and molecular interactions.

#### *1. Comparison with other methods*

In order to test the validity of the orientation theory, it would be desirable to have independent measurements of molecular size. Such measurements might be obtained from direct methods, such as the use of electron microscopy, or from indirect methods involving the use of models for the computation of

molecular size from sedimentation and diffusion constants, dissymmetry of light scattering, etc. So far, few such exhaustive tests of the orientation theory have been made for well-characterized monodisperse systems. However, we may still compare the results of flow birefringence studies with these other methods, keeping in mind the dependence of the results on the model chosen. For rigid particles this model, in all these methods, is usually an ellipsoid of revolution.

A direct comparison between electron microscopy and flow birefringence was made by Donnet (35) on tobacco mosaic virus molecules, which are elongated rod-like particles. However, his preparations were not monodisperse, so that a comparison could not be made directly with the Peterlin and Stuart theory without using Sadron's equations to take account of the polydispersity. The distribution of lengths was obtained from electron microscope observations. From this distribution equations 18 and 27 gave the apparent rotary diffusion constant at zero gradient as 303 sec.$^{-1}$ $\pm$ 20 per cent, while the application of equation 15 to the flow birefringence data at zero gradient gave a value of 280 sec.$^{-1}$ $\pm$ 10 per cent; this is good agreement, considering the experimental errors in both methods. The agreement between the two methods is considered by Donnet as experimental verification of the validity of the limiting law of Peterlin and Stuart and the hypothesis about Brownian motion upon which the orientation theory is based. Possible changes in particle structure in the preparation of specimens for electron microscopy should be kept in mind.

Donnet and coworkers (37) have also made similar comparisons for another system of rod-like particles, vanadium pentoxide sols, with poor agreement between these two methods and also with the method of electrical birefringence. The values of the rotary diffusion constants at 20°C. from these three methods are 8 sec.$^{-1}$ from flow birefringence, 90 sec.$^{-1}$ from electrical birefringence (5), and 3100 sec.$^{-1}$ from electron microscopy. In a subsequent publication Donnet (36) attributed the disagreement to the combined effects of polydispersity and slow flocculation.

Fairly good agreement has been obtained between lengths from frictional ratios and flow birefringence data for hemocyanin of *Helix pomatia* (39). This protein may be split under varying conditions of pH and salt concentration (15, 16). The molecular weights are $8.9 \times 10^6$, $4.3 \times 10^6$, and $1.03 \times 10^6$ for the original molecule and the split species, respectively (15); $f/f_0$ values give lengths of 1130, 820, and 820 Å., respectively, while flow birefringence data give 890, 890, and 960 Å., respectively (174). The splitting thus appears to take place parallel to the long axis of the molecule with little change in length.

Several of the asymmetrical proteins from plasma and other sources have been studied by Edsall and coworkers (41, 42, 43, 44, 53) in the high-velocity apparatus and fit the theory of rigid ellipsoids very well. Human fibrinogen (42) can be cited as an example of a relatively monodisperse preparation, the birefringence data being shown in figure 23, where they are expressed in terms of $\Delta$, defined in equation 1. The birefringence increases linearly at low $G\eta$, according to equations 10 and 16, and then tends towards a saturation value, as is predicted by the theory (figure 22) for the orientation of rigid particles. Many of the measure-

ments in this study were made at high $\alpha$ values, where equations 15 and 16 are not valid. At the time when these studies were made Edsall used a semiempirical method based upon Boeder's results for thin rods (12). The subsequent solutions of equations 9 and 12 (155) account for the behavior of the complete curves without changing the original conclusion that human fibrinogen has dimensions of 700 Å. by 38 Å. More recently, light-scattering data have been reported for bovine fibrinogen (177), giving a length of 850 Å. The question as to whether this represented a difference in length between human and bovine fibrinogen or else an apparent lack of agreement between flow birefringence and light scattering was investigated (83). A length of 670 Å. (figure 24) was obtained for the

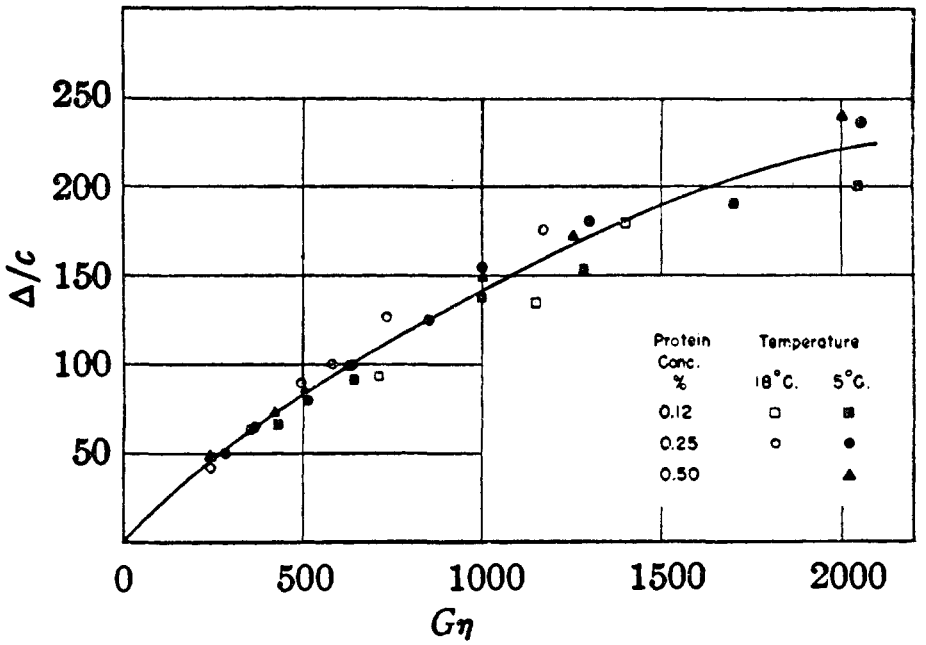


FIG. 23. Birefringence in solutions of human fibrinogen in 54 per cent aqueous glycerol (Edsall, Foster, and Scheinberg (42)).

bovine material, with the indication that the large value from light scattering was due to extremely small traces of impurities which could not affect the flow birefringence measurements. Comparisons between the flow birefringence data for human fibrinogen and the electron microscope results of Hall (76) have been made by Edsall (40).

Several data for other proteins studied by Edsall and coworkers are included in table 1, together with lengths calculated from $f/f_0$ values obtained from sedimentation, diffusion, and viscosity measurements (40). A prolate ellipsoid model was used in the computations.

The values of $n_1 - n_2$ for the proteins listed in table 1 were all found to be negative, indicating that these proteins are most polarizable in a direction per-

pendicular to the major axis. The significance of this finding for the arrangement of the peptide chains in the protein molecules is yet to be ascertained.

*2. Application of the flow birefringence technique to other systems*

Thus far the experimental results have been presented from the point of view of establishing the validity of the orientation theory. Many other investigations

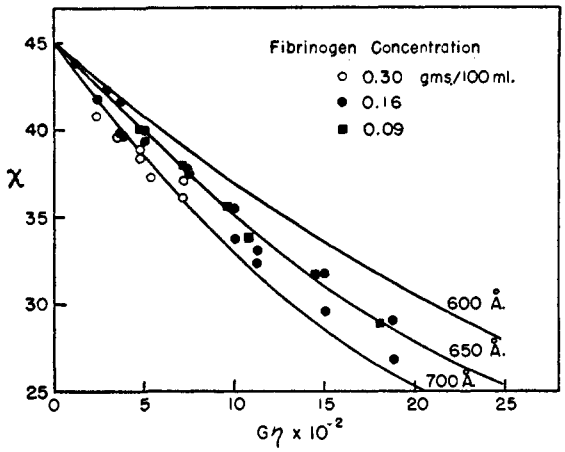


FIG. 24

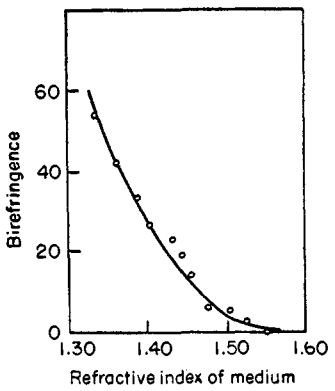


FIG. 25

FIG. 24. Extinction angle data for bovine fibrinogen (83). The curves are theoretical ones for the lengths indicated.

FIG. 25. Birefringence, in arbitrary units, in solutions of tobacco mosaic virus as a function of the refractive index of the medium (Lauffer (115)).

TABLE 1

*Comparison of data from flow birefringence and other methods for several proteins*

| PROTEIN | $a/b$ | $g_1 - g_2$ * | LENGTH FROM FLOW BIREFRINGENCE | LENGTH FROM $f/f_0$ |
|---|---|---|---|---|
| | | | Å. | Å. |
| Human fibrinogen | 18 | 0.00100 | 700 | 700 |
| Human γ-globulin | 5 | 0.00074 | 230 | 235 |
| Zein | 16 | 0.00036 | 350 | 320 |
| Human serum albumin | 4 | 0.00006 | 190 | 150 |

* See Edsall and Foster (41) for solvent composition and index of refraction.

have been carried out using flow birefringence as a tool for the determination of molecular parameters. The results of these investigations are presented herein.

(a) Determination of the principal indices of refraction for several substances

Studies have been carried out on tobacco mosaic virus by Lauffer (115) in an attempt to learn something of the intrinsic anisotropy of the virus particles. Lauffer examined the flow birefringence of several solutions of the material in glycerol–aniline–water mixtures of varying index of refraction, obtaining the

results shown in figure 25. It can be seen that when the solvent has an index of refraction of 1.57, equal to that of the virus particles, the birefringence is zero, indicating that the particles are intrinsically isotropic, even though they possess form anisotropy.

The use of flow birefringence and also refractive increment data for ascertaining the magnitudes of $n_1$ and $n_2$ has been made in the case of silk fibroin (20), bovine fibrinogen (83), and detergent micelles (2).

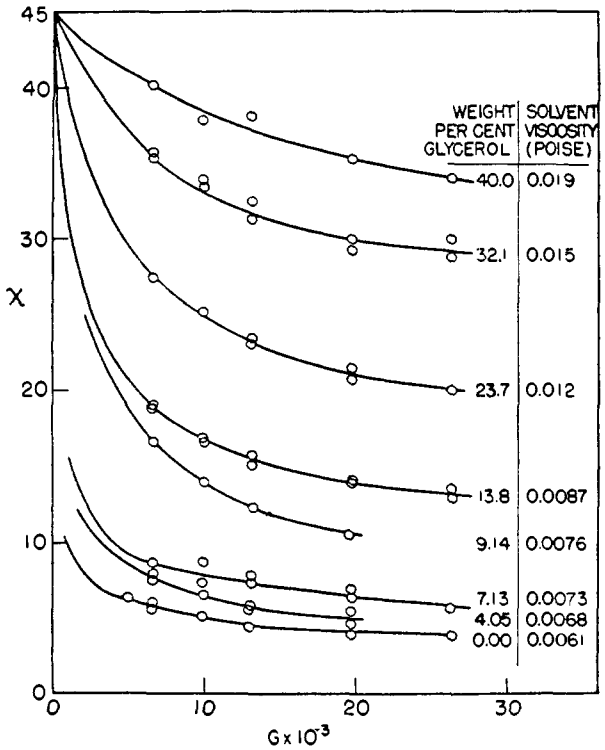


FIG. 26. Effect of glycerol on extinction angle curves for detergent micelles (2)

(b) Soap micelles

Bungenberg de Jong and van den Berg (19) made qualitative observations of flow birefringence in potassium chloride-sodium oleate mixtures. Gallay and Puddington (65) also observed flow birefringence in hydrated calcium stearate suspensions in mineral oil, while Arkin and Singleterry (1) have found that certain soaps of the alkali and alkaline earth metals in benzene solutions give highly viscous liquids showing flow birefringence.

For concentrations of the order of 12 per cent or higher sodium oleate forms large micelles. Snellman has explained his results (170) by assuming that the formation of large micelles does not occur at a definite concentration but over the broad range from 6 to 10 per cent. High temperatures displace the transition range toward higher concentrations.

Thiele has found that the sign of the streaming double refraction in soap solutions depends on the hydrogen-ion concentration, the inversion of the sign being reversible (184). This was interpreted in terms of changing micelle structure as the ratio of charged to uncharged carboxyl groups varied.

In the presence of relatively large amounts of potassium bromide the *n*-alkyltrimethylammonium bromides in which the alkyl group contains at least sixteen carbon atoms also form large asymmetrical micelles above a critical concentration of monomer. The size of the micelle increases with increasing salt concentration and increasing number of carbon atoms in the monomer, the birefringence curves showing the saturation effect characteristic of the orientation of rigid particles (2, 153).

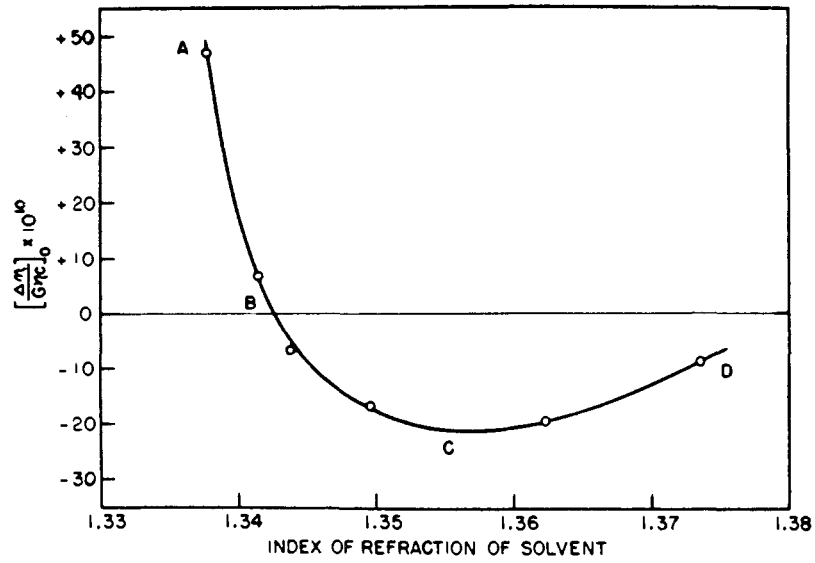


FIG. 27. Effect of glycerol on the birefringence of solutions of detergent micelles (2). The index of refraction of the solvent is a function of the glycerol content.

If glycerol is added to salt solutions of *n*-octadecyltrimethylammonium bromide, the large micelles decrease in size. This is illustrated (2) by the behavior of the extinction angle in figure 26. Figure 27 gives the corresponding birefringence as a function of the index of refraction of the solvent. The phenomenon illustrated in figure 27 arises from the simultaneous decrease of particle size with increasing glycerol concentration and also decreasing form birefringence arising from the increasing index of refraction of the solvent. While glycerol affects the micelle size, it does not change its optical parameters; therefore, the micelle structure is presumably unaltered by this additive.

### (c) γ-Globulin

Molecular aggregation has been studied by flow birefringence. In the case of γ-globulin (41), reported in table 1, there is evidence from ultracentrifuge studies

of the presence of a small amount of an end-to-end dimer in solutions of this protein. The system is therefore polydisperse, and the attempt was made to apply Sadron's equations.

(d) Cold-insoluble globulin

Another system where flow birefringence data indicate the possibility of dimerization is the so-called cold-insoluble globulin of fraction I of human plasma (43).

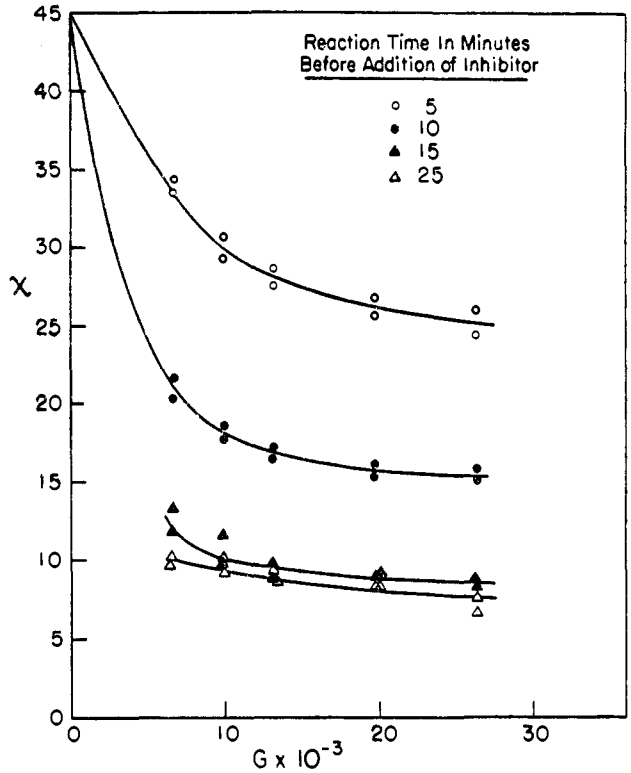


FIG. 28. Extinction angle curves for fibrinogen–thrombin mixtures in which the clotting process was arrested by addition of hexamethylene glycol at various stages of reaction (154).

The results indicated a particle of the same length but twice the cross-section of fibrinogen, suggesting the possibility of side-by-side dimerization of fibrinogen.

(e) Fibrinogen–thrombin clotting systems

By allowing fibrinogen–thrombin mixtures to react in the presence of hexamethylene glycol (56), or by adding this inhibitor after the clotting reaction had proceeded for a short time (154), it has been possible to demonstrate with the streaming birefringence technique the existence of long asymmetrical polymers in solution before the gel point. Figure 28 shows how the extinction angle curves

depart more and more from 45° as the reaction proceeds. Apparently the fibrinogen molecules aggregate end to end, so that prior to gelation the intermediate polymer reaches a length of about 5000 Å.

### (f) Actomyosin

Another interesting application to a problem of molecular aggregation was made by Binkley (7) in a study of actomyosin. From birefringence studies of the native actomyosin complex and also of synthetic mixtures of crystalline myosin and fibrous actin, he suggested that the actomyosin complex consists of three parts of myosin to one part of actin. Binkley's results are in agreement with those of Mommaerts (123, 124) for myosin and the earlier results of von Muralt and Edsall (125) for the actomyosin complex (denoted as myosin in the earlier terminology used by von Muralt and Edsall). An extensive study of the effects of various agents on the flow birefringence properties of myosin solutions has been carried out by Lawrence and coworkers (32, 116, 117, 126).

### (g) Pectin

Saverborn (149) investigated three types of polyuronides—pectic substances, alginic acid, and gum arabic—and concluded that the particles in solution were very elongated. Calculations based on an ellipsoidal model indicated that the pectin particles are made up of single chain molecules. However, Saverborn did not attach too much importance to this conclusion. Results of Snellman and Saverborn (175) on pectin solutions indicated considerable polydispersity. Hydrolysis of pectins led to increased length, indicating that these particles had been arranged in bundles before hydrolysis (175).

For pectin solutions Pilnik (134) found that the magnitude of the birefringence was positive and approached a saturation value with increasing gradient. The positive sign is due to the large form anisotropy, since the particles themselves have a negative intrinsic anisotropy (197). The extinction angles approached a limiting value greater than 0° with increasing gradient. This is similar to the behavior reported earlier by von Muralt and Edsall (125) for myosin and was interpreted in terms of polydispersity.

### (h) Silk fibroin

Signer and Straessle (168) found that the formula for rigid rods appeared to fit the data for silk fibroin, giving a length of 460 Å. Using a value of 79 for the axial ratio from viscosity measurements, they concluded that these results were compatible with other studies of Signer wherein the molecular weight was found to be of an order of magnitude comparable to that of synthetic polyamides, 10,000–20,000, and far below that of cellulose.

### (i) Nucleic acids

Mirsky and Pollister (122) indicated that nucleoproteins from a wide variety of animal cells are markedly elongated, as shown by their viscosity and flow birefringence properties. The elongated nucleoprotein molecule was considered

to be a loose combination of desoxyribosenucleic acid with basic protein (protamine or histone). Reversible changes, caused by variations of salt concentration, in the molecular configuration of nucleoprotein and their effects on flow birefringence were demonstrated by Jeener (84). The effects of various substances on the birefringence of thymonucleate solutions have been discussed by Greenstein (75).

Snellman and Widstrom (176) investigated the streaming birefringence of thymonucleic acid. The birefringence was negative and the extinction angle curve was independent of concentration below 20 mg./100 ml. While the data did not fit a curve for a monodisperse system of rigid particles, a length of 2000 Å. was estimated, corresponding to a molecular weight of 200,000 in agreement with the value from sedimentation found by Pedersen (180), who also studied a sample which was not monodisperse.

Schwander and Cerf (158) studied the streaming birefringence behavior of dilute solutions of thymonucleic acid. The $\eta\Theta$ value is 0.48 at 20°C. The region where the extinction angle is concentration-independent (10–20 mg./100 ml., the solvent being a solution of sodium chloride, 10 g./100 ml.) was attained. This value of $\eta\Theta$ corresponds to a length of 8000 Å. and a higher molecular weight (800,000) than for previously reported preparations. Other measurements (159), made in solutions containing glycerol (figure 29), indicate that the particle behaves as a rigid one. This conclusion is confirmed by recent experiments of Schwander and Signer (160) on the dependence of the extinction angle on the salt concentration. These results will be discussed in Section VI.

Recent studies have been made by Rich (47, 139), Goldstein (70), and Creeth *et al.* (31) on desoxyribosenucleic acids, including salt effects.

### (j) Poliomyelitis virus

A macromolecular substance from rat feces was investigated by Gard, Snellman, and Tyren (67) for possible identification as poliomyelitis virus. While this filamentous macromolecular material was found to be a nucleoprotein, it was not possible to demonstrate that it was the virus. One of the components of this material exhibited measurable streaming double refraction at concentrations as low as $10^{-7}$ g. per milliliter. In the concentration range $10^{-4}$ to $10^{-6}$ g. per milliliter the particle length was uniform and about 6000 Å. At the lowest measurable concentration the particle appeared shorter (4500 Å.); this was interpreted in terms of a dissociation phenomenon in the very dilute solutions.

### (k) Casein

Nitschmann and Guggisberg (127) investigated the streaming birefringence properties of sodium caseinate solutions together with salt effects. Changes in state of aggregation were produced by salt, the data being interpreted on the basis of a rod model, giving a length of 1880 Å. for sodium caseinate in 1.6 $N$ sodium sulfate solutions. Particles of different lengths were obtained at other salt concentrations.

(l) Chondroitinsulfuric acid and hyaluronic acid

Blix and Snellman (11) found that these substances in their native states have a long chain structure and a very high molecular weight. For native chondroitinsulfate the mean particle length was estimated to be about 4700 Å., corresponding to a molecular weight of the order of 260,000. Hyaluronate of different origin differed with regard to particle length, which was found to vary between 4800 Å. and 10,000 Å. The corresponding molecular weights were estimated to be of the order of 200,000 to 500,000. Dilute alkali produced depoly-

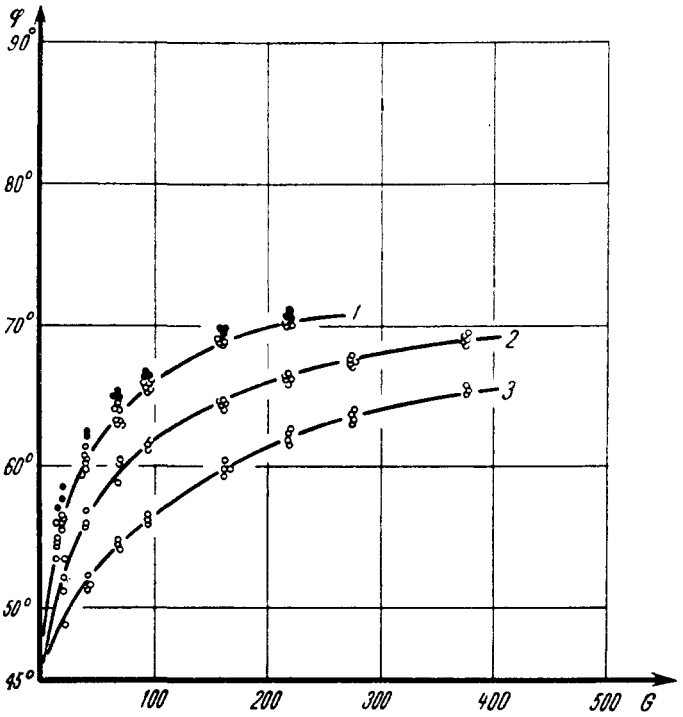


FIG. 29. Extinction angle, expressed as $\varphi$ (where $\varphi = 90 - \chi$), for thymonucleic acid (159). Each curve corresponds to a different glycerol concentration. For a given solvent composition, the data for several concentrations of thymonucleic acid fall on the same curve.

merization, as evidenced by a decrease in viscosity and a disappearance of the double refraction of flow in chondroitinsulfate. In the case of the hyaluronate solutions the birefringence did not completely disappear, the particle length of the alkali-degraded product being estimated at about 1300 Å., corresponding to a molecular weight of about 50,000. From sedimentation and diffusion constants the product appeared to be rather polydisperse with an estimated molecular weight of 37,000.

(m) Amylose

Peterlin and Samec (131) tried to orient the amylose and amylopectin components of starch without success, and concluded that both fractions appeared

to be very nearly spherical. Foster and Lepow (54), on the other hand, in studies on amylose solutions prepared from several different sources of starch, found that the amylose component is readily orientable. However, they concluded that the observed birefringence effects in the case of the amyloses are predominantly due to the elongation of coiled molecules rather than to simple orientation.

### (n) Gelatin

Scatchard, Oncley, Williams, and Brown (150) have reported some flow birefringence results obtained by Edsall and Foster for gelatin solutions, indicating few, if any, molecules longer than 1000 Å. in thiocyanate solutions but appreciable aggregation even at temperatures at which the gel rigidity is zero in 0.15 molal sodium chloride. These results are consistent with sedimentation and viscosity measurements carried out by these same workers.

Joly (87) applied the flow birefringence technique to a study of the mechanism of the gelation of gelatin and its interaction with other substances. From the fact that the extinction angle decreased from 45° at given $G$ as time increased he concluded that the molecules formed elongated fibers which increased in length as gelation proceeded. After a time, the phenomenon reversed itself, i.e., the extinction angle began to increase. This was interpreted as being due to the introduction of cross-linkages to set up the gel.

### (o) Protein denaturation

Flow birefringence measurements have also been applied to the investigation of particle sizes in protein denaturation. Edsall and Mehl (45) found that many denaturing agents cause the birefringence of myosin solutions to disappear, suggesting the breakdown of these asymmetrical molecules into smaller, more symmetrical units.

Joly and Barbu (3, 89, 90, 91) used this technique to investigate the thermal denaturation of serum albumin. In a similar type of investigation, Fredericq (57), and also Foster and Samsa (55), studied the denaturation of ovalbumin. In the case of ovalbumin, for example, denaturation was carried out by Foster and Samsa under such conditions that no precipitation, gelation, or appreciable turbidity occurred. Under certain conditions results were obtained which were compatible with the orientation theory for monodisperse rigid particles of length about 600 Å. In most cases, however, the systems were polydisperse, with aggregation playing an important part in the over-all denaturation process.

### (p) Tobacco mosaic virus

In studying the effects of various agents on this protein, Joly (88) first confirmed the earlier work of Robinson (140) and Lauffer (115) on the native material. He subsequently found that either prolonged freezing or gradients as high as 50,000 $sec.^{-1}$ caused at pH 4.5 a splitting of the virus particles which was partially reversible. The interaction of this protein with sodium dodecyl sulfate was also considered. Interaction studies on other protein complexes have also been carried out by Joly and Rybak (92), Lessiau, Cerf, and Macheboeuf (118), and Foster (52).

### (q) Coagulation phenomena in various substances

Frey-Wyssling and Weber (64) used measurements of double refraction to follow the changes in size and shape during growth of particles from supersaturated solutions of carnauba wax and Congo red in laminar flow. Similar studies by Berger (6, 48) on nickel hydroxide sols showed agreement between particle sizes determined from viscosity and streaming double refraction on the one hand and from x-ray measurements on the other hand. Sato (148a) investigated the effects of heat treatment of vanadium pentoxide sols on the viscosity and relaxation time of streaming double refraction.

### (r) Shellac

Basu (4) studied the flow birefringence properties of shellac solutions in several solvents. In all solutions the sign of the birefringence was negative. For shellac concentrations below 30 per cent the extinction angle was 45° at all gradients and the birefringence increased linearly with gradient. On the basis of the birefringence, viscosity, and diffusion measurements it was concluded that the shellac molecules are comparatively small and not flexible. Calculations based on a prolate ellipsoid model indicated major and minor axes of 68 Å. and 6.6 Å., respectively, for dewaxed shellac.

## VI. Recent Developments for Solutions of Chain Molecules

### A. Theory for deformable particles, in particular chain molecules

#### *1. Introduction*

The theory and results of flow birefringence for solutions of rigid particles having been presented, a consideration of the Maxwell effect in solutions containing particles which are deformable by the hydrodynamic field is now in order.

Much of the early experimental work on solutions of chain molecules was carried out by Signer and coworkers (162, 165). The experimental behavior of the extinction angle and birefringence has already been indicated in figures 4 and 5 for some of the more recent data of Tsvetkov and Frisman (186).

Early preliminary attempts were made by Kuhn (106) and Haller (77) to develop a theory for deformable molecules, with the greatest progress in this connection coming in the past decade. For chain molecules, however, the problem is much more difficult than in the case of rigid particles, whose dimensions are usually large compared with the dimensions of the molecules of the solvent. For chain molecules, where one has to consider the frictional forces on chain segments which are of dimensions of the order of the solvent molecules, difficulties arise in the application of the hydrodynamic equations of continuous media. Also, here a statistical problem must be solved and, in contradistinction to the problem of viscosity where the particle can be assumed to be undeformed in the hydrodynamic field, one must know the statistics of the deformed particle. As a result of these difficulties, resort has been had to the choice of simplified and idealized models. This procedure immediately imparts a limiting character to

the theories, with the result that the comparison with experimental observations has to be carried out very critically.

There will obviously be a great advantage in comparing the results of streaming birefringence measurements with those of other techniques involving the mechanical and optical properties of the dissolved molecules, in particular, those which involve a deformation of the particle. Several investigators have compared the velocity gradient dependence of the viscosity with the flow birefringence behavior of chain molecules (17, 187). Recently, relationships have been indicated (28) between flow birefringence measurements and results obtained by the newly developed technique of ultrasonic shear waves (119). However, each of these techniques involves its own problems, which are far from being settled. We shall restrict ourselves to the problem of flow birefringence, even if the discussion must therefore be incomplete at times.

Various models have been used for the theory of flow birefringence; the question of their validity has given rise to many discussions for the more extensively investigated problem of viscosity.

The first extensive attempts at the formulation of a theory for chain molecules were those of Hermans (79, 80) and also Kuhn and Kuhn (110, 111), who considered the case of a free-draining polymer, using a dumbbell model. Kuhn and Kuhn (112, 113) further introduced the concept of an internal viscosity for the particle and also a limitation on free draining (114), developing the theory for the dumbbell model in great detail and comparing the theoretical behavior of the extinction angle and the magnitude of the birefringence with the experimental results of Signer, Wissler, and others (110).

Another theory based on a free-draining polymer is Kramers' consideration of the necklace model (105), which takes into account the effect of intermediate chain elements.

A different point of view has been taken by Cerf (21, 25), who developed a theory of flow birefringence for the case of small velocity gradients, using as a model an elastic sphere, an earlier qualitative treatment of the elastic sphere having been given by Haller (77). This model is similar to the one used by Sadron (146) for the viscosity problem at high molecular weight. It also appears as a limiting case for high molecular weights in the viscosity theories based upon partial permeation as developed by Brinkman (14), Debye and Bueche (33), Kirkwood and Riseman (104), and Peterlin (130a). According to Flory (49, 50, 51), this limiting model of an effective hydrodynamic sphere should be valid even at low molecular weight ($\sim$50,000). The theory of the elastic sphere has been compared to the experimental results (magnitude of the birefringence) of Signer for polystyrene and those obtained more recently by Tsvetkov and Frisman for polyisobutylene (26).

As yet there is not sufficiently extensive experimental evidence available to decide on the realm of validity of the theories mentioned above. It has been shown that this question may be approached by making measurements of the extinction angle at low velocity gradients for different values of the viscosity of the solvent (22, 24). Such experiments would also yield information about the elasticity and

internal viscosity of flexible chain molecules; for less flexible chain molecules, where none of these theories is applicable, these experiments should give information about the degree of flexibility.

The following presentation will consider in more detail the various theories mentioned above and will include a comparison with experimental results.

### *2. Theory for an elastic dumbbell*

The theory for a dumbbell model has been developed independently but along similar lines by Kuhn and Kuhn (110–114) on the one hand and by Hermans (79, 80) on the other. This theory is based on earlier considerations of the statistical coil by Kuhn (107), wherein the molecule is regarded as more or less curled up because of the possibility of varying degrees of free rotation of successive links of the chain. Kuhn divided the coil into sections or statistical elements, the number of chain elements in the statistical element being chosen in such a way that the orientation of each statistical element could be considered as not being influenced by the other elements.

The statistical coil may be characterized in terms of the end-points, $P$ and $Q$, of the chain molecule. The mean square value of this end-to-end distance is denoted by $\overline{h_0^2}$. Using this statistical coil model and fixing end-point $P$ of the molecule at the origin of a coördinate system, Kuhn, in his earlier paper (107), obtained an expression for the distribution of $Q$ end-points around the origin in the absence of any external field.

When such a coil is placed in a hydrodynamic field it is subjected to shearing forces which cause a rotation of the whole molecule as well as a periodic extension and compression of the coil. Kuhn and Kuhn, as well as Hermans, expressed the hydrodynamic interaction between the coil and surrounding liquid in terms of the distance between $P$ and $Q$.

The frictional forces exerted upon the molecule by the liquid were calculated (110), using the assumption that one-fourth of the total chain is localized at each of the end-points $P$ and $Q$ and that the hydrodynamic effects of the intermediate chain parts can be neglected. The force acting on the end point $Q$, for example, is

$$f = V\eta_0\lambda\frac{L}{4}$$

where $V$ is the velocity of the $Q$ end-point relative to the surrounding liquid and $L$ is the maximum length of the chain without distortion of bond angles or interatomic distances (hydrodynamic length of the chain molecule); $\lambda$ is a frictional factor for which Kuhn and Kuhn have given alternative expressions depending on whether the chain is (110) or is not (114) free draining. For the case of free draining (i.e., the surrounding liquid passes freely through the coil) the frictional force $f$ was calculated as the resistance exerted on a sphere, with the result that $\lambda$ is a purely numerical coefficient. For partial draining, on the other hand, the frictional force was determined by means of macroscopic models (105a); in this case $\lambda$ appears to be a function of the length, $A$, and the thickness, $d$, of the statistical chain element, the degree of polymerization, $Z$ (i.e., the number of monomer

units in the chain), and the hydrodynamic length, $b$, of the monomer unit, where $b = L/Z$. For the related viscosity problem the free-draining case leads to Staudinger's law, while the partial-draining case leads to a molecular-weight dependence of the viscosity which is rather similar to that obtained by various investigators by means of more refined models (14, 33, 104). Kuhn and Kuhn have indicated that the free-draining approximation should be valid for rather low molecular weights, while an increasing degree of immobilization of the solvent should appear for increasing molecular weight.

The localization of the hydrodynamic forces at the ends of the molecule reduces this treatment to that of a dumbbell model, no matter what value is assigned to the factor $\lambda$. The end-points, however, are not at a fixed distance but are bound by a restoring force, so that the Kuhn–Hermans model can be defined as an elastic dumbbell. For this model these investigators calculated the disturbed distribution function of the end-points in the hydrodynamic field. For low velocity gradients, this calculation can be carried out by considering the molecules as an array of various shapes, each of which is rigid. It should be pointed out that Kuhn and Kuhn have considered the distribution problem in only two dimensions, whereas Hermans' treatment is a three-dimensional one.

If the distribution of end-points is determined, the optical properties of the medium may be calculated on the basis of earlier results of Kuhn and Grün (108) on the optical anisotropy of a chain molecule as a function of the end-to-end distance. Since there is no significant difference aside from numerical coefficients between the Kuhn and Kuhn results and those of Hermans, only the former will be reported here. Hermans (81) has made a comparison of the two sets of results.

($a$) The extinction angle, according to Kuhn and Kuhn, is given by the expression

$$\left(\frac{\tan 2\Omega}{G\eta_0}\right)_{c=0} = \frac{\lambda}{16}\frac{1}{kT}L\overline{h_0^2} = \frac{\lambda}{24}\frac{1}{kT}\frac{A^2b}{s}Z^2 \tag{28}$$

where $s$ is the number of monomeric units in a statistical chain element. $\Omega = (\pi/4) - \chi$. The other symbols have already been defined. From equation 28 it follows that the initial slope of the extinction angle curve may be written as

$$(\tan \alpha)_0 = \text{constant} \cdot \frac{\eta_0}{T} \tag{29}$$

where the constant depends on the parameters defined above but not on $\eta_0$ or $T$. Equation 29 has the same general form as equation 19 for rigid particles.

($i$) For the case of free draining $\lambda$ may be approximated by $3\pi/2$. Since $\lambda$ is thus independent of molecular weight, equation 28 may be written as:

$$\frac{1}{\eta_0}(\tan \alpha)_0 = K_\Omega \cdot Z^2 \tag{30}$$

where the factor

$$K_\Omega = \frac{\pi}{32} \cdot \frac{1}{kT}\frac{A^2b}{s} \tag{31}$$

is a constant within a homologous polymer series. Thus

$$\frac{1}{\eta_0}(\tan \alpha)_0$$

is proportional to the square of the degree of polymerization.

(*ii*) For the case of partial draining (105a)

$$1/\lambda = -0.05 + 0.12 \log_{10}(A/d) + 0.037\sqrt{Z/s} = \alpha + \beta\sqrt{Z}$$

where the coefficients $\alpha$ and $\beta$ do not depend on $Z$. Thus, for partial draining, $(\tan \alpha)_0$ increases more slowly with $Z$ than is indicated by equation 30.

(*b*) The corresponding formula for the magnitude of the birefringence is

$$\nu = \left(\frac{\Delta n}{G\eta_0 c}\right)_{c=0;G=0} = \frac{(n_0^2+2)^2}{6n_0}\frac{\pi\lambda}{30}\frac{N}{1000}\frac{1}{kT}\overline{bh_0^2}(\alpha_1 - \alpha_2)$$

$$= \frac{(n_0^2+2)^2}{6n_0}\frac{\pi\lambda}{45}\frac{N}{1000}\frac{1}{kT}\frac{A^2b}{s}Z(\alpha_1 - \alpha_2) \qquad (32)$$

where $c$ is the concentration in moles per liter, $n_0$ is the refractive index of the solvent, $N$ is Avogadro's number, and $\alpha_1$ and $\alpha_2$ are the principal polarizabilities of the statistical chain element. The dependence of $\alpha_1$ and $\alpha_2$ on $n_0$ involves the calculation of the internal field. This problem has yet to be investigated.

(*i*) For the case of free draining equation 32 may be written in the form

$$\nu = K_\nu \cdot Z \qquad (33)$$

where the factor $K_\nu$ is a constant within a homologous polymer series. In such a series $\nu$ is therefore proportional to the degree of polymerization. Equations 28 and 32 hold for a monodisperse system at infinite dilution.

As already indicated, the dumbbell model for the case of free draining leads to Staudinger's law, i.e., proportionality of the intrinsic viscosity to the degree of polymerization. Therefore, according to equation 33,

$$\frac{\nu}{[\eta]} = \text{constant} \qquad (34)$$

for several molecular-weight fractions of a given polymer.

(*ii*) For the case of partial draining the frictional coefficient $\lambda$ in equation 32 has the form given above. Thus $\nu$ increases more slowly with $Z$ than is indicated by equation 33.

For the case of free draining as well as for the case of partial draining $\nu$ and $[\eta]$ are both proportional to the frictional coefficient $\lambda$. This quantity therefore drops out in the quotient, and equation 34 holds for *any degree of permeation.*

The Kuhn–Hermans theory represents the first extensive approach to the problem of flow birefringence in solutions of chain molecules. A comparison with experiments will be made later. From a theoretical point of view there are some difficulties involved in the applicability of this theory to chain molecules; these have been discussed by Hermans (81) and also by Snellman (173). They are (*1*) the definition of the state of the molecule by the relative position of the end-

points and the localization of frictional forces at these end-points (dumbbell model), and (*2*) the question of the internal field in the optical problem.

*Introduction of an internal viscosity (112, 113):* The time required for a chain molecule to go from one configuration to a different one depends not only on the viscosity of the surrounding liquid but also on the internal viscosity of the chain, which is itself strongly influenced by the degree of free rotation around the valence bonds. Kuhn and Kuhn have introduced the effect of internal viscosity into their earlier treatment and obtained the following results.

(*a*) For low velocity gradients the distribution of end-points around the origin does not depend upon the internal viscosity of the particle. In order to calculate

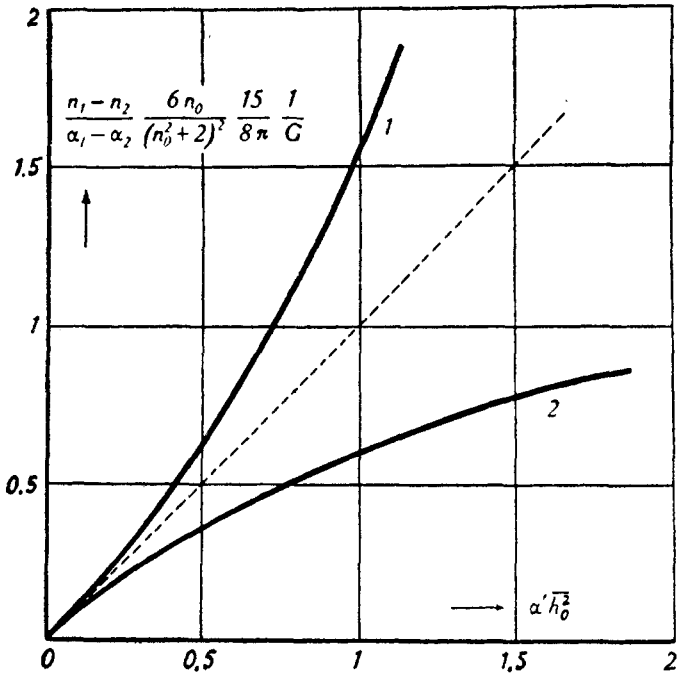


FIG. 30. Dependence of the birefringence on velocity gradient (Kuhn and Kuhn (112)). Curve 1, small internal viscosity; curve 2, large internal viscosity.

the initial slope of the birefringence curve the molecules may be considered as an array of various shapes each of which is rigid; that is, the initial birefringence has the character of an orientation effect. The initial slope of the birefringence curve has the same value for molecules of both large and small internal viscosity, as shown in figure 30. If the velocity gradients are high, on the other hand, the birefringence increases more rapidly than linearly with $G$ for molecules of small internal viscosity and more slowly than linearly for molecules of large internal viscosity, showing, in the latter case, a behavior in some way analogous to that of a rigid particle. Since the initial birefringence, as well as the intrinsic viscosity at zero gradient, is independent of the internal viscosity, equation 34 is valid for particles of arbitrary internal viscosity.

(*b*) The initial slope of the extinction angle curve, which depends on terms of higher order in $G$, arising from a development of the distribution function for the end-points, is a function of the ratio of internal viscosity to the viscosity of the solvent. For large values of this ratio the initial slope, $(\tan \alpha)_0$, is three times the size for the case where this ratio is small. Equation 35 gives the value of tan $2\Omega$ for high internal viscosity.

$$\left(\frac{\tan 2\Omega}{G\eta_0}\right)_{c=0} = \frac{3\lambda}{16}\frac{1}{kT}L\bar{h}_0^2 = \frac{\lambda}{8}\frac{1}{kT}\frac{A^2b}{s}Z^2 \tag{35}$$

In both limiting cases—small and large internal viscosities—the simultaneous measurement of the extinction angle and intrinsic viscosity would provide a method for determining molecular weight. The resulting formulas are, respectively,

$$Z = \frac{2RT}{1000}\frac{(\tan \alpha)_0}{\eta_0}\frac{1}{[\eta]} \qquad \text{for small internal viscosity} \tag{36}$$

and

$$Z = \frac{2RT}{3000}\frac{(\tan \alpha)_0}{\eta_0}\frac{1}{[\eta]} \qquad \text{for large internal viscosity} \tag{37}$$

Equations 36 and 37, like equation 34, are independent of the degree of permeation of the chain.

*Extension of the Kuhn-Hermans theory:* Peterlin (130a) has extended this theory by assuming that each statistical element can be replaced by a sphere for purposes of calculating the hydrodynamic resistance. A chain containing $N$ statistical elements is, therefore, equivalent to a set of $N - 1$ dumbbells, the orientation of each dumbbell not being influenced by the others in the absence of a hydrodynamic field. In the case of free draining this model must therefore lead to exactly the same result as the Kuhn-Hermans theory. However, Peterlin has taken into account the hydrodynamic interaction between the different statistical elements. The molecular-weight dependence of the intrinsic viscosity obtained by this simple model for the case of partial draining is quite similar to that obtained by Debye and Bueche (33) and by Kirkwood and Riseman (104). The equations obtained by Peterlin for the magnitude of the birefringence and for the extinction angle (with no internal viscosity) are quite similar to equations 34 and 36 of the Kuhn-Hermans theory. Peterlin has also investigated how the sedimentation constant, diffusion coefficient, intrinsic viscosity, magnitude of the birefringence, and extinction angle are modified by the excluded volume effect. In recent years this effect has been extensively studied by various investigators in connection with the viscosity problem.

### *3. Theory for a free-draining pearl necklace*

As a model for a deformable macromolecule Kramers (105) considered a single molecule as a number of particles in which every two successive particles are connected by a weightless rod of length $L$. The hydrodynamic force which the liquid exerts on a particle is written in the form $-\zeta V$, where $V$ is the velocity

of the particle with respect to the liquid and $\zeta$ is a frictional coefficient assumed to be the same for each particle.

Kramers considered alternative approximations: (*1*) one in which the possibility of completely free rotation of two successive rods with respect to each other was assumed, and (*2*) one in which a given value was assigned to the valence angle between two successive links with and without the possibility of free rotation. Thus, the effect of intermediate chain elements was taken into account as well as the correlation between the orientation of two different links; this latter consideration is still incomplete, in that only the effects of neighboring links were taken into account. Also, the treatment is restricted to the case of free draining.

Only the magnitude of the birefringence was calculated and the result obtained is of the same general form as those of Kuhn and Hermans; in particular, the quantity $\nu$ is proportional to the degree of polymerization; no expression for the extinction angle was given.

Kramers' treatment, which also includes a calculation of the specific viscosity of the solution, has been a starting point for a new approach to the viscosity of solutions of macromolecules. So far it has not been possible to carry out a theoretical treatment of streaming double refraction on a similar basis because of mathematical difficulties.

### *4. Theory for an elastic sphere; application to chain molecules*

#### (a) Theory for an elastic sphere

In 1932 Haller (77) presented a brief, qualitative description of the dynamo-optical phenomena for a solution of elastic spheres. He suggested that more theoretical and experimental investigations be carried out in order to see if such phenomena could appear in solutions of long-chain molecules.

The theory has recently been developed in a quantitative way for small velocity gradients by Cerf (21, 25) and has been applied to some flexible chain molecules. It has led to a new type of experiment on chain molecules, enabling one to determine whether the particle is rigid or easily deformable; a discussion of its formulation follows herein.

The theory is developed in three steps:

(*1*) On the basis of classical hydrodynamics, first neglecting Brownian motion, a study was made of the deformation of the elastic sphere in the hydrodynamic field. The elastic sphere was assumed to be homogeneous and isotropic with respect to its elastic properties and the solution was considered to be infinitely dilute. This study indicated that the physical coefficients which play a role in the characterization of the elastic sphere are Lamé's shearing elasticity coefficient, $\mu$, and a quantity already introduced by Haller (77), the internal viscosity, $\eta_i$, which is defined here as the viscosity of a continuous medium (i.e., the particle) and should be distinguished from Kuhn's internal viscosity. The radius of the particle does not appear in the formulas.

The behavior of the elastic sphere in the hydrodynamic field, wherein it is deformed into an ellipsoid, is similar to that of a liquid drop. For velocity gra-

dients approaching zero the axes of all the deformed particles in the system make an angle of $\psi = 45°$ with respect to the stream lines. The section of the deformed particle in the streaming plane is an ellipse (figure 8), the axial ratio of which is, at low gradients,

$$p = 1 + \frac{2.5}{\mu}\eta_0 G + \cdots \tag{38}$$

where $\eta_0$ is the viscosity of the solvent. The terms shown in equation 38 arise only from the terms of first order in $G$ in the stress tensor. For higher gradients the axes depart from 45°. If terms of second order in $G$ in the stress tensor are taken into account, then the initial departure of the position of the axes from 45° can be calculated.

$$\psi = \frac{\pi}{4} - \delta\psi = \frac{\pi}{4} - \frac{1.25}{\mu}(\eta_0 + 0.4\eta_i)G \tag{39}$$

A comparison has been made (25) between these results for an elastic sphere and the experimental results of Taylor (182), who photographed a visible deformable liquid drop in a hydrodynamic field at various velocity gradients.

(*2*) The position of the axes of the particle represents a state of *hydrodynamic* equilibrium which has been shown to be a stable one. As a consequence of this property the Brownian motion has quite a different effect upon an elastic spherical particle from its effect upon a rigid particle.

The effect of Brownian motion manifests itself by fluctuations in the shape of the particle (Brownian deformation) and by a slight dispersion of the position of the axes of the particle around the macroscopic position of hydrodynamic equilibrium (rotary Brownian motion). Both effects can be neglected as a first approximation if the particle is not too deformable and if the internal viscosity is not too large compared with the viscosity of the solvent, i.e., if the following conditions hold:

$$\frac{1}{\mu} < \frac{1}{\mu_0} \quad \text{with} \quad \frac{1}{\mu_0} = \frac{3v}{100kT} \tag{40}$$

$$\eta_i \ll 30\eta_0$$

$v$ is the volume of the particle and $\ll$ means here "about three times smaller than." For a given value of $\mu$ the volume of the sphere has to be larger than a certain limit, which can be calculated from the preceding conditions.

It may be recalled that in the case of a rigid ellipsoid the preferential axes in the flowing solution are obtained from a distribution function expressing the combined effect of the hydrodynamic field and of the Brownian motion. On the other hand, in the case of an elastic sphere the preferential axes are determined by the hydrodynamic field and are not disturbed in a first approximation by the effect of the thermal agitation. Therefore, for the elastic sphere no rotary diffusion constant appears in the first approximation.

(*3*) On the basis of the preceding results the dynamoöptical properties of the solution can then be calculated.

(*i*) *Extinction angle:* The preceding results immediately give the position of the neutral lines; as a consequence of the negligible effect of Brownian motion these neutral lines coincide with the hydrodynamically preferred axes, i.e., the extinction angle, $\chi$, is identical with $\psi$ of equation 39. Thus the initial slope of the extinction angle curve is given by

$$(\tan \alpha)_0 = \frac{1.25}{\mu} (\eta_0 + 0.4\eta_i) \tag{41}$$

where $(\tan \alpha)_0$ is defined in equation 19.

This equation holds for infinite dilution and for sufficiently small Brownian deformation (equation 40). The only upper limit imposed on the radius, $a$, of the sphere arises from the condition that the inertia terms in the hydrodynamic problem have been neglected. This requires that $a$ be less than 50,000 Å.

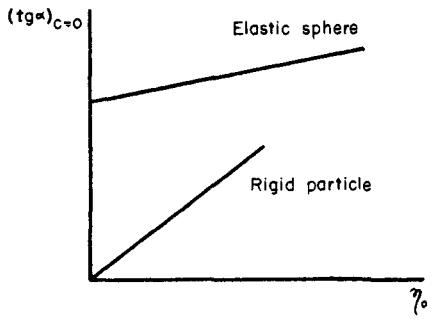


FIG. 31

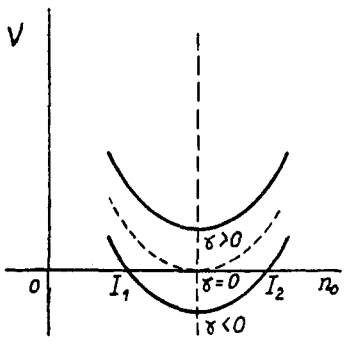


FIG. 32

FIG. 31. Behavior of $(\tan \alpha)_0$ as a function of $\eta_0$, illustrating equations 19 and 41 (26).

FIG. 32. Dependence of the Maxwell constant on the index of refraction of the solvent for several values of the elastoöptical coefficient (26).

It should be pointed out that equation 41 does not contain any rotary diffusion constant, in contradistinction to the corresponding equation for a solution of rigid ellipsoids (equation 19). It can also be seen from equation 41 that the extinction angle shows quite a different behavior from that of a solution of rigid particles if the viscosity, $\eta_0$, of the solvent is varied. Figure 31 shows the behavior of $(\tan \alpha)_0$ as a function of $\eta_0$ for an elastic sphere and for a rigid particle, i.e., equations 19 and 41. For the rigid particle and also the dumbbell model (equation 29) the curve is a straight line passing through the origin. For the elastic sphere, on the other hand, the straight line has a positive intercept when the internal viscosity is different from zero.

(*ii*) *Magnitude of the birefringence:* The quasi-static theory of propagation of light in disperse media provides a satisfactory solution of the question of internal field which arises in the optical problem. This treatment was introduced in the theory of induced double refraction by Peterlin and Stuart (132) in their rigid-particle theory.

The sphere is assumed to be optically isotropic in the undeformed state. Its optical properties are defined by means of two optical constants, the mean index of refraction, $n$, and the elastoöptic coefficient, $\gamma$, which characterizes the anisotropy acquired by the sphere when deformed. $\gamma$ is defined by the equation

$$\frac{n_1 - n_3}{n} = 2\gamma D \tag{42}$$

where the deformation, $D$, is $\frac{5}{4}\frac{\eta_0}{\mu} G$.

The birefringence at small gradients and small volume concentrations $\phi$ may then be derived. For small values of the difference in refractive indices, $n - n_0 = \partial n$, $n_0$ being the refractive index of the solvent, this reduces to

$$\frac{1}{n_0 \eta_0}\left(\frac{\Delta n}{G\phi}\right)_0 = \frac{w}{\mu}\left[5\gamma + 2\left(\frac{\partial n}{n}\right)^2\right] \tag{43}$$

$w$ is a mechanical factor depending on the intensity of the Brownian motion and is not too different from unity if equations 40 hold. Equation 43 is valid in the range of validity of the quasi-static theory of propagation of light in disperse media, i.e., if the radius, $a$, is less than 500 Å. for visible light. The lower limit of $a$ is still determined by equations 40.

In the small interval of variation of $n_0$ equation 43 predicts a parabolic dependence of $(\Delta n/G\phi)_0$ on $n_0$. If the elastoöptic coefficient, $\gamma$, is zero or positive, the birefringence is always positive. If $\gamma$ is negative, $\Delta n$ may change sign as the index of refraction of the solvent is varied. These results are illustrated schematically in figure 32. The minimum of the parabola occurs at a value of $n_0$ equal to that of the particle.

Cerf (25) has compared the dynamoöptical properties of a solution of elastic spheres with those of Peterlin and Stuart for a solution of rigid ellipsoids (132). His conclusions can be summarized in brief: A solution of elastic spheres exhibits a deformation effect of a nature completely different from the orientation effect of rigid particles. However, the two types of solution show a very similar macroscopically observable behavior. The only difference is to be found in the behavior of the extinction angle when the viscosity of the solvent is varied.

(b) Application of the elastic sphere model to chain molecules

The hypotheses involved in the use of elastic sphere as a model for a chain molecule have been discussed in more detail by Cerf (26). One of the main assumptions is that, as a first approximation, the solvent does not flow through the sphere which, nevertheless, is swollen with solvent. It should be kept in mind that all the coefficients characterizing the elastic sphere have only a phenomenological value in describing the properties of a chain molecule. It appears that the particle size enters in the quantity $\mu$, which must be related to the molecular weight and the thermodynamics of polymer–solvent interaction. The sphere represents an average configuration for the chain molecule, and the contribution to the optical effect of configurations deviating from the average configuration

is accounted for by considering the Brownian deformation of the sphere. The effect of non-spherical configurations of the chain is considered negligible when the effect of Brownian deformation of the sphere is negligible (see equations 40).

In order to compare the theoretical behavior of the birefringence with experimental data equation 43 has to be transformed to take account of the influence of the solvent on the mean index of refraction of the particle. The simple assumption of a linear dependence of index of refraction of the particle upon the index of refraction of the solvent was made (26). This assumption may have to be revised when more experimental data become available. Equation 43 then becomes

$$\frac{1}{n_0 \eta_0}\left(\frac{\Delta n}{G\phi}\right)_0 = \frac{w}{\mu}\left[5\gamma + 2\beta^2\left(\frac{\partial \mathbf{n}}{n}\right)^2\right] \tag{44}$$

where $\mathbf{n}$ is an index of refraction characteristic of the chain defined by $n = \beta\mathbf{n} + (1 - \beta)n_0$. The dependence of the birefringence on $n_0$ from equation 44 then shows the same behavior as predicted by equation 43, i.e., a parabolic dependence on $n_0$ and the possibility of inversion of the sign of the birefringence (see figure 32).

The difference between the two points of view, that of the elastic dumbbell and that of the elastic sphere, as applied to chain molecules may be summarized as follows: Both involve a deformation of the particle as well as an orientation of elongated configurations. In the case of the elastic dumbbell the initial birefringence for zero gradient arises entirely from an orientation effect, the deformation of the molecule by the shearing forces only affecting the behavior of the birefringence at higher gradients. In the case of the elastic sphere, on the other hand, the effect of configurations deviating from the mean spherical form is neglected, as a first approximation, for molecules which are large enough; the initial birefringence arises entirely from a deformation effect.

The question as to whether the initial effect exhibited at low velocity gradients is, for a given polymer, primarily a deformation effect or an orientation effect cannot be approached by considering the magnitude of the birefringence (26), since the elastic sphere model leads to a behavior similar to that obtained by Peterlin and Stuart for the ellipsoidal model. However, it should be recalled here that the dependence of the birefringence on the index of refraction of the solvent is quite different in the theory of Sadron (144); the latter may be applicable to rather extended linear chain molecules. The question of the validity of the different models may be approached (22, 26) on the basis of the difference between equations 19, 29, and 41, which give $(\tan \alpha)_0$ for a rigid ellipsoid, an elastic dumbbell, and an elastic sphere, as already indicated (figure 31). Thus, studies should be made of the behavior of $(\tan \alpha)_0$ as a function of $\eta_0$ (22), providing a test which can distinguish between the various models. Actually, the test is of a qualitative nature and of rather crude value, but nevertheless one which is adapted to the situation, in view of the poor state of our knowledge in this field (24). The test has the advantage that it is still valid even if the solutions under investigation are polydisperse, since the form of equations 19, 29, and 41

is the same for monodisperse and polydisperse systems with respect to the presence or absence of a positive intercept. The experiments which have been carried out thus far will be reported below.

### B. EXPERIMENTAL RESULTS FOR CHAIN MOLECULES

Although some experimental work has been started on concentrated solutions, all the existing theories apply only to infinitely dilute solutions. To compare the various theories with experimental results it is necessary to have data for monodisperse systems for which extrapolations of the extinction angle and birefringence to zero concentration and zero gradient have been carried out. Unfortunately these conditions have not always been fulfilled, especially since these extrapolations, for the extinction angle, are not always easy to carry out.

The experimental behavior of the extinction angle and birefringence at both low and high gradients (80, 112) has been compared with theory. As already pointed out, most of the theoretical treatments concern the behavior of these quantities, for chain molecules, at low rather than at high gradients. Also, most of the experimental results for chain molecules have been reported in terms of the initial behavior at low gradients, for example, as the initial slope of the birefringence curve. Since it has not yet been possible to reach a final explanation for these effects even at low gradients, the emphasis will be placed here on these low-gradient effects when comparing theory with experiment.

Section VI,B,1 will be concerned with some simple means of distinguishing between rigid and deformable particles. In Section VI,B,2 theoretical and experimental results for the magnitude of the birefringence at low gradients will be compared; Section VI,B,3 will deal primarily with the behavior of the extinction angle and will include a more precise test for distinguishing between rigid and deformable particles. The remaining sections will deal with other experimental results which may be regarded as the application of the flow birefringence technique to several problems in high-polymer physical chemistry rather than a direct test of the validity of the theories. Some consideration has been given to the effect of branching (161) and the addition of plasticizers (93) and non-solvents (98). However, such work is only in a preliminary stage and will not be considered in a separate section.

#### *1. Qualitative distinction between rigid and deformable particles*

In order to be able to decide on the validity of a model and interpret the Maxwell effect for chain molecules, it is first necessary to be able to distinguish between an orientation effect and a deformation effect. In this connection very simple observations have already given valuable information.

If the birefringence curve shows a saturation effect like that already described for a rigid particle, it is probable that the molecule under investigation is rather elongated and that the observed effect is, at least partially, an orientation effect. If the curve shows a greater-than-linear increase with $G$ (figure 4), a deformation of the molecule will appear most probable. As pointed out by several investigators (55, 186, 187), the combined observation of the behavior of the birefringence

and extinction angle with $G$ is particularly instructive. In some cases the birefringence continues to increase with $G$ even though the extinction angle has essentially approached zero (vystanex and oppanol in figures 4 and 5 and also polystyrene (27)). This is evidence for a deformation of the molecule.

The departure from rigidity was made evident in another way by Tsvetkov and Frisman for the case of polyisobutylene (186, 187). If the particle is assumed to be rigid, one can determine the anisotropy of the particle for different values of the velocity gradient by measuring the birefringence and extinction angle simultaneously and calculating $g_1 - g_2$ for each value of $G$ from equations 10, 15, and 16 of the Peterlin and Stuart theory for rigid ellipsoids. If the particles under investigation are really rigid, the particle anisotropy thus obtained should

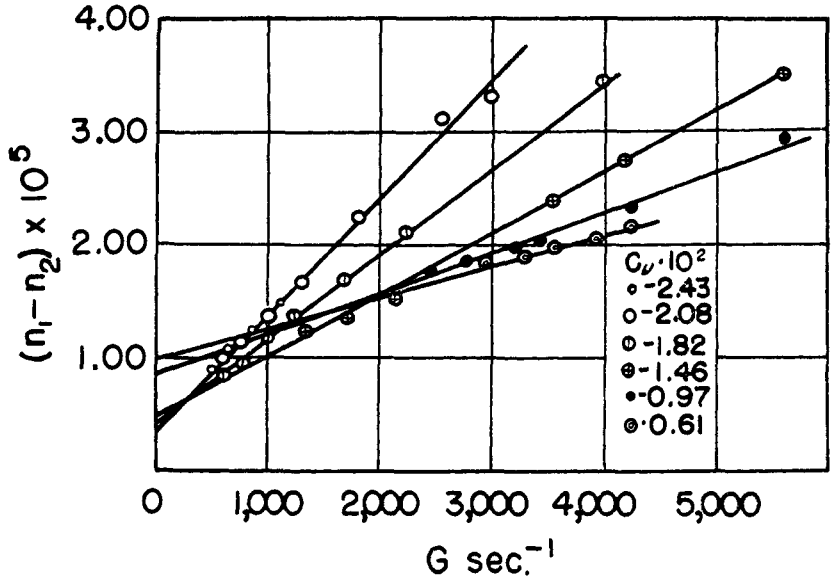


FIG. 33. Anisotropy of vystanex molecules in solution at various velocity gradients for several volume concentrations $C_v$ (Tsvetkov and Frisman (186)).

be the same at all velocity gradients. Figure 33 shows, on the contrary, that the anisotropy of vystanex molecules greatly depends on the velocity gradient, this being evidence of a strong contribution from a deformation effect. It should be noted that the form of the birefringence and extinction angle curves is affected by the polydispersity of the system, the samples reported in figure 33 being polydisperse.

Tsvetkov and Frisman tried to use the results of figure 33 in order to split the Maxwell effect into different parts, arising from the intrinsic molecular anisotropy, the form effect, and the effect of deformation of the molecule under flow. However, as pointed out by Tsvetkov and Frisman themselves, it would be preferable not to apply a theoretical approach which is actually applicable only to rigid particles.

*2. Measurements of the magnitude of the birefringence; comparison with theory*

(a) Dependence of the Maxwell constant on the molecular weight

Early results of Signer and Gross (165) on polystyrene of low molecular weight and more recent results of Wissler (196) on methylcellulose show a proportionality of $\nu$ to the molecular weight. Other studies have been carried out on nitrocellulose (95). The results of Signer and Gross and of Wissler are quoted by Kuhn and Kuhn (110) as being in agreement with equation 33. These are shown in figure 34; the discrepancies at high molecular weight are attributed by Kuhn and Kuhn to a limitation on the assumption of free draining.

The constancy of $\nu/[\eta]$ for various molecular weights, predicted by equation 34, is confirmed by the same results of Signer and Gross (165) and Wissler (196) and also by some results obtained by Wissler (196) for nitrocellulose. It should

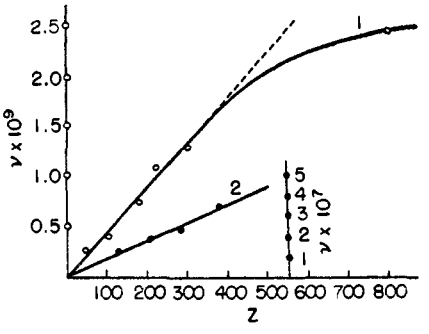


FIG. 34

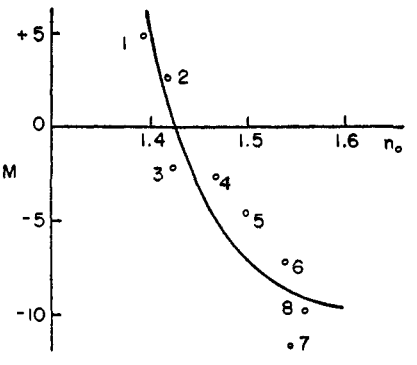


FIG. 35

FIG. 34. Dependence of the Maxwell constant on the degree of polymerization (Kuhn and Kuhn (110)). Curve 1, data of Signer and Gross for polystyrene; curve 2, data of Wissler for methylcellulose.

FIG. 35. Maxwell constant of polystyrene in eight solvents of different index of refraction (Cerf (26)). Curve drawn from data of Signer (163).

be recalled that equation 34 is independent of the internal viscosity of the particle and of the degree of permeation.

These results (table 2) are compatible with both the dumbbell and the necklace models. The theory for the elastic sphere does not provide an explicit expression for the dependence of the Maxwell constant on the molecular weight.

Further experimental work is required to examine the feasibility of the suggestion of Kuhn and Kuhn (112), and also of Wales (193), of using measurements of streaming double refraction to determine molecular weights.

(b) Dependence of the Maxwell constant on the index of refraction of the solvent

A comparison of the experimental results for the dependence of the Maxwell constant on $n_0$ has been made with the theory of the elastic sphere on the basis of equation 44 (26). The effects indicated by equation 44 are shown in figure 35 for

polystyrene ($\gamma < 0$) and in figure 36 for polyisobutylene ($\gamma > 0$). However, as pointed out by Cerf (26), this agreement is not a proof of the validity of the elastic sphere model, since a rigid ellipsoid model would lead to the same conclusions

TABLE 2

*Test of equation 34 for various polymers**

| POLYMER | $[\eta]$ | $\nu$ | $\frac{\nu}{[\eta]}$ |
|---|---|---|---|
| Polystyrene | 0.6 | $-2.5 \times 10^{-10}$ | $-4.16 \times 10^{-10}$ |
| | 1.0 | −3.9 | −3.9 |
| | 1.6 | −7.2 | −4.5 |
| | 2.2 | −10.9 | −4.96 |
| | 2.7 | −12.8 | −4.74 |
| | 5.6 | −24.4 | −4.35 |
| Methylcellulose | 28 | $1.29 \times 10^{-7}$ | $4.61 \times 10^{-9}$ |
| | 43 | 1.97 | 4.59 |
| | 55 | 2.35 | 4.27 |
| | 74 | 3.44 | 4.65 |
| Nitrocellulose | 108 | $-2.19 \times 10^{-7}$ | $-2.03 \times 10^{-9}$ |
| | 196 | −4.4 | −2.24 |
| | 340 | −6.24 | −1.83 |

* Data from Kuhn and Kuhn (110).

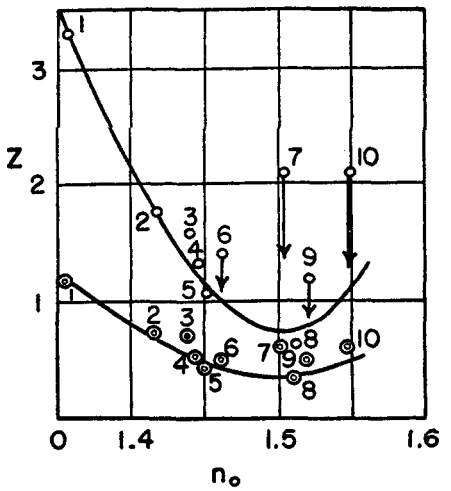


FIG. 36. Birefringence of two samples of polyisobutylene in ten solvents of different index of refraction (Tsvetkov and Frisman (187)).

(see figure 19). Figure 37 further shows the dependence of the Maxwell constant on $n_0^2$ for polymethylmethacrylate (191). The fact that $\nu$ is plotted against $n_0^2$ instead of $n_0$ does not affect the general form of the curve, since the range in

index of refraction is small for most organic solvents. The dispersion of the experimental points is much smaller in figure 37 than in figures 35 and 36. Experiments on the dependence of the birefringence on the nature of the solvent have also been carried out by Kanamaru, Yamamoto, and Tanaka (101).

No conclusion about the shape and rigidity of the solute molecules can be drawn from such experiments, since the results for the dependence of the birefringence on the index of refraction of the solvent are compatible with the theory of rigid ellipsoids as well as with the theory of the elastic sphere.

### *3. Test for the validity of the different models on the basis of measurements of the extinction angle*

Another approach to the question of distinguishing between the theories for deformable particles is through the behavior of the extinction angle at low veloc-

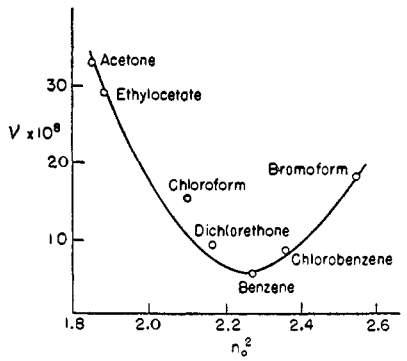


FIG. 37

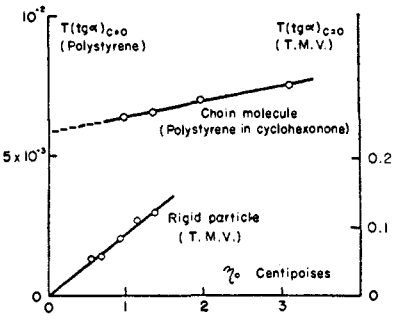


FIG. 38

FIG. 37. Maxwell constant of polymethylmethacrylate in several solvents of different index of refraction (Tsvetkov and Petrova (191)).

FIG. 38. Behavior of $T(\tan \alpha)_0$ as a function of $\eta_0$ for polystyrene and tobacco mosaic virus (22).

ity gradients. As already indicated (Section VI,A,4,(b)), one has to measure $(\tan \alpha)_0$ for different values of the viscosity $\eta_0$ of the solvent. The systems already investigated in this manner are polystyrene (22, 26), where the variation of $\eta_0$ was obtained by varying the temperature, and nucleic acids (159), where the variation of $\eta_0$ was obtained by adding various amounts of glycerol. As high precision is required in such experiments, the Bravais double-plate technique was used.

#### (a) Polystyrene; temperature dependence of the Maxwell effect

Early experiments on the temperature dependence of the Maxwell effect have been carried out by Signer and Gross on polystyrene (165) and by Kanamaru, Tanaka, and Sugiyama (97) on nitrocellulose. The data from these experiments are not sufficiently extensive to provide a basis for applying the test under consideration here.

To apply this test to the experiments carried out by Cerf (22, 26), the temperature dependence of $\mu$ and $\eta_i$ in equation 41 has to be taken into consideration. For theoretical reasons $\mu$ was considered as being proportional to the absolute temperature. On the other hand, on the basis of viscosity measurements, $\eta_i$ was assumed, as a first approximation, to be independent of $T$ (22, 26). This assumption may not be generally valid for chain molecules. Thus the quantity $T(\tan \alpha)_0$ should be of the form $m\eta_0 + n$ for the elastic sphere model, $m$ and $n$ being positive constants. For a rigid particle or a dumbbell model $T(\tan \alpha)_0$ should be proportional to $\eta_0$, according to equation 19 or 29. Figure 38 shows the behavior of $T(\tan \alpha)_0$ as a function of $\eta_0$ for a sample of polystyrene (molecular weight = 130,000) in cyclohexanone. Data for tobacco mosaic virus are also reported in figure 38. The curve for tobacco mosaic virus shows a behavior in agreement

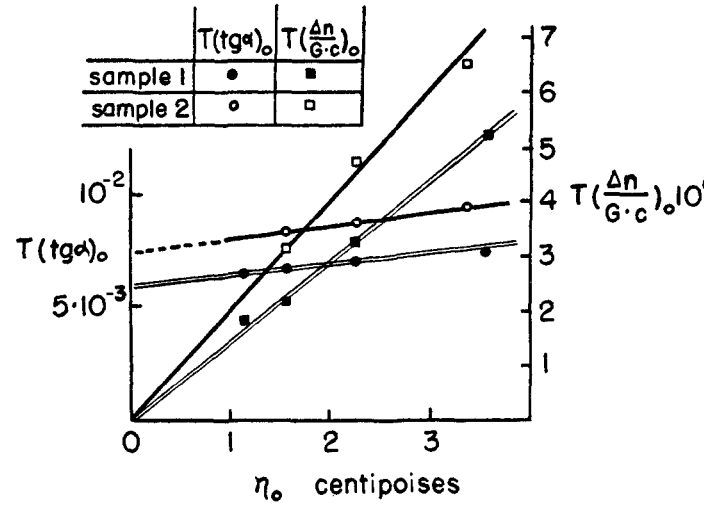


FIG. 39. Extinction angle and birefringence for two samples of polystyrene (26)

with the orientation theory, while polystyrene shows the behavior predicted by the theory of the elastic sphere.

Also, the theory for the dumbbell model predicts that the ratio of the slopes of this curve for large and small internal viscosity should be equal to 3 (see equations 28 and 35). It can be shown that the variation of $\eta_0$ from small to large values is equivalent to the variation of the internal viscosity from large values to small ones. Actually, it does not appear to be possible to draw an experimental curve of $T(\tan \alpha)_0$ *vs.* $\eta_0$ through the experimental points satisfying the Kuhn condition. These particular data would seem to be in disagreement with the predictions of the Kuhn theory. However, since it is a difficult experimental problem to make such extinction angle measurements of high precision, it would be instructive to have them repeated, if possible in a larger range of viscosities.

Figure 39 shows $T(\tan \alpha)_0$ and $T(\Delta n/Gc)_{c=0,G=0}$ as a function of $\eta_0$ for the preceding sample of polystyrene (No. 1) and for a fractionated sample (molecular weight = 202,000, No. 2). It can be seen that the quantity $T(\Delta n/Gc)_{c=0,G=0}$ is

proportional to $\eta_0$. This seems to be an experimental verification of the proportionality of $\mu$ to $T$, as assumed in the theory (equation 44).

The existence of the positive intercept for these two samples of polystyrene is qualitative evidence for the validity of the theory of the elastic sphere, although conditions 40 are not exactly fulfilled here. It should be noticed that the intercepts for samples 1 and 2 are not identical, indicating a dependence of $\mu$ and/or $\eta_i$ on the molecular weight.

Figures 40 and 41 illustrate the concentration dependence of $(\Delta n/Gc)_{G=0}$ and of $(\tan \alpha)_0$ for polystyrene No. 2 at different temperatures. Empirical relations have been given for representing these curves (26). Other empirical relations for the concentration dependence have been given for nitrocellulose (99) and for polyisobutylene (96, 190).

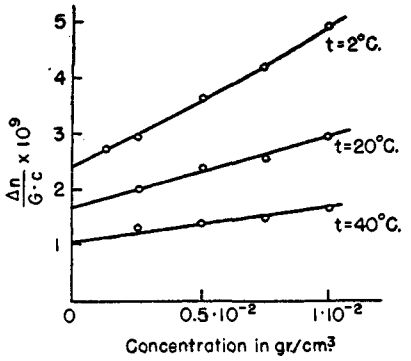


FIG. 40

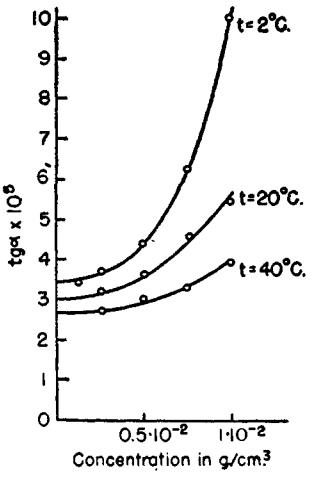


FIG. 41

FIG. 40. Concentration dependence of the birefringence for polystyrene at several temperatures (26).

FIG. 41. Concentration dependence of the extinction angle for polystyrene at several temperatures (26).

It appears that some progress has been made in the range of low velocity gradients and some evidence has been obtained that the effect, for the particular molecules studied, is more a deformation effect than an orientation one. Since this limiting theory for an impermeable molecule appears to apply, this provides additional evidence for the use of the impermeable sphere as a model for a polymer molecule.

*Determination of the elasticity and internal viscosity coefficients:* Since the theory of the elastic sphere appears to be in qualitative agreement with the experiments described above and since the description of the mechanical properties of the molecule by means of the two coefficients $\mu$ and $\eta_i$ seems to be plausible, it can be seen that measurements of streaming double refraction provide a method for evaluating $\mu$ and $\eta_i$ (24, 26).

From a determination of the slope and intercept, $m$ and $n$, it follows that

$$\mu_T \sim 1.25 \frac{T}{m}$$
$$\eta_i \sim 2.5 \frac{n}{m} \tag{45}$$

$\mu_T$ is the value of $\mu$ at the temperature $T$. The symbol $\sim$ is used to indicate that these equations may have only a semiquantitative value. Table 3 gives the values of $\mu_T$ and $\eta_i$ in C.G.S. units obtained for two samples of polystyrene.

It should be emphasized once again that so far the coefficients $\mu$ and $\eta_i$ have only a phenomenological character and have not as yet been related to the parameters of the chain molecule. In particular, it is very desirable to know the dependence of these coefficients on the molecular weight. The coefficient $\mu$ is related to quantities of statistical character which, if calculated for a chain molecule, would provide a basis for the determination of $\mu$ for such chains (25). The

TABLE 3

*Elasticity and internal viscosity coefficients for two samples of polystyrene*

| SAMPLE NO. | MOLECULAR WEIGHT | $\mu_{20°}$ | $\eta_i$ |
|---|---|---|---|
| 1 | 130,000 | $7 \times 10^3$ | 0.3 |
| 2 | 202,000 | $6 \times 10^3$* | 0.3 |

* The value previously reported by Cerf (24, 26) is erroneous.

question of the possible quantitative significance of equation 45 has to be investigated further. Measurements with ultrasonic shear waves will very likely give useful information in this respect (28). In any event, as emphasized by Cerf (26), it is very desirable that the coefficients $m$ and $n$ be determined for many chain-molecule systems of varying molecular weights, even for less flexible molecules for which the theory is certainly not applicable.

### (b) Thymonucleic acids

Similar studies have been carried out for thymonucleic acids by Schwander and Cerf (159). As already indicated, in these experiments the variation of viscosity of the solvent was obtained by using a mixture of salt, water, and glycerol with different concentrations of glycerol. As shown in figure 42, the curve giving $(\tan \alpha)_0$ as a function of $\eta_0$ is a straight line going through the origin except for values of $\eta_0$ larger than 10 centipoises. This departure has not yet been explained.

## *4. Behavior of the birefringence and the extinction angle at high velocity gradients*

### (a) Birefringence

Before discussing some of the recent effects observed at high velocity gradients it is well to recall that discontinuities had earlier been observed in the birefrin-

gence and extinction angle curves, for a critical velocity gradient, $G_c$, by Signer and Gross (165) in the case of high-molecular-weight polystyrene and by Sadron (142) in the case of pure liquids. The results of Signer and Gross were attributed by Sadron (143) to the transition between laminar and turbulent flow. However, these same authors, in reporting similar effects in other samples of polystyrene, attributed the phenomenon to an abrupt deformation of the molecule at the critical gradient, without discussing the possibility that these discontinuities might also be due to the onset of turbulence (167).

Such discontinuities were observed by deRosset (34) for polymethylmethacrylate and by Tsvetkov and Frisman (186, 187) for polyisobutylene, where the effect on the birefringence was not as pronounced as for polystyrene. It was

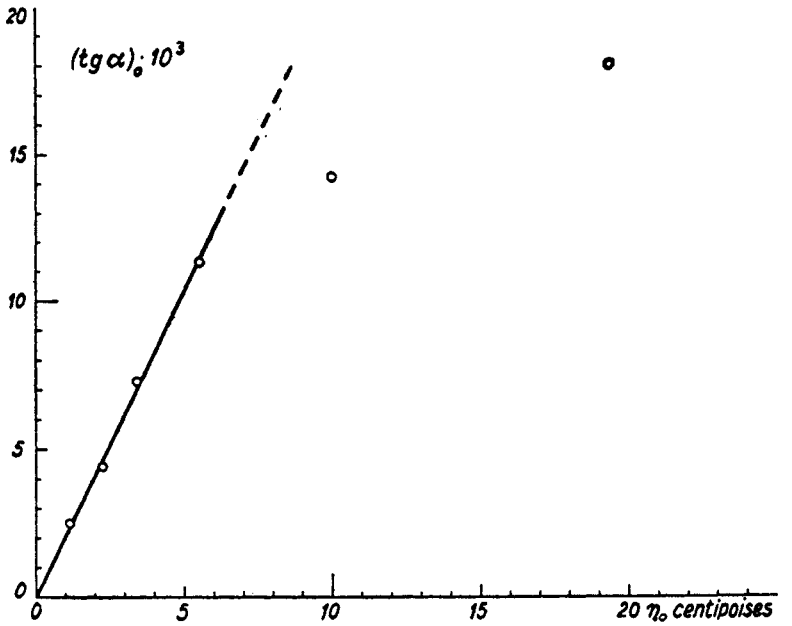


FIG. 42. $(\tan \alpha)_0$ *vs.* $\eta_0$ for thymonucleic acid (159)

attributed by Tsvetkov and Frisman to an abrupt elongation of the molecule, the value of the critical velocity gradient being in agreement with the value predicted by a theory of Frenkel (59), wherein the curled-up molecule was thought to uncurl at a critical velocity gradient in such a way that its entire middle portion straightened out. This agreement, however, was regarded as fortuitous by Rehner (138), because of the non-validity of Hooke's law under conditions of rupture in Frenkel's treatment. Nevertheless, the assumption that the configuration of the molecule changes substantially under flow is supported, according to Tsvetkov and Frisman, by the fact that further increases of the velocity gradient in solutions of oppanol give rise to irreversible changes resulting in a diminution of the solution viscosity and also of the magnitude of the birefringence. These

changes are illustrated in figure 43, where the birefringence curves are plotted both for fresh solutions and for the same solutions kept for 3 min. at $G = 30{,}000$ sec.$^{-1}$ in the cylindrical apparatus. The mechanical action is seen to result in a very marked reduction of the birefringence and an increase in the range of velocity gradients where the slope of the curves is changing. There is also a corresponding effect on the extinction angle. This is illustrated in figure 44, showing curves obtained with a fresh oppanol solution ($c_v = 0.842 \times 10^{-2}$) and with the same solution after it had been treated in the cylindrical apparatus for 5 min. at a velocity gradient of 20,000 sec.$^{-1}$ Thus measurements of the extinction angle support the assumption of the breaking of molecular chains, thereby indicating

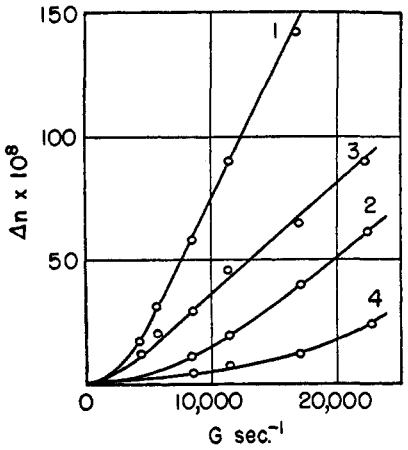


FIG. 43

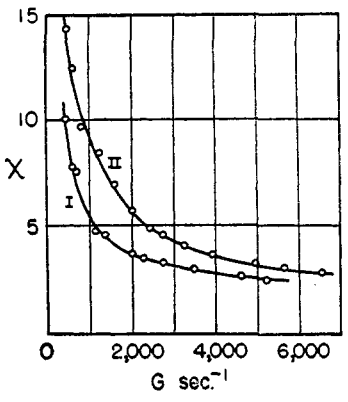


FIG. 44

FIG. 43. Influence of mechanical treatment on birefringence for oppanol solutions (Tsvetkov and Frisman (186)). $C_v = 0.187 \times 10^{-2}$ (curve 1, fresh solution; curve 2, after 3-min. treatment). $C_v = 0.0932 \times 10^{-2}$ (curve 3, fresh solution; curve 4, after 3-min. treatment).

FIG. 44. Influence of mechanical treatment on extinction angle for oppanol solutions (Tsvetkov and Frisman (186)). $C_v = 0.842 \times 10^{-2}$: curve I, fresh solution; curve II, after 5-min. treatment at $G = 20{,}000$ sec.$^{-1}$

directly that the molecular weight of the dissolved particles diminishes in a hydrodynamic field.

On the other hand, discontinuities recently observed in polystyrene (26) solutions seem very likely to be due to turbulence. Thus, there remains the possibility of the coexistence of two different phenomena at high gradients, turbulence on the one hand and an abrupt deformation of the molecule on the other.

### (b) Extinction angle; empirical approach

Some attempts have been made at an empirical formulation for the extinction angle. The formulation was based on Boeder's results for a solution of rod-shaped particles,

$$\tan 2\chi = \frac{c\Theta}{G} = \frac{cKT}{G\eta_0\zeta} \tag{46}$$

where $\Theta$ is the rotary diffusion constant and $\zeta$ is the rotary frictional coefficient. $c$ is a numerical factor. Measurements of the extinction angle made by Tsvetkov and Frisman (186, 187) on solutions of polyisobutylene have shown that, if $\zeta$ is assumed constant, the experimental extinction angle curves do not correspond qualitatively to equation 46 but are much better expressed by the empirical equation

$$\tan 2\chi - \tan 2\chi_0 = \frac{c\Theta}{G} = \frac{ckT}{G\eta_0\zeta} \tag{47}$$

where $\chi_0$ is a constant angle, characteristic of the given polymer, and the limit that the extinction angle should attain at very high velocity gradients. However, in this approach uncertainties may arise in the behavior of the extinction angle at high gradients, owing to the possibility of turbulent motion. Also, an experimental extinction angle curve with $\chi_0$ different from zero is strongly suggestive of polydispersity. Furthermore, there is some doubt, in the light of the theory of the elastic sphere, about the possibility of interpreting the behavior of the extinction angle with $G$, for chain molecules, by means of a rotary diffusion constant. The same remarks apply to an attempt of Schoenberg, Riseman, and Eirich (157) to use the rotary diffusion constant of the Kirkwood–Riseman theory (104) in the interpretation of the extinction angle. Other empirical formulas for the dependence of the extinction angle and birefringence on velocity gradient have been given for nitrocellulose (99) and polyisobutylene (96).

### *5. Anomalous behavior of the extinction angle and the birefringence*

Anomalies in the extinction angle and birefringence curves have already been indicated as being due to polydispersity. Recent results of this kind in polydisperse systems were observed by Signer, Liechti, and Liechti (164) for nitrocelluloses as well as by Snellman and Saverborn (175) for pectic substances. Such anomalous effects have also been observed by Tsvetkov and Petrova (190) in rubber solutions and attributed to the presence of impurities of large size. This hypothesis was confirmed by the fact that purified solutions showed a normal effect.

The anomaly due to the presence of large particles is of a rather peculiar form in concentrated solutions of aluminum soaps, where Gray and Alexander (74) found a birefringence different from zero for zero gradient. Also, the extinction angle at zero gradient is not 45° but 0°, as shown in figure 45. It seems that these effects are due to a preferential orientation of long chains in the neighborhood of the walls and parallel to them. Theoretical considerations in connection with these experiments have been presented by Gray (73).

### *6. Effect of electric charges; polyelectrolytes*

If a chain molecule possesses charges, then the resulting intramolecular repulsions will give rise to expanded configurations. The influence of these charges may be suppressed to varying degrees by the presence of counter-ions in the solution. The presence of the charges, therefore, affects the random-coil statistics used for uncharged polymers. As a result of the change in shape of the molecule

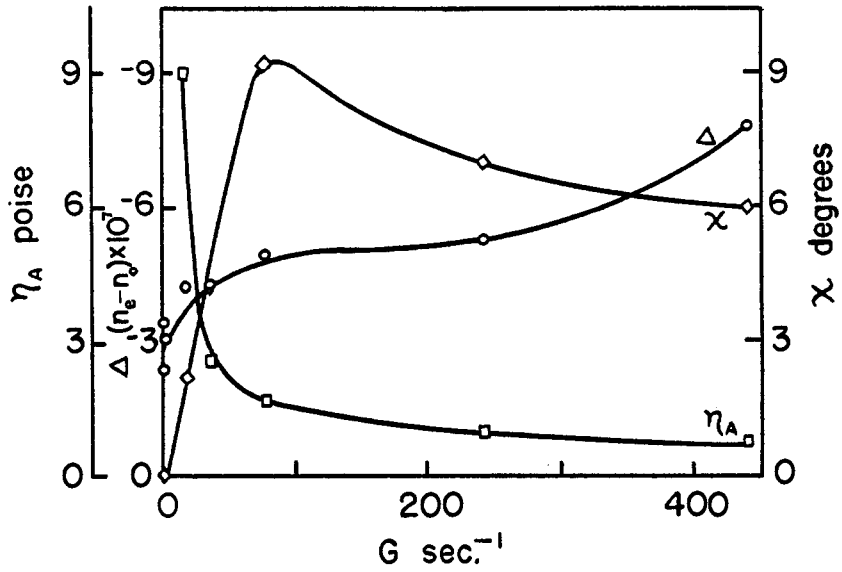


FIG. 45. Anomalous behavior of birefringence ($\Delta$) and extinction angle ($\chi$) as a function of velocity gradient for a 2 per cent solution of aluminum laurate P in benzene (Gray and Alexander (74)).

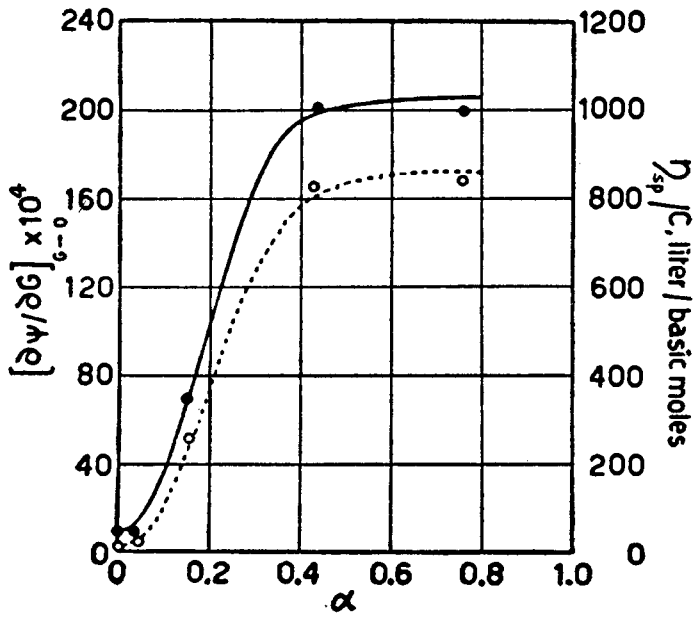


FIG. 46. Streaming birefringence and viscosity measurements of polymethylmethacrylate solutions *vs.* degree of ionization $\alpha$. (●), $\partial\psi/\partial G \equiv (\tan\alpha)_0$; ○, $\eta_{sp}/C$. Polymer concentration = 1/50 base moles per liter; degree of polymerization = 3000. (Katchalsky (102)).

the viscosity, flow birefringence, and sedimentation behavior of polyelectrolytes should be significantly different from that of uncharged polymers.

For polymethylmethacrylate Katchalsky found that the quantity $\eta_{sp}/c$ for the unionized macromolecule at low pH in dilute hydrochloric acid solution is proportional to the square root of the molecular weight, while $\eta_{sp}/c$ for the ionized polymer increases much more rapidly, approaching proportionality to the square of the molecular weight (102). At low degrees of ionization the molecule seems to be a compact spherical coil obeying Einstein's law; it opens up with increasing ionization and finally seems to stretch to a rod-like filament at high degrees of ionization. The conclusion that the molecule is expanded by ionization is substantiated by parallel measurements of the flow birefringence of the solution. The quantity $(\tan \alpha)_0$ increases in a manner similar to that of the viscosity, as shown in figure 46.

In the last few years theoretical investigations have been carried out by Hermans and Overbeek (82) and by Kuhn, Künzle, and Katchalsky (103, 109), primarily to account for the viscosity behavior of solutions of polyelectrolytes. Both theories contain approximations indicated by the respective authors.

The Kuhn, Künzle, and Katchalsky theory is based on the Kuhn and Kuhn treatment of the viscosity problem (110), in which the mean square end-to-end distance, $\overline{h_0^2}$, of the polymer chain is the essential parameter for calculating the viscosity of the solution. In this theory the determination of the viscosity of a solution of ionized polymer molecules is, therefore, equivalent to the determination of the change of $\overline{h_0^2}$ due to the presence of charges. In a similar way the behavior of the extinction angle and the magnitude of the birefringence have been computed. The few experimental results which are available show that for polymethacrylic acid the behavior of the anisotropy of the statistical chain element does not fit the present theoretical scheme, since the anisotropy is observed to decrease instead of increasing when the degree of ionization increases (109).

Other experimental results have been obtained by Rosen, Kamath, and Eirich (141) on polyvinyl pyridonium bromide. The quantity $\Theta$, plotted against the polyelectrolyte concentration in figure 47, is an equivalent rotary diffusion constant calculated for a velocity gradient of 10,000 sec.$^{-1}$ from the data of Scheraga, Edsall, and Gadd (155) based on the Peterlin and Stuart theory for rigid particles (132). Since it is not yet completely known whether polyelectrolytes can be treated with the theory for rigid particles, we shall consider here only the experimental results. Curves 2, 3, 4, and 5, which correspond to isoionic dilution, show that the extinction angles move toward 45° on dilution, as is normally observed. Curve 1, on the other hand, obtained by dilution with water, shows that the extinction angles have the opposite behavior, i.e., they move away from 45° on dilution. This effect may correspond to a stretching of the molecule. In these experiments it was not possible to carry out an extrapolation to infinite dilution, owing to the strong concentration dependence. In view of this concentration dependence it will be of great importance to carry out measurements on polyelectrolytes at very low concentrations with the best precision possible with the flow birefringence technique.

If the polyelectrolyte is a rigid particle instead of a flexible coil, then the salt concentration should not affect the shape. Schwander and Signer (160) have investigated sodium thymonucleate for different salt concentrations ranging from 1 to 10,000 mg. per 100 g. of solution, and also for different polymer concentrations ranging from 8 to 20 mg. per 100 g. of solution. The extinction angle was found to be independent of salt and sodium thymonucleate concentrations within the precision of the measurements. These results, which differ from those for polyvinyl pyridonium bromide, provide evidence for the fact that flow birefringence of sodium thymonucleate solutions is due to the orientation of rigid particles, confirming in a convincing way the similar earlier conclusion of Schwander and Cerf (159).

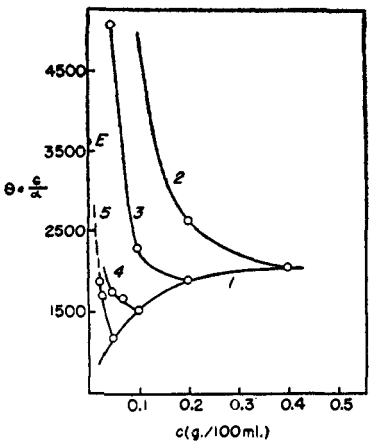


FIG. 47. Apparent rotary diffusion constant *vs.* concentration of polyelectrolyte. Curve 1, dilution with water; curves 2–5, dilution starting from potassium bromide concentrations of 0.0165 *M*, 0.0083 *M*, 0.0042 *M*, and 0.0021 *M*, respectively, and diluting with the same concentration of potassium bromide. *E*, estimated intercept of curve 5. (Rosen, Kamath, and Eirich (141)).

### *7. Kinetic studies*

Tsvetkov and Frisman (188) studied the dynamooptical properties of a styrene monomer-polymer mixture at different stages of the polymerization process. Figure 48 shows the behavior of the birefringence as a function of the velocity gradient at various stages. The positive ordinates correspond to negative double refraction. The double refraction of flow of liquid styrene monomer is positive, while that of a partially polymerized system is negative. For each curve the corresponding relative viscosity, $\eta_r$, of the system is reported. The curves reveal that polymerization of styrene leads to a gradual decrease of its positive double refraction and finally to a reversal of its sign.

Figure 49 shows the viscosity and optical properties for another sample of styrene at different stages of polymerization. The magnitude of the extinction angle suffers an abrupt decrease at the same stage of polymerization at which a decrease of the degree of depolarization, $\Delta u$, of scattered light and the change

of sign of the double refraction are observed. Further polymerization leads to a change in the sign of the birefringence and a small increase of its positive value, whereupon it remains practically constant and begins to decrease slowly at advanced stages of polymerization.

In order to draw quantitative conclusions from these results it should be noted that the system is a solution of polystyrene in its monomer. Consequently the dynamoöptical properties of the solution must be considered as the properties of

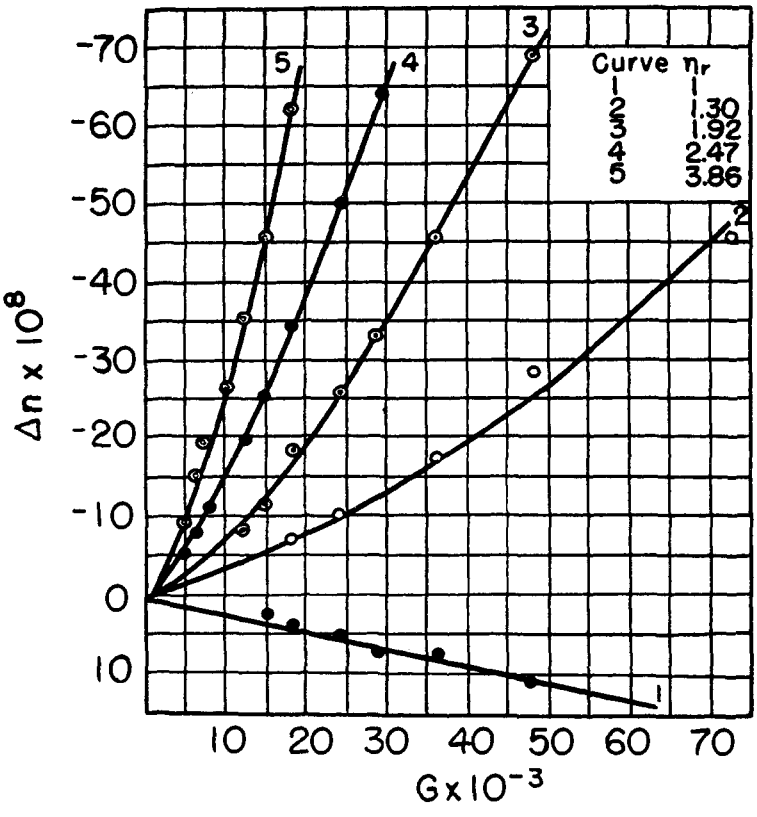


FIG. 48. Birefringence curves obtained during polymerization of styrene (Tsvetkov and Frisman (188)). $\eta_r$ is the viscosity of the monomer–polymer mixture relative to that of the monomer, curve 1 being that for pure styrene.

a polydisperse system consisting of many components falling into two classes: (*a*) Liquid styrene monomer giving a positive double refraction $\Delta n_m$ and an extinction angle $\chi_m = 45°$ at all gradients. (*b*) Polymer molecules dissolved in this liquid and giving a negative double refraction $\Delta n_p$ and an extinction angle $\chi_p$ which is a function of the gradient. The observed birefringence and extinction angle are related to both these factors through Sadron's equations for polydisperse media, the validity of these equations, of course, not being restricted only to rigid particles. Thus, $\chi_p$ can be determined, assuming the system to be a binary

one. From $\chi_p$ and the results of Kuhn and Kuhn for the dumbbell model, the determination of the mean molecular weight of the polymer fraction at each stage of the polymerization can be made.

As Tsvetkov and Frisman themselves have pointed out, there may be limitations on the quantitative exactness of the result. Nevertheless, very useful information is obtained and, as these investigators have indicated, flow birefrin-

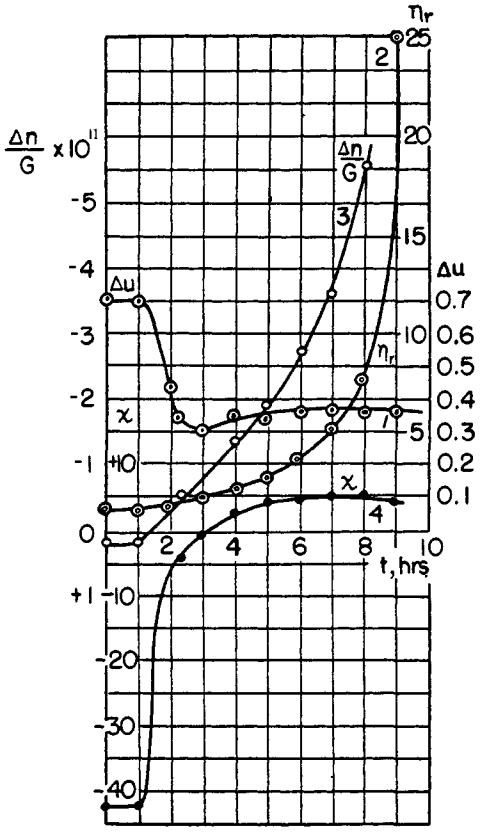


FIG. 49. Time dependence of birefringence ($\Delta n/G$) and extinction angle $\chi$ during the polymerization of styrene (Tsvetkov and Frisman (188)).

gence should be a particularly fruitful method when the low concentration of polymer in the mixture prevents the application of any other method.

The ripening of viscose (cellulose xanthate) in dilute solutions has been studied by means of flow birefringence by Signer and Meyer (121, 166). Figure 50 shows the extinction angle as a function of the velocity gradient at different stages of ripening. Combining these results with viscosity measurements made during the course of ripening, Signer and Meyer were able to describe in detail the complicated processes which take place during the ripening. At the first stage the solution shows the behavior characteristic of chain molecules with a molecular weight of the

order of $10^5$. Then a decrease in length of the molecule and decrease in molecular weight takes place, owing to oxidation and hydrolysis of dithiocarbonate groups; this is accompanied by an approach of the extinction angle towards 45°. After 25 days the extinction angle curve is of the type obtained for mixtures of two components, one of which is composed of large aggregates. The birefringence, on the other hand, increases during the first 13 days of ripening, although the extinction angle comes close to 45°, which means that the anisotropy of the single molecule increases during the splitting of the dithiocarbonate groups from the dissolved molecules.

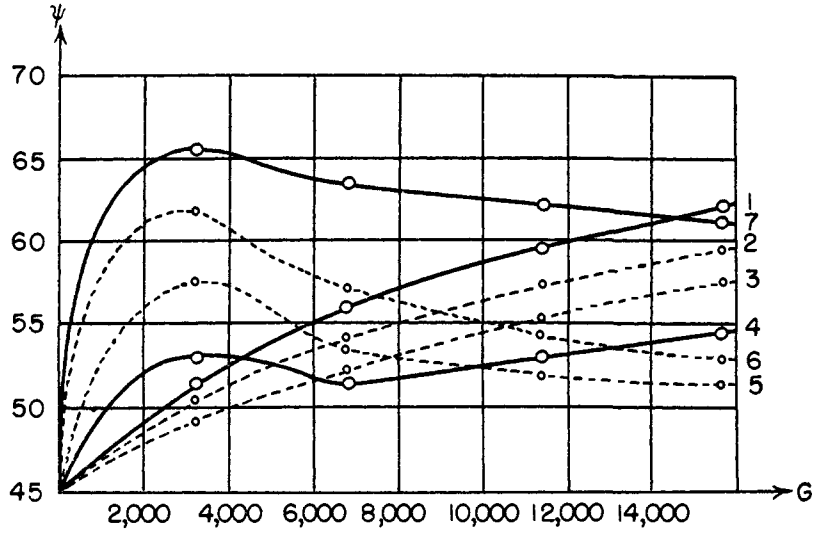


FIG. 50. Extinction angle ($\psi = 90 - \chi$) as a function of velocity gradient in viscose solutions (Signer and Meyer (166)): curve 1, beginning of ripening; curve 2, after 4 days; curve 3, after 12 days; curve 4, after 25 days; curve 5, after 40 days; curve 6, after 67 days; curve 7, after 132 days.

### *8. Measurements of relaxation time*

The apparatus devised by Gonsalves (72) and by Conner and Donnelly (30) for measuring relaxation times (see Section IV,C) has been used for studying concentrated solutions of viscose (cellulose xanthate). One of the most remarkable features in these measurements is that for most of the solutions there is only one relaxation time, $\tau$, measured. Figure 51 shows the relationship between $\tau$ and the degree of polymerization. From these results it can be concluded that the relaxation time must be directly connected with the magnitude of the individual particles.

According to Conner and Donnelly the viscosity of the solution must also be one of the main factors determining the relaxation time. Figure 52 shows values of the relaxation time plotted against the viscosity of the corresponding solution. In the graph are lumped data obtained for solutions having different aging times,

different carbon disulfide contents, different press ratios, different sources of cellulose, and other differences described in detail by Conner and Donnelly (30).

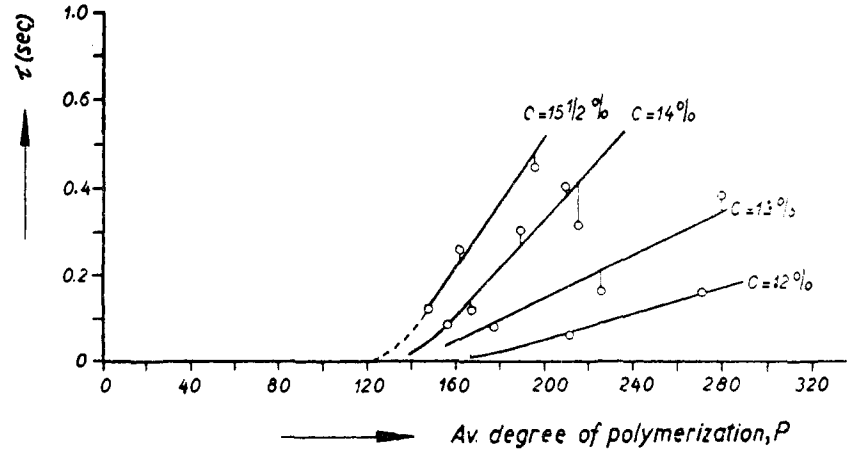


FIG. 51. Effect of degree of polymerization on relaxation time in solutions of cellulose xanthate at different concentrations (Gonsalves (72)).

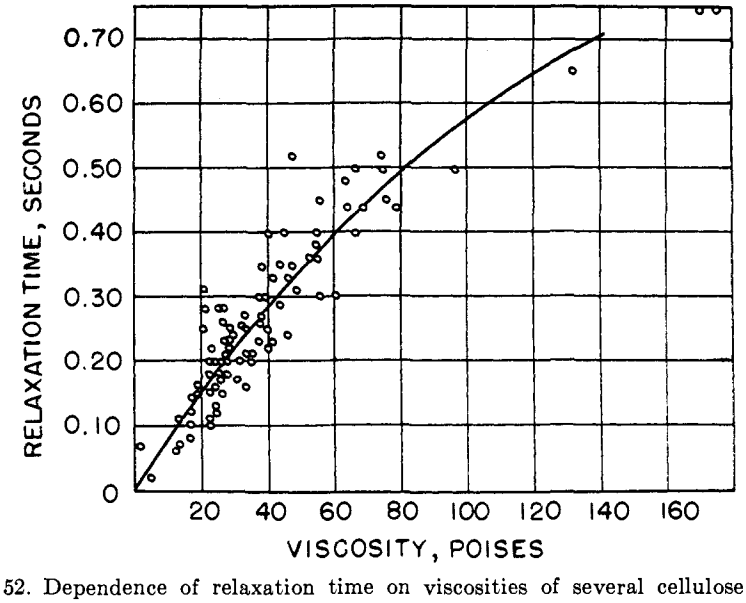


FIG. 52. Dependence of relaxation time on viscosities of several cellulose xanthate solutions (Conner and Donnelly (30)).

In figure 53 are plotted the dependence of the relaxation time, the birefringence, and the viscosity as a function of the shearing stress. The birefringence rises abruptly to a plateau and then continues its increase at higher shearing stresses. Two distinct processes appear to be present. The plateau would be more striking

if a single shearing stress could be maintained during observation. As pointed out by Conner and Donnelly, the fact that the shearing stress during flow in a round tube varies from zero at the center of the tube to a maximum at the periphery limits greatly the resolving power of the type of apparatus used in this experiment.

It also appears in figure 53 that the relaxation time drops very quickly in the range of shearing stress during which the plateau of the birefringence is forming and disappearing. A noticeable distribution of relaxation times was evident for the region in which the relaxation time was changing abruptly. This rapid drop is evidence for the belief that the structure causing the plateau is being broken up by the higher frictional forces acting upon it. Since the relative birefringence

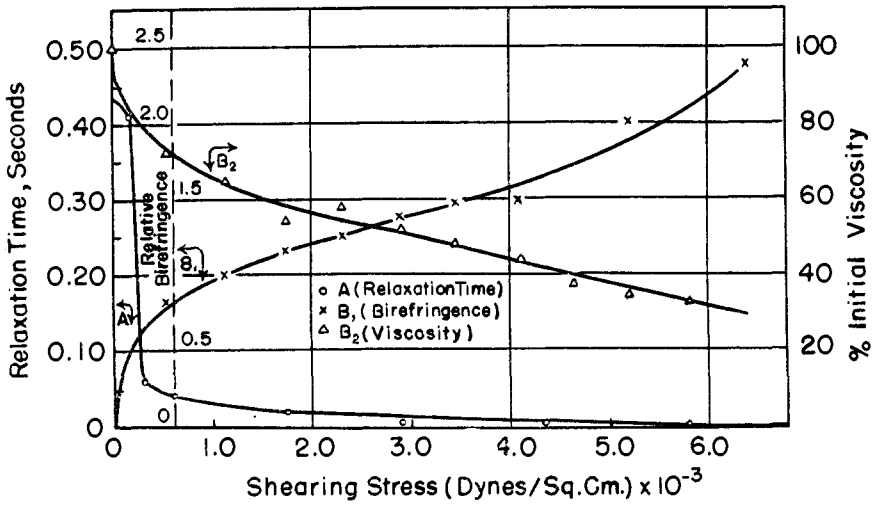


FIG. 53. Decrease in relaxation time with increasing shearing stress (Conner and Donnelly (30)).

at low velocity gradients was not changed by the experiments at high gradients, the aggregates are apparently capable of re-forming.

From these results and also from some additional studies these investigators have concluded that probably one has to deal with loose aggregations of molecular chains which have temporarily formed in solution and which will disperse again if solubility conditions become more favorable.

## VII. CONCLUSIONS

The flow birefringence technique for the study of the size, shape, and optical properties of rigid particles has been extensively applied in recent years, especially since the orientation theory for rigid ellipsoids has been shown to have quantitative validity. Molecular parameters have been determined for many rigid molecules, especially from measurements over a wide range of velocity gradients. The method has been very helpful for the investigation of proteins

and other biological materials; it is particularly useful when employed in conjunction with the other well-established methods for physical-chemical studies of these molecules.

The situation for chain molecules is not as satisfactory as for rigid particles. From the experimental point of view it would be very helpful to have more systematic results for dilute solutions of well-characterized, fractionated chain molecules covering a large range of molecular weights. From the theoretical point of view we now have limiting theories for dilute solutions, the theory of the elastic dumbbell attributing the effect at low gradients mainly to an orientation of the molecules, and the theory of the elastic sphere attributing it mainly to a deformation. Both of these theories are successful in particular cases, although such success is not always a proof of the validity of the basic model of the theory. However, by measuring the extinction angle for various solvent viscosities it should be possible to decide which theory is applicable to a given material so that information may be obtained for that substance by means of measurements of flow birefringence. While these investigations have been primarily concerned with dilute solutions, some experimental work has been started in the last few years on more concentrated solutions, especially studies of relaxation time.

The authors wish to express their appreciation to Professor John T. Edsall of Harvard Medical School, to Professor Anton Peterlin of the University of Ljubljana, and to Professor Charles Sadron of the University of Strasbourg for reading this manuscript and giving invaluable suggestions.

## VIII. References

(1) Arkin, L., and Singleterry, C. R.: J. Colloid Sci. **4**, 537 (1949).
(2) Backus, J. K., and Scheraga, H. A.: J. Colloid Sci. **6**, 508 (1951).
(3) Barbu, E., and Joly, M.: Bull. soc. chim. biol. **32**, 116, 123 (1950).
(4) Basu, S.: Science and Culture **13**, 508 (1948); J. Indian Chem. Soc. **24**, 148, 157, 263 (1947).
(5) Benoit, H.: Compt. rend. **228**, 1716 (1949); **229**, 30 (1949); Thesis, Strasbourg, 1950.
(6) Berger, A.: Kolloid-Z. **103**, 185 (1943); **104**, 24 (1943).
(7) Binkley, F.: J. Biol. Chem. **174**, 385 (1948).
(8) Björnstahl, Y.: J. Optical Soc. Am. **29**, 201 (1939).
(9) Björnstahl, Y.: Kolloid-Z. **97**, 46 (1941).
(10) Björnstahl, Y.: Z. Physik **119**, 245 (1942).
(11) Blix, G., and Snellman, O.: Nature **153**, 587 (1944); Arkiv Kemi, Mineral. Geol. **19A**, No. 32 (1945).
(12) Boeder, P.: Z. Physik **75**, 258 (1932).
(13) Boehm, G.: Abderhalden's *Handbuch der biologischen Arbeitsmethoden*, Abt. II, Teil 3, p. 3939 (1939).
(14) Brinkman, H. C.: Physica **13**, 447 (1947).
(15) Brohult, S.: Nova Acta Regiae Soc. Sci. Upsaliensis **12**, No. 4, 69 pp. (1940).
(16) Brohult, S., and Borgman, K.: *The Svedberg*, p. 429. Almquist and Wiksells Boktryckeri, Uppsala (1944).
(17) Buchheim, W., and Philippoff, W.: Naturwissenschaften **26**, 694 (1938).
(18) Buchheim, W., Stuart, H. A., and Menz, H.: Z. Physik **112**, 407 (1939).
(19) Bungenberg de Jong, H. G., and Berg, H. J. van den: Proc. Koninkl. Nederland. Akad. Wetenschap. **51**, 1197 (1948).

(20) CERF, R.: Compt. rend. **226**, 405 (1948).
(21) CERF, R.: Compt. rend. **226**, 1586 (1948); **227**, 1221 (1948); **227**, 1352 (1948).
(22) CERF, R.: Compt. rend. **230**, 81 (1950).
(23) CERF, R.: Rev. optique **29**, 200 (1950).
(24) CERF, R.: J. chim. phys. **47**, 663 (1950).
(25) CERF, R.: J. chim. phys. **48**, 59 (1951).
(26) CERF, R.: J. chim. phys. **48**, 85 (1951).
(27) CERF, R.: J. Colloid Sci. **6**, 293 (1951).
(28) CERF, R.: Compt. rend. **233**, 1099 (1951); J. Chem. Phys. **20**, 395 (1952).
(29) COHN, E. J., AND EDSALL, J. T.: *Proteins, Amino Acids and Peptides as Ions and Dipolar Ions*, Chap. 21. Reinhold Publishing Corporation, New York (1943).
(30) CONNER, W. P., AND DONNELLY, P. I.: Ind. Eng. Chem. **43**, 1136 (1951).
(31) CREETH, J. M., GULLAND, J. M., AND JORDAN, D. O.: J. Chem. Soc. **1947**, 1141.
(32) DAINTY, M., KLEINZELLER, A., LAWRENCE, A. S. C., MIALL, M., NEEDHAM, J., NEEDHAM, D. M., AND SHEN, S. C.: J. Gen. Physiol. **27**, 355 (1944).
(33) DEBYE, P., AND BUECHE, A. M.: J. Chem. Phys. **16**, 573 (1948).
(34) DEROSSET, A. J.: J. Chem. Phys. **9**, 766 (1941).
(35) DONNET, J. B.: Compt. rend. **229**, 189 (1949).
(36) DONNET, J. B.: J. chim. phys. **47**, 698 (1950).
(37) DONNET, J. B., ZBINDEN, H., BENOIT, H., DAUNE, M., DUBOIS, N., POUYET, J., SCHEIBLING, G., AND VALLET, G.: J. phys. radium [8] **10**, 25S (1949).
(38) EDSALL, J. T.: Advances in Colloid Sci. **1**, 269 (1942).
(39) EDSALL, J. T.: Ann. Rev. Biochem. **11**, 151 (1942).
(40) EDSALL, J. T.: Fortschr. chem. Forsch. **1**, 119 (1949).
(41) EDSALL, J. T., AND FOSTER, J. F.: J. Am. Chem. Soc. **70**, 1860 (1948).
(42) EDSALL, J. T., FOSTER, J. F., AND SCHEINBERG, H.: J. Am. Chem. Soc. **69**, 2731 (1947).
(43) EDSALL, J. T., GILBERT, G. A., AND SCHERAGA, H. A.: Abstracts of Papers Presented at the 112th Meeting of the American Chemical Society, September 1947, p. 33C.
(44) EDSALL, J. T., GORDON, C. G., MEHL, J. W., SCHEINBERG, H., AND MANN, D. W.: Rev. Sci. Instruments **15**, 243 (1944).
(45) EDSALL, J. T., AND MEHL, J. W.: J. Biol. Chem. **133**, 409 (1940).
(46) EDSALL, J. T., RICH, A., AND GOLDSTEIN, M.: Rev. Sci. Instruments, in press.
(47) EDSALL, J. T., SCHERAGA, H. A., AND RICH, A.: Abstracts of Papers Presented at the 119th Meeting of the American Chemical Society, April, 1951, p. 5J.
(48) FEITKNECHT, W., SIGNER, R., AND BERGER, A.: Kolloid-Z. **101**, 12 (1942).
(49) FLORY, P. J.: J. Chem. Phys. **17**, 303 (1949).
(50) FLORY, P. J., AND FOX, T. G, JR.: J. Am. Chem. Soc. **73**, 1904 (1951).
(51) FOX, T. G, JR., AND FLORY, P. J.: J. Am. Chem. Soc. **73**, 1909, 1915 (1951).
(52) FOSTER, J. F.: J. Phys. & Colloid Chem. **53**, 175 (1949).
(53) FOSTER, J. F., AND EDSALL, J. T.: J. Am. Chem. Soc. **67**, 617 (1945).
(54) FOSTER, J. F., AND LEPOW, I. H.: J. Am. Chem. Soc. **70**, 4169 (1948).
(55) FOSTER, J. F., AND SAMSA, E. G.: Science **112**, 473 (1950); J. Am. Chem. Soc. **73**, 3187, 3190, 5388 (1951).
(56) FOSTER, J. F., SAMSA, E. G., SHULMAN, S., AND FERRY, J. D.: Arch. Biochem. Biophys. **34**, 417 (1951).
(57) FREDERICQ, E.: Bull. soc. chim. Belg. **56**, 223 (1947).
(58) FREDERICQ, E., AND DESREUX, V.: Bull. soc. chim. Belg. **56**, 208 (1947).
(59) FRENKEL, J.: Acta Physicochim. U.R.S.S. **19**, 51 (1944).
(60) FREUNDLICH, H., STAPELFELDT, F. AND ZOCHER, H.: Z. physik. Chem. **114**, 161, 190 (1924-25).
(61) FREY-WYSSLING, A.: Helv. Phys. Acta **16**, 437 (1943).
(62) FREY-WYSSLING, A., AND WALCHLI, O.: J. Polymer Sci. **1**, 266 (1946).
(63) FREY-WYSSLING, A., AND WEBER, E.: Helv. Chim. Acta **24**, 278 (1941).

(64) FREY-WYSSLING, A., AND WEBER, E.: Kolloid-Z. **101**, 199 (1942).
(65) GALLAY, W., AND PUDDINGTON, I. E.: Can. J. Research **22B**, 173 (1944).
(66) GANS, R.: Ann. Physik **86**, 628 (1928).
(67) GARD, S., SNELLMAN, O., AND TYREN, H.: *The Svedberg*, p. 530. Almquist and Wiksells Boktryckeri, Uppsala (1944).
(68) GERENDAS, M.: Enzymologia **9**, 123 (1941).
(69) GERENDAS, M., AND MATOLTSY, A. G.: Hung. Acta Physiol. **1**, 124 (1948).
(70) GOLDSTEIN, M.: Abstracts of Papers Presented at the 119th meeting of the American Chemical Society, April, 1951, p. 12J.
(71) GOLDSTEIN, M.: J. Chem. Phys. **20**, 677 (1952).
(72) GONSALVES, V. E.: Proc. Intern. Rheol. Congr., Holland, 1948, II, 239 (1949).
(73) GRAY, V. R.: Proc. Intern. Rheol. Congr., Holland, 1948, II, 23 (1949).
(74) GRAY, V. R., AND ALEXANDER, A. E.: J. Phys. & Colloid Chem. **53**, 9 (1949).
(75) GREENSTEIN, J. P.: Advances in Protein Chem. **1**, 209 (1944).
(76) HALL, C. E.: J. Biol. Chem. **179**, 857 (1949).
(77) HALLER, W.: Kolloid-Z. **61**, 26 (1932).
(78) HEGETSCHWEILER, R.: Makromol. Chem. **4**, 156 (1949).
(79) HERMANS, J. J.: Physica **10**, 777 (1943).
(80) HERMANS, J. J.: Rec. trav. chim. **63**, 25 (1944).
(81) HERMANS, J. J.: Rec. trav. chim. **63**, 205 (1944).
(82) HERMANS, J. J., AND OVERBEEK, J. TH. G.: Bull. soc. chim. Belg. **57**, 154 (1948); Rec. trav. chim. **67**, 761 (1948).
(83) HOCKING, C., LASKOWSKI, M., JR., AND SCHERAGA, H. A.: J. Am. Chem. Soc. **74**, 775 (1952).
(84) JEENER, R.: Compt. rend. soc. biol. **140**, 1138 (1946).
(85) JEFFERY, G. B.: Proc. Roy. Soc. (London) **A102**, 161 (1922).
(86) JERRARD, H. G.: J. Applied Phys. **21**, 1007 (1950).
(87) JOLY, M.: Bull. soc. chim. biol. **30**, 398 (1948); **31**, 105 (1949).
(88) JOLY, M.: Bull. soc. chim. biol. **30**, 404 (1948); **31**, 108 (1949).
(89) JOLY, M.: Kolloid-Z. **115**, 83 (1949).
(90) JOLY, M., AND BARBU, E.: Bull. soc. chim. biol. **31**, 1642 (1949).
(91) JOLY, M., AND BARBU, E.: Bull. soc. chim. biol. **32**, 908 (1950).
(92) JOLY, M., AND RYBAK, B.: Compt. rend. **230**, 1214 (1950).
(93) KANAMARU, K., SUGIYAMA, S., AND TANAKA, T.: J. Soc. Chem. Ind. Japan **45**, Suppl. binding, 263 (1942).
(94) KANAMARU, K., AND TANAKA, T., J. Soc. Chem. Ind. Japan **45**, Suppl. binding, 190 (1942).
(95) KANAMARU, K., TANAKA, T., AND KOMATU, W.: J. Soc. Chem. Ind. Japan **45**, Suppl. binding, 237 (1942).
(96) KANAMARU, K., TANAKA, T., AND MIMURA, M.: J. Soc. Chem. Ind. Japan **45**, Suppl. binding, 270 (1942).
(97) KANAMARU, K., TANAKA, T., AND SUGIYAMA, S.: J. Soc. Chem. Ind. Japan **45**, Suppl. binding, 232 (1942).
(98) KANAMARU, K., TANAKA, T., AND SUGIYAMA, S.: J. Soc. Chem. Ind. Japan **45**, Suppl. binding, 266 (1942).
(99) KANAMARU, K., TANAKA, T., AND YAMAMOTO, M.: J. Soc. Chem. Ind. Japan **45**, Suppl. binding, 200 (1942).
(100) KANAMARU, K., AND TANIOKU, T.: J. Soc. Chem. Ind. Japan **45**, Suppl. binding, 196 (1942).
(101) KANAMARU, K., YAMAMOTO, S., AND TANAKA, T.: J. Soc. Chem. Ind. Japan **45**, Suppl. binding, 242 (1942).
(102) KATCHALSKY, A.: J. Polymer Sci. **7**, 393 (1951).
(103) KATCHALSKY, A., KÜNZLE, O., AND KUHN, W.: J. Polymer Sci. **5**, 283 (1950).
(104) KIRKWOOD, J. G., AND RISEMAN, J.: J. Chem. Phys. **16**, 565 (1948).

(105) KRAMERS, H. A.: J. Chem. Phys. **14**, 415 (1946); this is a translation of Physica **11**, 1 (1944).
(105a) KUHN, H.: Habilitationsschrift, Basel, 1946; Proc. Intern. Rheol. Congr., Holland, 1948, II, 44 (1949); J. Colloid Sci. **5**, 331 (1950).
(106) KUHN, W.: Kolloid-Z. **62**, 269 (1933).
(107) KUHN, W.: Kolloid-Z. **68**, 2 (1934).
(108) KUHN, W., AND GRÜN, F.: Kolloid-Z. **101**, 248 (1942).
(109) KUHN, W., KÜNZLE, O., AND KATCHALSKY, A.: Helv. Chim. Acta **31**, 1994 (1948); Bull. soc. chim. Belg. **57**, 421 (1948).
(110) KUHN, W., AND KUHN, H.: Helv. Chim. Acta **26**, 1394 (1943).
(111) KUHN, W., AND KUHN, H.: Helv. Chim. Acta **28**, 1533 (1945).
(112) KUHN, W., AND KUHN, H.: Helv. Chim. Acta **29**, 71 (1946).
(113) KUHN, W., AND KUHN, H.: Helv. Chim. Acta **29**, 609 (1946).
(114) KUHN, W., AND KUHN, H.: J. Colloid Sci. **3**, 11 (1948).
(115) LAUFFER, M. A.: J. Phys. Chem. **42**, 935 (1938).
(116) LAWRENCE, A. S. C., MIALL, M., NEEDHAM, J., AND SHEN, S. C.: J. Gen. Physiol. **27**, 233 (1944).
(117) LAWRENCE, A. S. C., NEEDHAM, J., AND SHEN, S. C.: J. Gen. Physiol. **27**, 201 (1944).
(118) LESSIAU, J., CERF, R., AND MACHEBOEUF, M.: Ann. inst. Pasteur **74**, 341 (1948).
(119) MASON, W. P.: Trans. Am. Soc. Mech. Engrs. **69**, 359 (1947); J. Colloid Sci. **3**, 147 (1948).
(120) MEHL, J. W.: Cold Spring Harbor Symposia Quant. Biol. **6**, 218 (1938).
(121) MEYER, W.: Thesis, Bern, 1943.
(122) MIRSKY, A. E., AND POLLISTER, A. W.: Proc. Natl. Acad. Sci. U. S. **28**, 344 (1942).
(123) MOMMAERTS, W. F. H. M.: Arkiv kemi, Mineral. Geol. **19A**, No. 17, No. 18 (1945).
(124) MOMMAERTS, W. F. H. M.: Nature **156**, 631 (1945).
(125) MURALT, A. L. v., AND EDSALL, J. T.: J. Biol. Chem. **89**, 315, 351 (1930); Trans. Faraday Soc. **26**, 837 (1930).
(126) NEEDHAM, J., SHEN, S. C., NEEDHAM, D. M., AND LAWRENCE, A. S. C.: Nature **147**, 766 (1941).
(127) NITSCHMANN, H., AND GUGGISBERG, H.: Helv. Chim. Acta **24**, 434, 574 (1941).
(128) ONCLEY, J. L.: Chem. Revs. **30**, 433 (1942).
(129) PERRIN, F.: J. phys. radium [7] **5**, 497 (1934).
(130) PETERLIN, A.: Z. Physik **111**, 232 (1938).
(130a) PETERLIN, A.: *Les grosses molécules en solution*, p. 70. Collège de France, Paris (1948).
(131) PETERLIN, A., AND SAMEC, M.: Kolloid-Z. **109**, 96 (1944).
(132) PETERLIN, A., AND STUART, H. A.: Z. Physik **112**, 1, 129 (1939).
(133) PETERLIN, A., AND STUART, H. A.: *Hand- und Jahrbuch der chemischen Physik*, Bd. VIII, Abt. IB. Becker & Erler, Leipzig (1943).
(134) PILNIK, W.: Ber. schweiz. botan. Ges. **56**, 208 (1946).
(135) PRICE, W. C.: Science **101**, 515 (1945).
(136) PRICE, W. C., WILLIAMS, R. C., AND WYCKOFF, R. W. G.: Arch. Biochem. **9**, 175 (1946).
(137) RAMAN, C. V., AND KRISHNAN, K. S.: Proc. Roy. Soc. (London) **117A**, 589 (1928).
(138) REHNER, J., JR.: J. Chem. Phys. **13**, 450 (1945).
(139) RICH, A.: Abstracts of Papers Presented at the 119th Meeting of the American Chemical Society, April, 1951, p. 35C.
(140) ROBINSON, J. R.: Proc. Roy. Soc. (London) **170A**, 519 (1939).
(141) ROSEN, B., KAMATH, P., AND EIRICH, F.: Discussions of the Faraday Society **11**, 135 (1951).
(142) SADRON, C.: J. phys. radium [7] **7**, 263 (1936).
(143) SADRON, C.: Schweiz. Arch. angew. Wiss. u. Tech. **3**, 8 (1937).
(144) SADRON, C.: J. phys. radium [7] **8**, 481 (1937).
(145) SADRON, C.: J. phys. radium [7] **9**, 381 (1938).

(146) SADRON, C.: J. chim. phys. **44**, 22 (1947).
(147) SADRON, C., BONOT, A., AND MOSIMANN, H.: J. chim. phys. **36**, 78 (1939).
(148) SADRON, C., AND MOSIMANN, H.: J. phys. radium [7] **9**, 384 (1938).
(148a) SATO, K.: J. Chem. Soc. Japan **64**, 197 (1943).
(149) SAVERBORN, S.: "A Contribution to the Knowledge of the Acid Polyuronides," Dissertation, Uppsala, 1945.
(150) SCATCHARD, G., ONCLEY, J. L., WILLIAMS, J. W., AND BROWN, A.: J. Am. Chem. Soc. **66**, 1980 (1944).
(151) SCHERAGA, H. A.: Arch. Biochem. Biophys. **33**, 277 (1951).
(152) SCHERAGA, H. A.: J. Chem. Phys. **19**, 983 (1951).
(153) SCHERAGA, H. A., AND BACKUS, J. K.: J. Am. Chem. Soc. **73**, 5108 (1951).
(154) SCHERAGA, H. A., AND BACKUS, J. K.: J. Am. Chem. Soc. **74**, 1979 (1952).
(155) SCHERAGA, H. A., EDSALL, J. T., AND GADD, J. O., JR.: J. Chem. Phys. **19**, 1101 (1951).
(156) SCHERAGA, H. A., EDSALL, J. T., AND GADD, J. O., JR.: Annals of the Computation Laboratory of Harvard University **26**, 219 (1951).
(157) SCHOENBERG, M. D., RISEMAN, J., AND EIRICH, F. R.: J. Colloid Sci. **5**, 393 (1950).
(158) SCHWANDER, H., AND CERF, R.: Helv. Chim. Acta **32**, 2356 (1949).
(159) SCHWANDER, H., AND CERF, R.: Helv. Chim. Acta **34**, 436 (1951); Experientia **7**, 95 (1951).
(160) SCHWANDER, H., AND SIGNER, R.: Helv. Chim. Acta **34**, 1344 (1951).
(161) SIGNER, R.: Helv. Chim. Acta **19**, 897 (1936).
(162) SIGNER, R.: Trans. Faraday Soc. **32**, 296 (1936).
(163) SIGNER, R.: Unpublished, quoted by Sadron (144).
(164) SIGNER, R., LIECHTI, V., AND LIECHTI, H.: J. chim. phys. **44**, 58 (1947).
(165) SIGNER, R., AND GROSS, H.: Z. physik. Chem. **165A**, 161 (1933).
(166) SIGNER, R., AND MEYER, V.: Helv. Chim. Acta **28**, 325 (1945).
(167) SIGNER, R., AND SADRON, C.: Helv. Chim. Acta **19**, 1324 (1936).
(168) SIGNER, R., AND STRAESSLE, R.: Helv. Chim. Acta **30**, 155 (1947).
(169) SNELLMAN, O.: Arkiv Kemi, Mineral. Geol. **19A**, No. 30 (1945).
(170) SNELLMAN, O.: Arkiv Kemi, Mineral. Geol. **19B**, No. 5 (1945).
(171) SNELLMAN, O.: Arkiv Kemi, Mineral. Geol. **24B**, No. 1 (1947).
(172) SNELLMAN, O.: Arkiv Kemi, Mineral. Geol. **24B**, No. 2 (1947).
(173) SNELLMAN, O.: Acta Chem. Scand. **1**, 291 (1947).
(174) SNELLMAN, O., AND BJÖRNSTAHL, Y.: Kolloid-Beihefte **52**, 403 (1941).
(175) SNELLMAN, O., AND SAVERBORN, S.: Kolloid-Beihefte **52**, 467 (1941).
(176) SNELLMAN, O., AND WIDSTROM, G.: Arkiv Kemi, Mineral. Geol. **19A**, No. 31 (1945).
(177) STEINER, R. F., AND LAKI, K.: J. Am. Chem. Soc. **73**, 882 (1951).
(178) STUART, H. A.: *Hand- und Jahrbuch der chemischen Physik* **10**, 27 (1939).
(179) STUART, H., AND PETERLIN, A.: J. Polymer Sci. **5**, 551 (1950).
(180) SVEDBERG, T., AND PEDERSEN, K. O.: *The Ultracentrifuge*, p. 443. University Press, Oxford (1940).
(181) TAYLOR, G. I.: Phil. Trans. Roy. Soc. (London) **A223**, 289 (1923).
(182) TAYLOR, G. I.: Proc. Roy. Soc. (London) **A146**, 501 (1934).
(183) TAYLOR, G. I.: Proc. Roy. Soc. (London) **A157**, 546, 565 (1936).
(184) THIELE, H.: Kolloid-Z. **112**, 73 (1949); **113**, 155 (1949).
(185) TOLSTOI, N. A.: Doklady Akad. Nauk S.S.S.R. **59**, 1563 (1948).
(186) TSVETKOV, V. N., AND FRISMAN, E.: Acta Physicochim. U.R.S.S. **20**, 61 (1945).
(187) TSVETKOV, V. N., AND FRISMAN, E.: Acta Physicochim. U.R.S.S. **20**, 363 (1945).
(188) TSVETKOV, V. N., AND FRISMAN, E.: Acta Physicochim. U.R.S.S. **21**, 978 (1946); J. Phys. Chem. (U.S.S.R.) **21**, 261 (1947).
(189) TSVETKOV, V. N., AND PETROVA, A.: J. Tech. Phys. U.R.S.S. **12**, 423 (1942).
(190) TSVETKOV, V. N., AND PETROVA, A.: J. Tech. Phys. U.R.S.S. **14**, 289 (1944); Rubber Chem. and Technol. **19**, 360 (1946).

(191) TSVETKOV, V. N., AND PETROVA, A.: J. Phys. Chem. (U.S.S.R.) **23**, 368 (1949).
(192) TSVETKOV, V. N., PETROVA, A. I., AND PODDUBNYĬ, I. Y.: Zhur. Fiz. Khim. **24**, 994 (1950); Chem. Abstracts **45**, 1407f (1951).
(193) WALES, M.: J. Phys. & Colloid Chem. **52**, 976 (1948).
(194) WEBER, H. H.: Arch. ges. Physiol. (Pflügers) **235**, 205 (1934).
(195) WIENER, O.: Abhandl. math.-phys. Klasse Königl. Sächs. Gesellschaft der Wissenschaften (Leipzig) **32**, 509 (1912).
(196) WISSLER, A.: Thesis, Bern, 1940.
(197) WUHRMANN, K., AND PILNIK, W.: Experientia **1**, 330 (1945).